Measurement techniques of scattering parameters based on six-port technology for microwave applications

by

Rabih BARAKAT

THESIS PRESENTED TO ÉCOLE DE TECHNOLOGIE SUPÉRIEURE
IN PARTIAL FULFILLMENT FOR THE DEGREE OF
DOCTOR OF PHILOSOPHY
Ph. D.

MONTREAL, APRIL 06, 2022

ÉCOLE DE TECHNOLOGIE SUPÉRIEURE
UNIVERSITÉ DU QUÉBEC

BOARD OF EXAMINERS

THIS THESIS HAS BEEN EVALUATED

BY THE FOLLOWING BOARD OF EXAMINERS

Mr. Vahé Nerguizian, Thesis Supervisor
Department of Electrical Engineering, École de technologie supérieure

Mr. Serioja Tatu, Thesis Co-supervisor
Institut National de la Recherche Scientifique, Énergie Matériaux Télécommunications

Mr. Mohammad Jahazi, President of the Board of Examiners
Department of Electrical Engineering, École de technologie supérieure

Mr. Nicolas Constantin, Member of the jury
Department of Electrical Engineering, École de technologie supérieure

Mr. Halim Boutayeb, External Evaluator
Université du Québec en Outaouais

THIS THESIS WAS PRENSENTED AND DEFENDED

IN THE PRESENCE OF A BOARD OF EXAMINERS AND PUBLIC

MARCH 15, 2022

AT ÉCOLE DE TECHNOLOGIE SUPÉRIEURE

ACKNOWLEDGMENT

First of all, I would like to express my deepest gratitude for my supervisor professor Vahé Nerguizian for giving me the opportunity to prepare for this doctoral study. I thank him for trusting me from the beginning. He provided me with many helpful suggestions and important advices during this study period and through the process of research and writing of this thesis.

I would like to warmly thank my co-supervisor professor Serioja Tatu for the motivational words and the helpful suggestions during this long journey. I will always be grateful for all the ideas and time he dedicated to help me, his excellent guidance, endless caring and patience. I wouldn't have come this far without you.

I would also to show my appreciation to my colleague Djilali Hammou, for his valuable assistance provided during the measurements at INRS Lab. I express my gratitude to him for the help and support he gave me while submitting my first journal paper.

Besides my supervisors, I would like to thank the members of my Ph.D. committee: Professor Mohammad Jahazi, professor Nicolas Constantin and professor Halim Boutayeb for their valuable time in reviewing this thesis.

My sincere gratitude extends to all the staff and technicians at Polygrames Research Center, in particular, Mr. Jules Gauthier, Mr. Traian Antonescu and Mr. Steve Dubé for their technical support in the realization of my circuits' fabrication.

Last but not least, I would like to express my deepest gratitude to my beloved wife, Samah, for her understanding and encouragement which helped in the achievement of this thesis.

Techniques de mesures des paramètres de dispersion basées sur la technologie six-port pour applications micro-ondes

Rabih BARAKAT

RÉSUMÉ

Les analyseurs de réseaux vectoriels ont été utilisés pour fournir des mesures précises des paramètres-S d'un réseau micro-ondes et sont des instruments essentiels qui suscitent de plus en plus d'intérêt dans l'industrie biomédicale. Dans ce contexte, les ondes électromagnétiques de faible puissance qui sont transmises dans les cellules testées peuvent être efficaces dans la détection du cancer en raison de la différence de comportement diélectrique entre les tumeurs cancéreuses et les cellules normales aux fréquences micro-ondes. Cependant, ces instruments sont souvent encombrants et coûteux, ce qui ne convient pas aux tests de dépistage rapides aux points de service. Par conséquent, de nombreuses recherches ont été menées pour les remplacer par des systèmes de mesure alternatifs à base de la technologie six-port, peu coûteux et portatifs. L'objectif de cette thèse est de présenter un système micro-ondes à six-port large-bande capable de mesurer les coefficients de réflexion et de transmission d'un dispositif sous test (DST). La conception du système de mesure proposé doit donner la précision nécessaire pour que les mesures soient effectuées dans une large bande de fréquences dans la bande S.

Bien que de nombreuses études aient été menées pour développer des réflectomètres six-port, il est toujours essentiel d'optimiser les performances des circuits six-port en gardant une faible complexité de conception et aussi en réduisant l'effort de calcul pour le calibrage. Pour ce faire, le coupleur hybride et le diviseur de puissance doivent être optimisés car ils constituent les éléments de base de l'architecture six-port proposée. À cette fin, la conception d'un diviseur de puissance en anneau modifié, construit à l'aide d'un diviseur de puissance en anneau classique et d'un résonateur à impédance échelonnée supplémentaire, est présentée afin d'améliorer sa bande passante et ses performances. Une étude comparative entre le dispositif conçu et le diviseur de puissance en anneau classique est accomplie. Les résultats de la simulation électromagnétique (EM) montrent que le diviseur proposé présente une largeur de bande fractionnelle de 90.2 % à la fréquence centrale de 3.17 GHz. Les résultats de mesure du prototype fabriqué démontrent une haute performance sur la bande passante opérationnelle considérée de 1.7 GHz à 4.64 GHz avec une perte de retour inférieure à -10 dB tout en maintenant une bonne perte d'insertion et une bonne isolation entre les ports de sortie. Le déséquilibre d'amplitude maximal est inférieur à 0.21 dB et le déséquilibre de phase est inférieur à 2.5 degrés entre les signaux de sortie. En outre, un coupleur à 90-degrés compact à deux-sections avec une structure arrondie est conçu pour fonctionner à 3 GHz. Le coefficient de réflexion d'entrée S_{11} est inférieur à -10 dB entre 2.3 GHz et 3.96 GHz, ce qui signifie une large bande de fréquences opérationnelle du coupleur proposé. De plus, la perte d'insertion est de -3.09 dB à la fréquence centrale avec un déséquilibre d'amplitude inférieur à ±1 dB entre 2.6 GHz et 3.7 GHz.

La jonction six-port composée d'un diviseur de puissance en anneau modifié et de trois coupleurs hybrides identiques à 90 degrés est ensuite conçue et fabriquée pour fonctionner à la fréquence centrale de 3 GHz. Les performances du système six-port sont démontrées par des mesures de la perte de retour S_{11} qui est inférieur à -17 dB dans la bande de fréquence de 2.2-3.67 GHz. En outre, les coefficients de transmission par rapport au port 1 sont de – 6.3 dB ± 1 dB de 2.2 GHz à 3.55 GHz. Ces résultats montrent l'excellente performance de la jonction six-port.

Afin de réaliser le réflectomètre six-port, la source micro-ondes et le dispositif à tester sont connectés à la jonction six-port par le biais d'un circuit additionnel formé par un hybride 90-degrés et un diviseur de puissance en anneau modifié. Les performances du réflectomètre six-port sont ensuite évaluées en effectuant des mesures en temps réel et en mesurant le coefficient de réflexion de différents dispositifs testés. Les résultats mesurés sont ensuite corrigés par une méthode de calibration appropriée pour supprimer les imperfections du système. Comparé aux méthodes de calibration six-port classiques, le processus de calibration proposé est facile à utiliser et permet des mesures précises du coefficient de réflexion tout en réduisant la complexité et les efforts de calcul des techniques de calibration six-port classiques.

Enfin, un analyseur de réseau six-port portatif et peu coûteux pour mesurer les coefficients de réflexion et de transmission complexes est conçu pour fonctionner à la fréquence centrale de 3 GHz. L'analyseur de réseau proposé est constitué de deux jonctions six-port avec des détecteurs de puissance connectés aux ports de sortie, ainsi que d'un circuit additionnel pour la distribution de la puissance, formé d'un coupleur et d'un diviseur de puissance. Le système de mesure proposé combine les avantages de la simplicité et du fonctionnement en temps réel ainsi que la fabrication à faible coût car il est construit en technologie micro-ruban. Une approche simplifiée de calibration basée sur la correction d'erreur à deux ports avec seulement quatre standards est mise en œuvre. Après la calibration, les coefficients de réflexion et de transmission complexes obtenus à partir des différents tests effectués sont évalués, ce qui démontre la validité de la méthode de calibration. Cette thèse ouvre une nouvelle voie prometteuse pour la mesure des paramètres S à deux ports, basée sur la technique six-port à faible coût.

Mots-clés: Microruban, diviseur de puissance en anneau, résonateur à impédance échelonnée, réflectomètre six-port, analyseur de réseau à six ports, permittivité complexe, micro-ondes

Measurement techniques of scattering parameters based on six-port technology for microwave applications

Rabih BARAKAT

ABSTRACT

Vector network analyzers have been used to provide accurate measurements of the scattering parameters of a microwave network and are essential instruments that have gained more and more attention in biomedical industry. In this context, low-power electromagnetic waves that are transmitted into the cells under test can be successful in cancer detection due to the dielectric contrast between malignant tumors and normal cells at microwave frequencies. However, these instruments are often bulky and expensive which is not suitable for clinical and Point-of-care rapid tests. Therefore, many research activities have been made to replace them by low cost and portable alternative six-port measurement systems. The aim of this thesis is to present a wideband microwave six-port system that is able to measure the reflection and the transmission coefficients of a device under test (DUT). The proposed six-port design is required to give the accuracy needed for the measurements to be done in a wide band of operation in the S-band.

While many studies have been carried out to develop six-port reflectometers, there is still a need to optimize the six-port circuit performance by keeping the design complexity low and by reducing the computational effort for six-port calibration. To do this, hybrid couplers and power dividers need to be optimized as they are building blocks in the proposed six-port architecture. To this end, the design of a modified ring power divider, built by using a conventional ring power divider and an additional Stepped-Impedance Resonator (SIR) is introduced to improve its operational bandwidth and performance compared to the reported ring structure. A comparative study between the designed device and the previously reported ring power divider is conducted. The electromagnetic (EM) simulated results show that the proposed divider has a fractional bandwidth of 90.2 % at the center frequency of 3.17 GHz. The measurement results of the fabricated prototype demonstrate high performance over the considered operational bandwidth from 1.7 GHz to 4.64 GHz with a return loss lower than -10 dB while maintaining a good insertion loss and a good isolation between the output ports. The maximum amplitude imbalance is better than 0.21 dB and the phase imbalance is better than 2.5 degrees between the output signals. In addition, a compact two-section 90-degree coupler with a rounded structure is designed to operate at 3 GHz. The input reflection coefficient S_{11} is under -10 dB between 2.3 GHz and 3.96 GHz which means a wide operational bandwidth of the proposed coupler. In addition, the insertion loss is -3.09 dB at the center frequency with magnitude imbalance less than ±1 dB between 2.6 GHz and 3.7 GHz.

The six-port junction made up of a modified ring power divider and three identical 90-degree hybrid couplers is then designed and fabricated to operate at the center frequency of 3 GHz. The six-port system's performance is demonstrated by measurements of the return loss S_{11} which is lower than -17 dB in the frequency band of 2.2 – 3.67 GHz. Besides, the transmission

coefficients with respect to port 1 are - 6.3 dB ± 1 dB from 2.2 to 3.55 GHz. These results show the excellent performance of the six-port junction.

In order to build the six-port reflectometer, the microwave source and the device under test (DUT) are connected to the six-port junction unit through an additional circuit formed by a 90-degree hybrid and a ring power divider. The performance of the six-port reflectometer is then evaluated for real-time measurements by measuring the reflection coefficient of different devices under test. The measured results are then corrected by a proper calibration method to remove hardware imperfection. Compared to conventional six-port calibration methods, the proposed calibration process is easy to use and allows accurate reflection coefficient measurements while reducing the complexity and computational efforts of traditional six-port calibration techniques.

Finally, a low-cost and portable six-port network analyzer (SPNA) for measuring the complex reflection and transmission coefficients is designed to operate at the center frequency of 3 GHz. The proposed network analyzer is built by two six-port junctions and 8 power detectors and an additional circuit for power distribution which is formed by one coupler and one power divider. The proposed measurement system combines the advantages of simplicity and real-time operation as well as low-cost fabrication since it is built on a single layer microstrip technology. A simplified approach for calibration based on two-port error correction with only four standards is implemented. After calibration, the measured complex reflection and transmission coefficients obtained from the different tests performed is evaluated which demonstrate the validity of calibration method. This thesis opens a new promising route for two-port S-parameter measurements based on low-cost six-port technique.

Keywords: Microstrip, Ring Power divider, Stepped-impedance resonator, six-port reflectometer, six-port network analyzer, complex permittivity, microwave

TABLE OF CONTENTS

Page

LIST OF TABLES

Page

LIST OF FIGURES

Page

LIST OF ABREVIATIONS

ANA	Automatic network analyzer
VNA	Vector network analyzer
SPR	Six-port reflectometer
SPNA	Six-port network analyzer
SPFD	Six-port phase/frequency discriminator
PCB	Printed circuit board
DUT	Device under test
GaAs	Gallium arsenide
ADS	Advanced Design System
LMS	Least mean square
RF	Radio frequency
EVM	Error vector modulation
MRI	Magnetic resonance imaging
DSP	Digital signal processor
FBW	Fractional bandwidth
HLL	High-Low line
CUT	Cell under test
POC	Point of care
SIR	Stepped impedance resonator
EM	Electromagnetic
dB	Decibel
IL	Insertion loss

RL	Return Loss
TL	Transmission Line

INTRODUCTION

0.1 Motivation

Detecting cancer in its first stages is the most effective way to reduce mortality from this disease. In order to detect cancer, different methods can be used like magnetic resonance imaging (MRI), ultrasound and X-ray radiography, among others. However, not all screening tests are helpful, and most have risks and side effects. Besides, some test procedures can cause bleeding or other problems. Recently, microwave measurement techniques (Basu & Purkait, 2019; Nerguizian et al., 2017) that are non-ionizing, non-invasive have been considered as a good method for early cancer detection with the lowest possible side effects and without any destruction of cells. In this context, low-power electromagnetic waves that are sent into the cells under test (CUT) can be successful in cancer detection due to the dielectric contrast between normal cells and malignant tumours at microwave frequencies. “The principle is the detection of scattered waves generated by the difference in complex permittivity between tissues in the microwave band. In general, cancer tissues are rich in blood vessels and have higher relative permittivity and conductivity than other tissues” (Kuwahara et al., 2019). In addition, the characterization and identification of several cancer cell lines at microwave frequencies were reported in (Nerguizian et al., 2017) where the complex permittivity of different cell lines in the frequency range from 2 GHz to 4.5 GHz is evaluated. “The information of high frequency dielectric properties of different types of cell lines enables the detection and signature identification of cells in a microfluidic device at microwave frequencies. It was observed that the measured dielectric constant of each cancer cell was almost constant in the S-Band frequency range between 2 and 4.5 GHz” (Nerguizian et al., 2017). The main equipment used during these tests was the conventional network analyzer particularly useful for return loss and insertion loss measurements.

0.2 Problem statement

In general, the vector network analyzer (VNA) is normally a high-cost instrument and has a large size, which may not be practical to use in point-of-care (POC) testing. Therefore, it's a good approach to replace this bulky and costly equipment by a small, portable measurement system which is specific to our needs, and which is capable, along with a dedicated calibration algorithm, of measuring complex reflection and transmission coefficients. The fabricated unit will not be very expensive and would be limited to a specific operational frequency band needed for the measurement's requirements. For cancer cell detection, a portable network analyzer which can deliver accurate results with wideband performance is needed. Therefore, the main challenge in this thesis is to optimize the design of a portable wideband six-port network analyzer used in the S-band frequency range, which can be used in cancer detection systems in order to make it a good alternative to the commercial network analyzer.

0.3 Research Objectives

In this thesis, the objective is to investigate the design and fabrication of a wideband microwave six-port system that is able to measure the reflection and the transmission coefficients of different devices under test (DUTs). The proposed measurement system apart from having the advantages of low cost and portable system should have high accuracy in comparison to conventional vector network analyzer over the S-band frequency range, which is generally a bulky and expensive instrument used in the laboratory.

0.4 Thesis outline

This thesis is organized in five chapters.

Chapter 1 presents the literature review for the six-port measurement theory including all its applications; it also includes the calibration procedures used in these measurement systems and a comparison between the different calibration methods.

Chapter 2 presents the six-port technique and all the theory regarding six-port measurement systems as a low-cost alternative method to measure complex reflection and transmission coefficients. A detailed analysis of the six-port junction is made in order to obtain the reflection coefficient. The dual six-port network analyzer is then described.

Chapter 3 presents the design and optimization of the wideband six-port components which will be included in our six-port system. A detailed analysis of the modified ring power divider and the two-section rounded coupler is conducted in order to design these components in a wide operational bandwidth. The modified ring power divider described in this chapter was the subject of the published article: “Modified ring power divider using stepped-impedance resonator”.

Chapter 4 presents the design and fabrication of the proposed six-port reflectometer which is then tested by measuring the reflection coefficient of different DUTs over a large frequency band. The measured results are then corrected by a simplified calibration method to consider the imperfections of the proposed system and to make further corrections of measured results.

Chapter 5 presents the design and fabrication of the proposed six-port network analyzer along with its calibration procedure. After a brief description of the six-port network analyzer SPNA operation, the validation of the designed SPNA in Advanced Design System (ADS) the verify its correct operation to obtain both the transmission and the reflection coefficients of a device under test (DUT) is described. Then, the experimental setup is used to make real-time measurements of two passive loads. The two-port calibration process is then used to correct errors resulting from system imperfections over the frequency range 2.4- 4 GHz. Then, the conclusion and future work are presented to conclude this work.

CHAPTER 1

LITERATURE REVIEW

1.1 Introduction

Since 1972, the six-port technique which was introduced by Engen & Hoer (1972) has gained more and more interest in several fields of microwave engineering. An arbitrary six-port junction is composed of a passive device having two inputs, one for the source signal and the other for the device under test (DUT), and four outputs consisting of four power detectors. The block diagram of the six-port reflectometer (Engen, 1977) is illustrated in Figure 1.1.

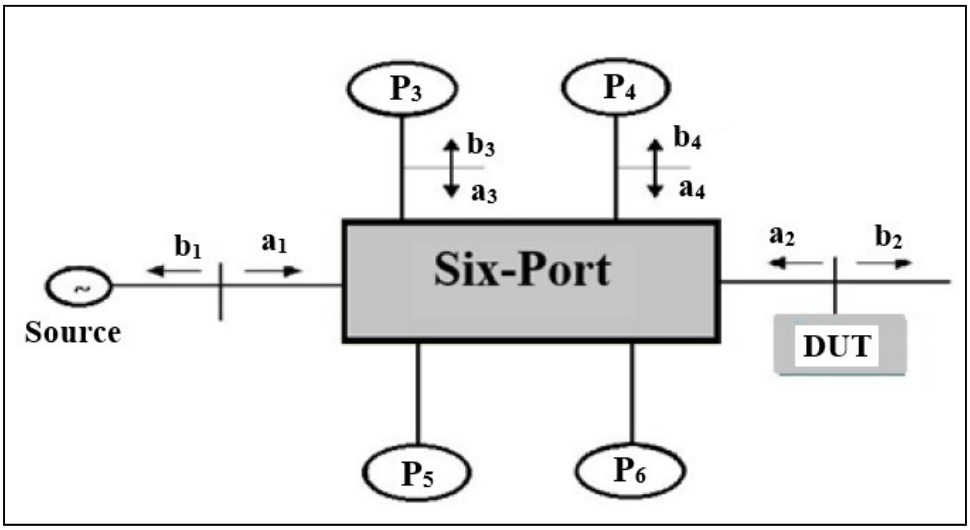

Figure 1.1 Six-port reflectometer block diagram

1.2 Six-port reflectometer

The six-port technique was originally described by Engen (1977) as an alternative method of implementing an automatic network analyzer (ANA). By measuring the output powers, the six-port reflectometer allows measuring the amplitude ratio as well as the phase difference of two electromagnetic signals (Engen, 1977). It is mostly used to measure the reflection coefficient of a device under test (DUT), which is the ratio of the wave reflected by the DUT

to the incident wave sent towards the DUT. However, the dual six-port network analyzer (Hoer, 1977; Juroshek & Hoer, 1984) measures both reflection and transmission coefficients. The complex reflection coefficient is determined as the intersection of three circles and the major design question remains in the choice of the circle's centers (q_i points) as shown in Figure 1.2. In practice, there is ambiguity in the solution as the three circles will not generally meet in one point because of measurement errors. The position of the q_i points depends on the topology of the reflectometer. Ideally, the three q_i points have the same amplitude, and their arguments differ by 120 °.

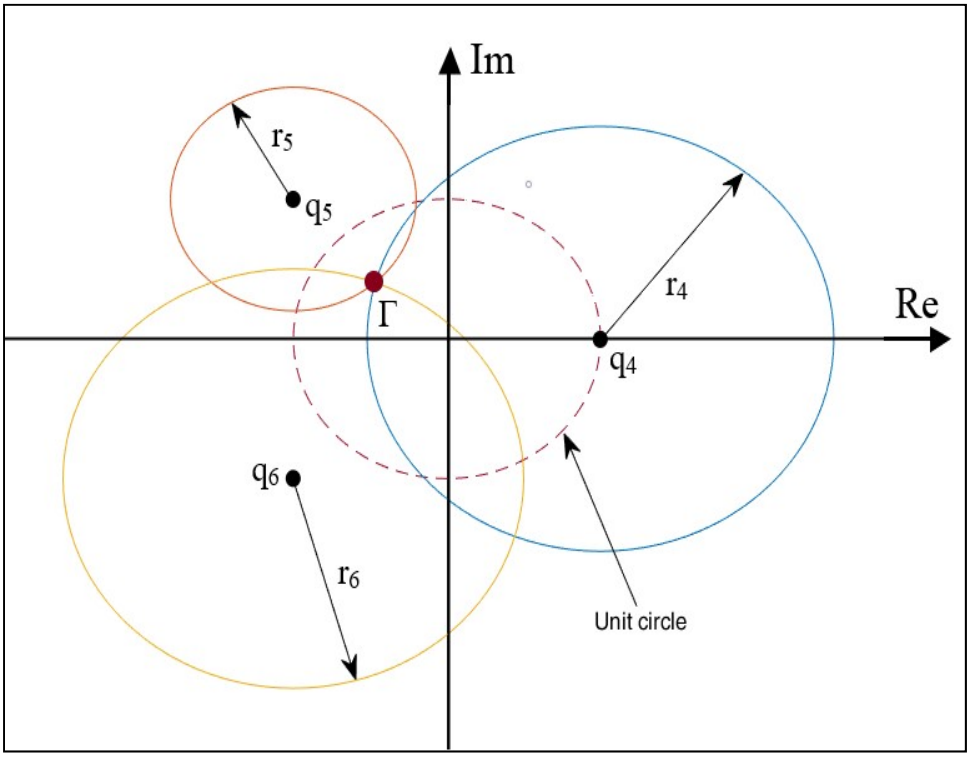

Figure 1.2 Graphical method for determining the reflection coefficient

In addition, Hoer (1977) described the design of a microwave network analyzer which was able to measure the S-parameters of a DUT by incorporating two identical six-port reflectometers. The broadband measurement system can be theoretically studied at a single frequency from 2–18 GHz after calibration at this frequency. Since then, the six-port technique was used intensively in the literature to develop measurement systems. Specifically, research

activities related to load-pull characterization methods of power transistors were carried out by Fadhel M Ghannouchi et al. (1989) which permit to measure the power transferred to the load as well as the load impedance seen by the transistor. The proposed technique bypasses the need to use extra directional couplers and power meters usually required in microwave power measurements (Fadhel M Ghannouchi et al., 1990). Moreover, a six-port measurement circuit with a GaAs monolithic microwave integrated-circuit (MMIC) device working in the frequency range of 0.08–7 GHz was proposed in (Bilik et al., 1990). The circuit consisted of lumped elements and its major inconvenience was its very high losses, which can reach 16 dB between the source and detectors. Another new structure for a six-port reflectometer using non-matched diode detectors working in the operating frequency range of 1.3–3 GHz and realized in MMIC technology was proposed in (Frank Wiedmann et al., 1997). It had a low attenuation of about 6 to 10 dB between the power source and the output measurement ports. Furthermore, a novel miniaturized microstrip six-port junction made up of a 3 dB Wilkinson power divider and three quadrature hybrid couplers was presented in (Fang et al., 2011). It has transmission coefficients less than - 6.7 dB and a return loss lower than -10 dB in the frequency range from 2.2 GHz to 2.6 GHz. In (Chagtmi et al., 2017), a dual-band six-port reflectometer composed of a six-port junction with a diode detection circuit has been designed, calibrated and used to find the reflection coefficient of an unknown load. The proposed reflectometer has been achieved to work at two operating frequencies of 1.5 GHz and 2.7 GHz. Recently, a six-port reflectometer producing an ameliorated power distribution has been proposed in (Kamil Staszek et al., 2016). The presented six-port reflectometer has been designed and fabricated in stripline technology with the use of single-section directional couplers and power dividers in the operational frequency band of 2.5–3.5 GHz. The comparison of the measurement results clearly shows significant enhancement of the measurement accuracy of the proposed six-port with respect to the classical six-port reflectometer. Later, a portable six-port reflectometer working at a single frequency of 5.13 GHz to determine the moisture content of a biomass material has been proposed in (Julrat & Trabelsi, 2017). The proposed six-port reflectometer (SPR) was applied to measure the relative complex permittivity ε of several biomass samples to determine the moisture content of the biomass. Moreover, a wideband six-port reflectometer based on Buttler matrix using broadside coupled lines has been realized in (Hassan & Abbas,

2018). The proposed reflectometer used four couplers having three conductor layers with two substrates between each layer. The measured S-parameters showed good behavior in the operational frequency band from 1.75 GHz to 3.25 GHz.

To date, many studies have shown the effectiveness of microwave technology as a potential non-invasive approach for biomedical applications and cancer detection, especially for breast cancer. It has been shown that "the cancerous cells demonstrate greater permittivity and larger surface area for which there is large increase in capacitance components due to the Capacitance Relaxation phenomenon" (Basu & Purkait, 2019). "The principle is the detection of scattered waves generated by the difference in complex permittivity between tissues in the microwave band" (Kuwahara et al., 2019). Since the main measurement equipment used in these systems is the vector network analyzer, many efforts have been done to replace the traditional vector network analyzer (VNA) by a portable and low-cost microwave six-port reflectometer that would be limited to a specific operational frequency band needed for the measurements requirements. For example, a wideband microwave six-port reflectometer was designed to be inserted in a microwave breast cancer detection system in (Bialkowski et al., 2006). The simulation results showed that the obtained reflection coefficients have a magnitude of 1 ± 0.2 when the DUT is made of either an open or short load in a frequency band from 4 to 8 GHz. In (Kissinger et al., 2013), a 60 GHz six-port reflectometer for biomedical applications which is able to measure the reflection coefficient of different sensors both in amplitude and phase has been reported. In (Lee et al., 2016), a six-port reflectometer with a dielectric probe sensor has been manufactured and utilized to define the dielectric ε_r of normal and malignant breast tissue in the frequency band 2.34– 3.0 GHz by using an improved five-port ring circuit reflectometer. Even though the measurement errors seem noticeable, the difference between normal and malignant breast tissue samples was recognizable on the basis of the magnitude measurement of reflection coefficients of unknown loads (Lee et al., 2016). In addition, a two-port vector network analyzer (VNA) composed of two six-port-junctions for biomedical applications has been proposed in (Hofmann et al., 2013). This six-port has been conceived to work with a 10% fractional bandwidth around the three frequencies of 6.6 GHz, 19.7 GHz, and 32.4 GHz with an embedded permittivity sensor in order to measure various glucose

concentrations in binary solutions. Likewise, a new six-port reflectometer operating at a single frequency (8 GHz) has been reported in (K Staszek et al., 2017), which had an improved measurement accuracy for the reflection coefficient measurements. The introduced detector based on microwave measurements can be used in a portable exhaled breath analyzer for diabetes patients.

1.3 Six-port digital receiver and radar system

Along the years, various six-port circuits were proposed in many other applications such as in telecommunications and radar systems as well as for biomedical applications. In this regard, Ji Li et al. (1995) introduced a new six-port digital receiver for direct demodulation of different digitally modulated signals utilizing a six-port phase/frequency discriminator. In addition, Tatu et al. (2001) proposed a new direct conversion six-port receiver suitable for low-cost wideband millimeter-wave application. This receiver presented a possible alternative for mobile terminals as it operated without the need for accurate output power readings and without a DSP, as required in the previous six-port receivers' designs. Furthermore, Zhang et al. (2017) proposed a new dual-band six-port receiver working in the operational frequency bandwidth of 2–3 GHz on the basis of real time-delay neural network. The six-port receiver offered reduced error vector modulation (EVM) value less than 2 % which verified the system's implementation accuracy. Moreover, a compact six-port junction using broadside-coupled waveguide operating from 1.5 GHz to 2.5 GHz has been presented in (Qayyum & Negra, 2017). The proposed six-port junction, having amplitude and phase imbalance of 2.8 dB and ± 10˚, respectively, was suitable to be used in six-port receiver applications. Also, a wideband six-port correlator with an integrated filtering function operating from 1.6 GHz to 2.6 GHz has been proposed in (S. Sun et al., 2017). The measurement results showed wideband performance with transmission coefficients of -8.1 ± 1.6 dB and a return loss less than -10 dB in the whole operating band. Recently, an LTCC six- port device operating from 24 GHz to 24.25 GHz band has been presented in (Barbara & Yevhen, 2020). The proposed six-port, having phase and amplitude imbalance of ± 1.5˚ and 0.98 dB, was constituted of strip-line quadrature couplers and microstrip power divider. In (Sunil et al., 2020), a wideband six-port network

operating from 2.3 GHz to 4.0 GHz consisting of a Wilkinson power divider and wideband Lange couplers has been reported. The designed six-port network showed phase errors less than 4.7° and magnitude imbalance of 1.98 dB over the operating frequency bandwidth.

So far, the six-port technique was also used in automobile radar for collision avoidance. For example, a novel six-port digital phase/frequency discriminator (SPFD) has been presented in (J Li et al., 1994) to measure Doppler frequency shifts. This new radar system has the advantages of low-cost and small volume and offers a faster sampling rate. Similarly, many works in the literature were devoted to the use of six-port radar systems in several frequency ranges. In (Gutierrez Miguelez et al., 2000), another radar according to the six-port phase/frequency discriminator (SPFD) operating at a 2 GHz has been described for automobile collision avoidance usage. In (Vinci et al., 2012), a six-port medical radar operating at 24 GHz built on a multilayer printed circuit board (PCB) has been presented. This six-port radar system was able to detect breath rate and heartbeat frequency without using electrodes on the patient's body. Additionally, a six-port interferometer operating between 5 to 8 GHz has been reported in (Ibrahim et al., 2016) for direction of arrival detection. The simulation results of the six-port network showed good performance in the operational bandwidth from 5.5 GHz to 7.8 GHz where the return loss at Port 1 is greater than 10 dB and the phase shifts are near ± 90° in the bandwidth from 5 GHz to 8 GHz.

1.4 Six-port architectures

Different six-port structures exist in the literature. The most well-known architecture is composed of a Wilkinson power divider and three 90° hybrid couplers like the one used in (Hammou et al., 2016; Tatu et al., 2001) where a new six-port architecture having good phase and amplitude balance in the frequency band 57–65 GHz has been reported. In this structure, the ring power divider is used instead of the Wilkinson power divider by adding two half-wave transmission lines to connect the 100 Ω integrated resistor in order to improve the circuit performance. The basic diagram of this architecture is shown in Figure 1.3 (Hammou et al., 2016).

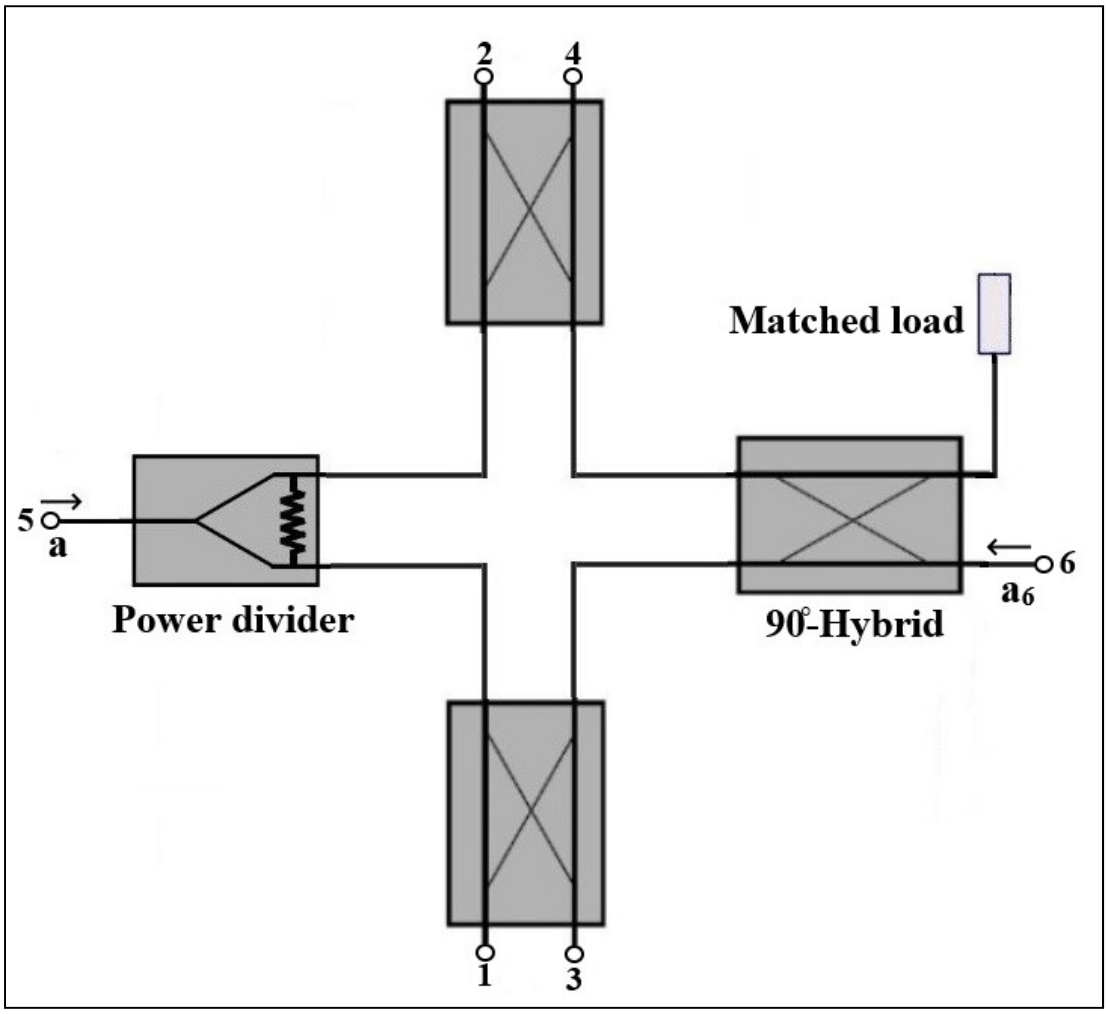

Figure 1.3 The most known six-port architecture

The second most popular architecture is constituted of four quadrature branch-line couplers and a 90-degree phase shifter as shown in Figure 1.4. It is similar to the most known six-port architecture, but the power divider is replaced by a phase shifter and a quadrature branch-line coupler in this configuration. This six-port architecture was used in (Tatu & Moldovan, 2006) in order to realize a six-port heterodyne receiver which can be dedicated for future high-speed wireless communication systems. The simulation results of the reported six-port circuit show that the insertion loss is near -6.3 dB at the center frequency of 60 GHz.

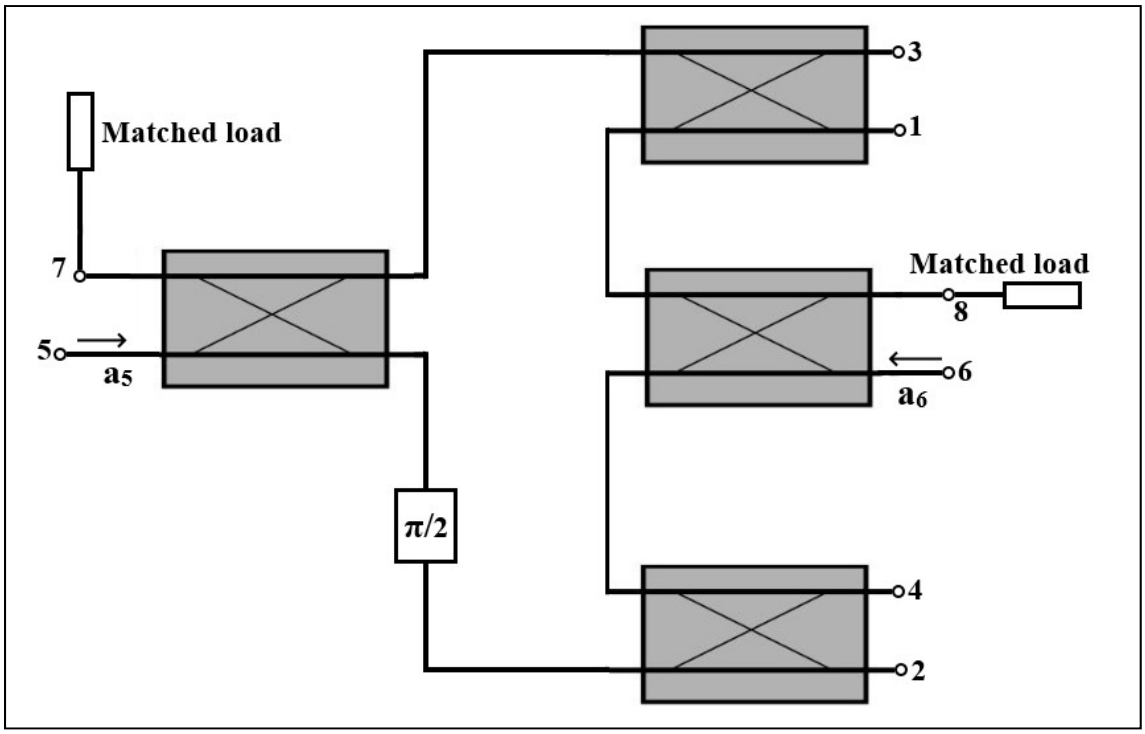

Figure 1.4 The six-port second most popular reported architecture

The third reported six-port architecture is composed of one rat-race coupler and three 90° couplers as shown in Figure 1.5. In comparison with the previous architecture, the phase shifter and the quadrature hybrid coupler are replaced with a rat-race coupler. In (Chew et al., 2015), a new six-port correlator using this architecture has been built to work in the 60 GHz band (57 to 66 GHz). The reported six-port junction had a phase and amplitude imbalance of 1.5° and 0.7 dB respectively through the whole operational bandwidth. However, the simulation results showed that the insertion loss for ports 5 and 6 is bigger than that for ports 3 and 4 and this is caused by the higher insertion loss of the rat-race coupler (Chew et al., 2015). In addition, the transmission coefficients for port 1 and 2 vary between - 8.2 and - 10 dB, which is considered as a high loss compared to the typical case of - 6 dB in the previous architectures.

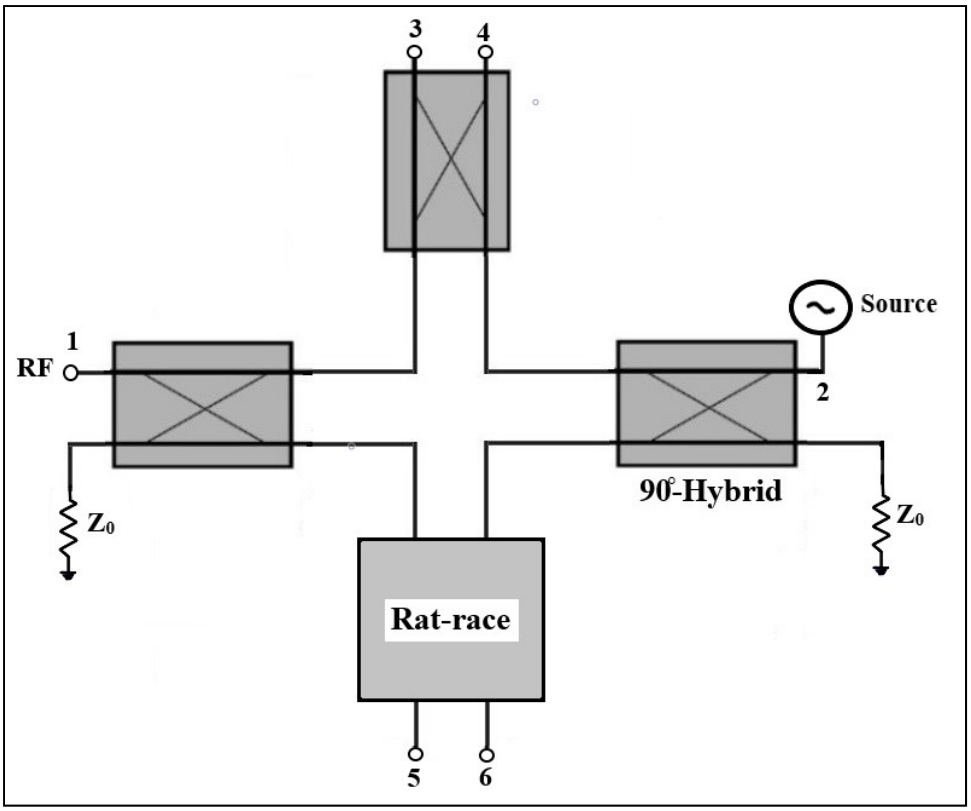

Figure 1.5 The third reported six-port architecture

The fourth reported six-port architecture shown in Figure 1.6 was proposed in (Yu et al., 2008) and consisted of two Wilkinson power dividers, one rat-race coupler and one 90° coupler. The proposed correlator using this architecture and operating at the central frequency of 2.5 GHz has got wider bandwidth compared to three other six-port phase correlators presented and analyzed in this paper (Yu et al., 2008).

The second architecture uses a 90-degree phase shifter whose additional insertion loss may degrade the performance of the six-port system. According to the analysis of wideband vector reflectometers done in (Kothari et al., 2013), the phase-shifter has non-ideal characteristics that can considerably affect the performance of the system and represent the prominent sources of error when evaluating the reflection coefficient. Thus, the second architecture will be discarded. Based on the study done in (Yu et al., 2008), a performance comparison for various

six-port structures composed with Wilkinson power divider, quadrature hybrid coupler and/or 180°rat-race ring coupler operating at the central frequency of 2.5 GHz is shown in Table 1.1.

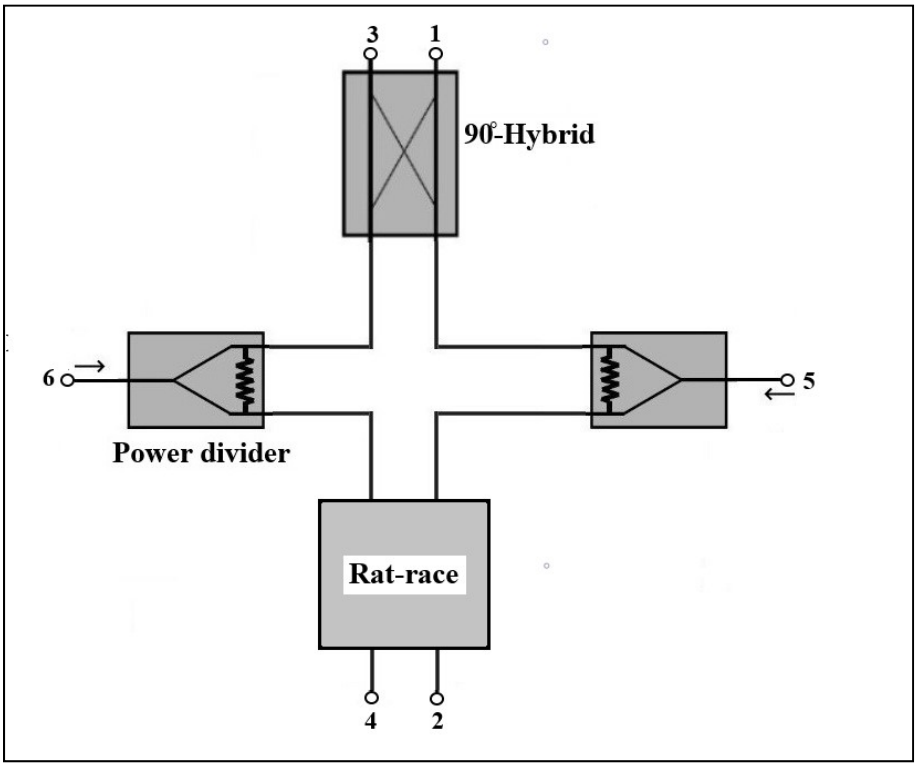

Figure 1.6 The fourth reported six-port architecture

Table 1.1 Performance comparison of different six-port architectures

	Bandwidth	**Insertion loss**	**Phase error**
Architecture 1	**420 MHz**	**-6.0 ± 1.5 dB**	**4°**
Architecture 3	**420 MHz**	**-6.3 ± 1 dB**	**8°**
Architecture 4	**630 MHz**	**-6.1 ± 1.2 dB**	**13°**

According to Table 1.1, the first architecture using one Wilkinson and three hybrid couplers presents less errors in terms of insertion loss and phase error among the considered structures. In addition, the conventional rat race coupler has some drawbacks such as a comparatively narrower bandwidth and a considerable occupied area due to the use of transmission lines (H.-X. Xu et al., 2011). This will affect the global performance of the six-port structure for the

third and fourth structures. For all these reasons, the first architecture will be chosen, and its components are optimized to get better performance and wider bandwidth throughout this thesis.

1.5 Calibration

In order to minimise measurement imperfections of the various elements constituting the six-port system and get accurate results, the six-port needs to be calibrated before being used. Calibration is used to obtain the calibration constants of the six-port system which then makes it possible to calculate the reflection coefficient of the DUT. Calibration techniques for six-port devices have been widely described in the literature (F M Ghannouchi & Bosisio, 1988; Hunter & Somlo, 1985; F Wiedmann et al., 1999; Yakabe et al., 1994). All these methods were based on the relationship between the output power readings by the detectors and the reflection coefficient of the DUT.

However, the most famous and widely used method till these days was developed by Engen (1978). In this method, the solution of the complex reflection coefficient Γ is given by determining eleven constants describing the six-port circuit into two distinct parts. The first part involves reducing the six-port reflectometer to a four-port circuit with an associated complex ratio detector. In this part, five of the eleven constants of the six-port reflectometer are determined. In the second part, it remains to determine the six real constants which describe the equivalent four-port system (Engen, 1978). Since then, a lot of work has been performed to find an accurate solution for the reflection coefficient while minimizing the number of standard loads, restrictions on the used standards and the computational effort.

Li and Bosisio (1982) developed a calibration method with four reflection standards having the reflection coefficient magnitude $|\Gamma| = 1$. The calibration errors from the standards were significantly reduced, which makes this method appropriate to calibrate a potential five or six-port reflectometer based on crystal diode detectors. Similarly, Hunter & Somlo (1985) developed an explicit six-port calibration method employing five calibration standards and

giving unambiguous solution for the calibration constants. The five standards used include four sliding short circuits and the fifth standard was a load element (Z_0 = 50 Ω). However, even though the method allowed exact specification of the standards to be used, the tests with the fifth standard, significantly different from Z_0, showed growing sensitivity to the measurement noise of the reported results. Moreover, Qian (Qian, 1985) presented an iterative method for six-port calibration using only four standards including a matched load and three offset shorts. In this method, there was no constraint on the incident wave on each of the four terminations, and there was no need to determine the sign ambiguity. The remaining redundancy could be used to determine errors produced by the six-port measurement system.

Ghannouchi and Bosisio (1988) also developed an explicit method for six-port calibration requiring five standards based on matrix formalism. The algorithm converged rapidly and the relatively few loads employed enabled rapid calculations which decreased the computational effort. Later, Yakabe et al. (Yakabe et al., 1994) proposed an explicit six-port calibration method using one short and one sliding load with unknown reflection coefficient as a calibration standard. The formulas used were expressed without any ambiguity and were rapidly estimated based on Fourier series of power ratios. Moreover, F. Wiedmann et al. (F Wiedmann et al., 1999) presented a six-port calibration method to find the first estimations of the parameters of Engen's six to four-port conversion algorithm. The method used five standards having unknown but fixed absolute value of the reflection coefficient. In addition, Haddadi & Lasri (2012) proposed a six-port calibration method based on a spatial Fourier analysis, which uses impedance data scattered on the whole Smith chart to enhance the measurement precision followed by a least square algorithm. The suggested technique allowed a great flexibility in the achievement of planar six-port reflectometers by giving the opportunity to relax the design restrictions. However, the computational effort was increased by increasing the number of calibration standards at the expense of obtaining accurate calibration results. Furthermore, Staszek et al. (2013) proposed a six-port calibration realized in two-steps. The first step consisted of solving a least-squares problem. Next, four distinct calibration standards excluding a matched load should be used, and the error terms were evaluated as the average values.

Recently, an explicit six-port calibration method for a compact six-port junction operating from 3 GHz to 6 GHz was proposed in (Moubarek et al., 2019). It was based on matrix formalism expressing I and Q as a function of the measured output voltages on the detectors (V_3..., V_6) and the number of calibration standards was reduced to six. This method used the second order model algorithm introduced by Haddadi & Lasri(2012), which was based on a spatial Fourier analysis. Another six-port calibration method using unknown calibration standards having arbitrary magnitude and phase and a matched load was presented in (K Staszek, 2018).Since the calibration loads were unknown, a normalization was needed. The method used eight segments of matched transmission lines having different lengths as calibration standards. The major drawback of this method was the complicated mathematical concepts and increased computational effort used through the proposed calibration procedure.

Table 1.2 shows a detailed description of the most relevant six-port calibration methods previously present in the literature. As seen in Table 1.2, most of the calibration methods used in the literature for six-port systems calibration demand high computational efforts and high level of expertise on behalf of the operator in the field of microwave engineering as well as complicated mathematical concepts.

Given the high computational costs and the painful and time-consuming efforts involved in these methods, there is a need for a new calibration method that can combine accuracy with ease of use at a low computational cost. The simplified calibration approach based on error correction models for one port and two-ports systems proposed in this thesis addresses these challenges. More specifically, the proposed method uses an analytical approach to find the corrected reflection and transmission coefficients for six-port measurement systems. The experimental results prove the efficiency and good performance of the proposed six-port calibration approach as will be seen in detail in chapters 4 and 5 of this thesis.

Table 1.2 Detailed description of the most relevant calibration methods used for six-port systems

Calibration Method	**Advantages**	**Disadvantages**	**Calibration Standards**
(Engen, 1978)	This method permits to separate the problem into two distinct steps. The first step transforms the SPR into a virtual four-port. It is not required to find all eleven constants together. In addition, the four-port problem has already existing solutions for traditional network analyzers.	This method includes a lengthy mathematical approach. In addition, there is the ambiguity of having to choose square-root signs. It also includes an iterative process, and the solution may get a wrong root or diverge.	Nine calibration standards allow solving a linear system of nine equations having nine unknowns.
(S. Li & Bosisio, 1982)	This is an explicit method where there are no ambiguities for the solution of reflection coefficients and no singularity occurs in a wide range of phase distribution.	Too high computational effort required to find the calibration constants. To resolve the sign ambiguity, a supplementary measurement must be done in which a matched load is connected to port 2.	Four reflection standards, having $\|\Gamma\|=1$ and a different phase distribution, are required.
(Hunter & Somlo, 1985)	This is an explicit method using five standards providing unambiguous and clear solutions for the calibration constants.	Restrictions imposed by the type of calibration standards; the choice of the fifth standard (Z_0) showed increased sensitivity of the results to the measurement noise.	Four standards used as a sliding short and the fifth standard is a matched load.
(Qian, 1985)	This is an iterative calibration method using only four standards, there is no restriction on the incident wave on each of the four terminations, and there is no need to determine the sign ambiguity.	The assumptions of initial constant values must be made and at least two solution sets could be obtained; redundancies are used to determine errors produced by the system.	Four standards including three offset short circuits and a matched load are used.
(F M Ghannouchi & Bosisio, 1988)	This is an explicit method based on matrix formalism that converges rapidly and the relatively few loads employed enable rapid calculations. There is no restriction that a particular reference port must be used.	The limitation on the choice of the type of standards used; long and complicated mathematical process.	Five standards: 3 sliding shorts, a matched load and a 6-dB attenuator terminated by a short circuit.

Table 1.3 Detailed description of the most relevant calibration methods used for six-port systems (continued)

Calibration Method	**Advantages**	**Disadvantages**	**Calibration Standards**
(Haddadi & Lasri, 2012)	The calibration model proposed based on a spatial Fourier analysis allows a great flexibility in the achievement of planar SPRs by giving the opportunity to relax the design restrictions. Mismatching effects and nonlinearity of power detectors are considered in this calibration method.	The algorithm developed includes an iterative process where Γ_0 is considered as an initial guess. The computational effort is increased by incrementing the number of calibration standards at the expense of obtaining accurate calibration results.	Eight calibration standards are required for the simultaneous resolution of the matrix system.
(K Staszek et al., 2013)	A two-step calibration method is used. The first step consists of solving a least-squares problem. In the second step, four calibration standards excluding a matched load must be used, and the error parameters can be evaluated as the average values.	The numerical least-square algorithm includes an iterative process which implies that it can be divergent despite of choosing good estimates of the initial values. The computational effort to find the calibration constants is high.	Four different calibration standards (excluding a matched load) are required.
(Moubarek et al., 2019)	This method is based on spatial Fourier analysis and on matrix formalism expressing I and Q as a function of the measured output voltages on the detectors. A linearization of power detectors and an AC detection procedure are used to enhance the precision.	This method is based on the second order model algorithm introduced in a previous reported method by Haddadi & Lasri (2012) in which a high computational effort is adopted. In addition, the solution includes an iterative process.	The number of calibration standards is six as the authors used the second calibration model described in a previous reported method.
(K Staszek, 2018)	In comparison to other calibration methods, this method consists of using unknown calibration standards having arbitrary magnitude and phase and a matched load which releases the limitation on the type of calibration standards.	The calibration method uses complicated mathematical concepts including graphical concepts in the complex plane and increased computational effort used through the proposed calibration procedure.	The method uses eight segments of matched transmission lines having different lengths as calibration standards.

1.6 Conclusion

As seen through the literature review, the six-port technique can be used in different applications including measurement systems and digital receivers as well as radar systems. In this thesis, a six-port measurement system which can be used to measure both the complex reflection and transmission coefficients of a DUT is fully described. Since some applications need only the reflection coefficient to be found, the complete design and fabrication of a six-port reflectometer is first described. In order to enhance the six-port circuit performance, the ring power divider and the 90° hybrid coupler are optimized in terms of S-parameters and bandwidth. Then, a six-port reflectometer (One-port network analyzer) is designed and fabricated using the six-port junction and an additional circuit. Furthermore, a complete six-port (two ports) network analyzer is designed and fabricated in a single low-cost layer substrate. In addition, a simplified calibration method based on virtual error box calibration method is proposed, which therefore can be applied for any type of six-port reflectometer and network analyzer. The number of known standard loads required for calibration has also been reduced to three standards for one port calibration as is normally used in commercial network analyzer calibration kits. For two-port calibration, an additional Thru standard is used. Since the proposed six-port system is relatively simple to design and can provide high performance with a low-cost technique. Our results clearly show that the proposed measurement system, along with the new calibration technique, can improve the existing six-port measurement system designs in terms of accuracy for wideband applications and proves that it can be a good candidate to replace the conventional network analyzer in low-cost measurement systems. In general, six-port techniques are adaptable to practically any frequency (Koelpin et al., 2010), which makes the proposed design possible at any microwave and millimeter-wave frequency bands with a modification of design parameters. To this end, the simplified calibration algorithm, which uses well-known calibration standards widely available and used in existing industrial calibration kits will reduce the computational efforts and can significantly reduce the time needed compared to the traditional methods used so far in the literature.

CHAPTER 2

SIX-PORT THEORY

As mentioned in the literature review, the six-port technique is considered as a low-cost alternative method to measure the reflection coefficient (Γ) of a device under test (DUT) by using simple power detectors rather than complex heterodyne schemes (Engen, 1977). In this chapter, we will review the basic theory of the six-port technique and the design of the six-port junction and network analyzer. Before describing the six-port technique, we will introduce some background theory regarding power dividers and 90-degree hybrids, which are the main components of the six-port circuit.

2.1 Wilkinson Power Divider

The Wilkinson Power Divider is a passive three-port device that can divide the input signal evenly between the two output ports while keeping a matched condition on all three ports. The Wilkinson power divider is a common component, broadly used in microwave and communications systems. The Scattering matrix of the Wilkinson power divider (Pozar, 2012) is given by:

$$[S] = \frac{-j}{\sqrt{2}} \begin{bmatrix} 0 & 1 & 1 \\ 1 & 0 & 0 \\ 1 & 0 & 0 \end{bmatrix} \tag{2.1}$$

The basic schematic of the Wilkinson power divider (Pozar, 2012) having port 1 as input and ports 2 and 3 as outputs is shown in Figure 2.1. The input port is connected to output ports by quarter wave lines of characteristic impedance $\sqrt{2}.Z_0$. The two output ports are connected by a 100 Ω resistor, which provides isolation between the two outputs.

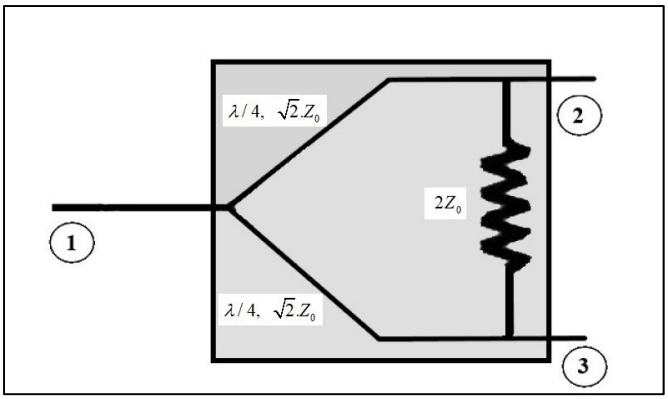

Figure 2.1 The Wilkinson power divider

2.2 Ring Power divider

In order to enhance the traditional Wilkinson divider, it has been modified by extending the quarter-wave transformers by half wave transmission lines to better integrate the 100 Ω isolation resistance, thereby reducing the coupling between the quarter wave transformers. These new lines transform the layout of the circuit into a ring structure of electrical length 1.5 λ_g (Hammou et al., 2011) as shown in Figure 2.2 where a new power divider has been designed operating at 61 GHz for wireless communications.

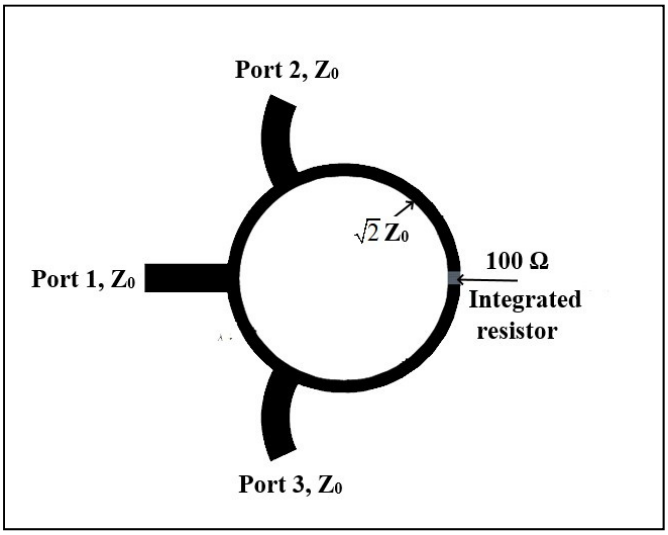

Figure 2.2 The Ring power divider

The Scattering matrix of the Ring power divider is similar to that of the Wilkinson power divider. In order to further enhance the performance of this structure in a wideband operational bandwidth, a modified ring power divider (Barakat et al., 2020) consisting of the same circular structure is proposed with the addition of a stepped impedance resonator (SIR) to the old structure. The modified ring power divider structure will be studied in detail in the next chapter.

2.3 Quadrature hybrid coupler

A quadrature hybrid coupler is a passive device widely used in microwave circuits which splits the input power evenly between the two output ports with a 90º phase difference between them while maintaining high isolation between the input ports. It is generally used in circuits requiring an equal division of power into the output ports with 90º phase shift between them. This device is reciprocal because any port can act as an input, and it still operates in the same manner. The 90˚hybrid can be implemented in low-cost planar microstrip single layer technology which makes it the best choice to include in the proposed six-port measurement system. In general, port 1 is the input port, port 2 and port 3 the through and coupled ports and port 4 is the isolated port. The basic configuration of the quadrature hybrid used as a combiner is shown in Figure 2.3. In this diagram, the two input signals a_1 and a_2 are combined to give the two output signals shown below with 90-degree phase shift between them (Pozar, 2012).

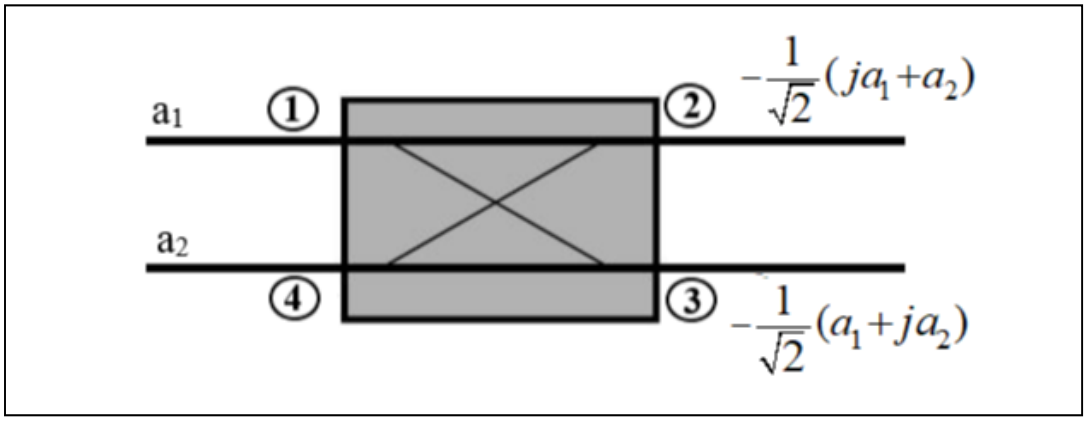

Figure 2.3 The 90-degree hybrid coupler used as combiner

The Scattering matrix of the 90-degree hybrid coupler is given by (Pozar, 2012):

$$[S]=\frac{-1}{\sqrt{2}}\begin{bmatrix}0 & j & 1 & 0\\ j & 0 & 0 & 1\\ 1 & 0 & 0 & j\\ 0 & 1 & j & 0\end{bmatrix} \tag{2.2}$$

The basic layout of the 90° hybrid coupler is shown in Figure 2.4 (Pozar, 2012). This coupler is made of four sections of quarter wavelength microstrip transmission lines. Two sections have a characteristic impedance of Z_0, and the other two have an impedance of $Z_0/\sqrt{2}$. Each port is fed with a transmission line of impedance Z_0.

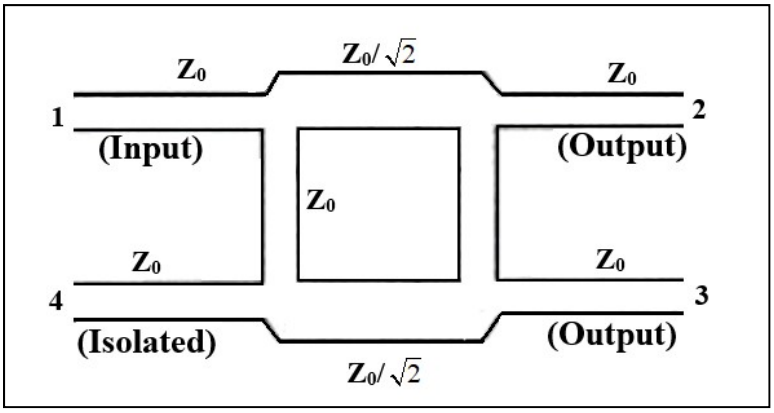

Figure 2.4 Layout of the 90-degree coupler

2.4 The Six-port reflectometer

The block diagram of a traditional six-port reflectometer as introduced by Engen (1977) is shown in Figure 2-5. The microwave source is usually connected to port 1, and the DUT is connected to port 2. The four output ports are normally connected to power meters P_3 to P_6. The incident waves a_i and reflected waves b_i of the six-port circuit are related together with six equations (Fadhel M Ghannouchi & Mohammadi, 2009) by:

$$b_i=\sum_{j=1}^{6}S_{ij}a_j \quad \ldots\ldots\ldots for\ i=1,\ldots,6 \tag{2.3}$$

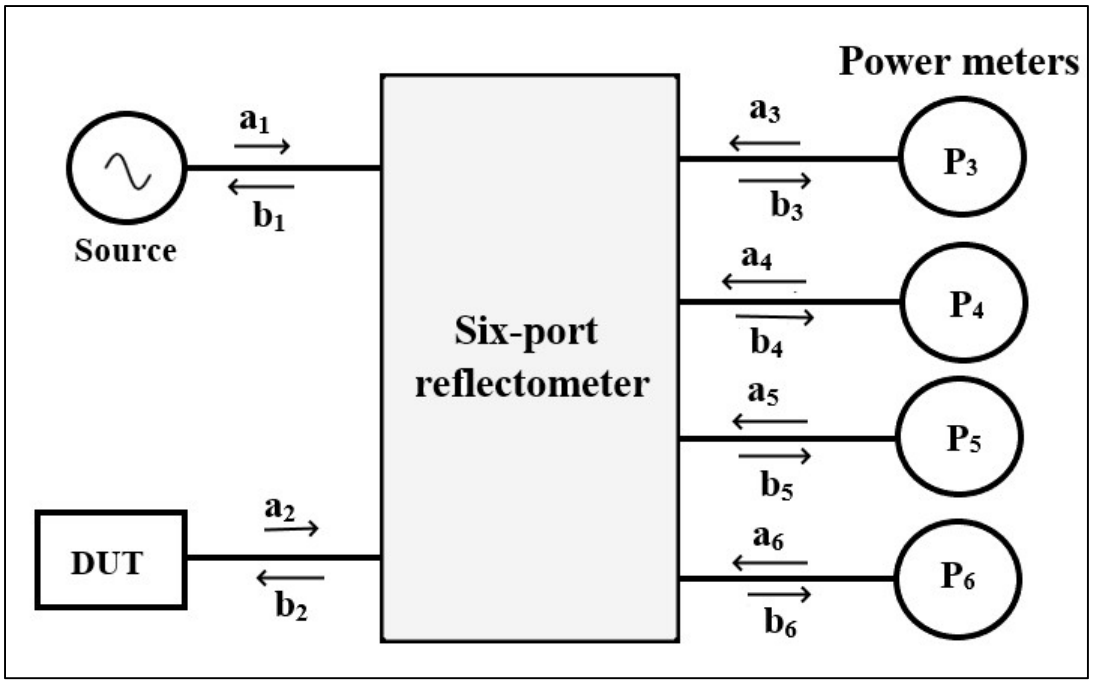

Figure 2.5 The six-port reflectometer block diagram

In addition, since ports 3 to 6 are connected to power meters P_3 to P_6, the incident and reflected waves at the output ports can be written as:

$$a_i = b_i \Gamma_i \quad \ldots\ldots\ldots for\ i=3,\ldots,6 \tag{2.4}$$

Where Γ_i is the complex reflection coefficient of the connected power detector at port i.

The waves arriving at the power detectors can be written as:

$$b_i = A_i\, a_2 + B_i\, b_2 \quad ; \ldots . for\ i=3,\ldots,6 \tag{2.5}$$

Where A_i and B_i are complex quantities specific to the reflectometer. Therefore, the four output waves can be written as follows:

$$b_3 = A_3 a_2 + B_3 b_2 \tag{2.6}$$

$$b_4 = A_4 a_2 + B_4 b_2 \tag{2.7}$$

$$b_5 = A_5 a_2 + B_5 b_2 \tag{2.8}$$

$$b_6 = A_6 a_2 + B_6 b_2 \tag{2.9}$$

The four output power readings (P_3 to P_6) from the power meters are used to get the unknown reflection coefficient of the DUT:

$$P_3 = |b_3|^2 = |A_3 a_2 + B_3 b_2|^2 = |b_2|^2 |A_3^2| \left| \Gamma + \frac{B_3}{A_3} \right|^2 \tag{2.10}$$

$$P_4 = |b_4|^2 = |A_4 a_2 + B_4 b_2|^2 = |b_2|^2 |A_4|^2 \left| \Gamma + \frac{B_4}{A_4} \right|^2 \tag{2.11}$$

$$P_5 = |b_5|^2 = |A_5 a_2 + B_5 b_2|^2 = |b_2|^2 |A_5|^2 \left| \Gamma + \frac{B_5}{A_5} \right|^2 \tag{2.12}$$

$$P_6 = |b_6|^2 = |A_6 a_2 + B_6 b_2|^2 \tag{2.13}$$

Where $A_3, \ldots, B_6$ are eight complex constants to be identified by appropriate calibration procedures, and $\Gamma = a_2 / b_2$ is the reflection coefficient to be measured.

The six-port reflectometer is normally designed such as the output of one port is proportional to $|b_2|^2$ and thus used as a reference detector. Choosing detector 6 as reference, the first design objective will be for $A_6 = 0$, so that:

$$P_6 = |b_2|^2 |B_6|^2 \tag{2.14}$$

Then, by normalizing the detected powers P_3, P_4, and P_5 to that detected at port 6, we can write:

$$p_3 = P_3 / P_6 = \left| \frac{A_3}{B_6} \right|^2 |\Gamma - q_3|^2 \tag{2.15}$$

$$p_4 = P_4 / P_6 = \left| \frac{A_4}{B_6} \right|^2 |\Gamma - q_4|^2 \tag{2.16}$$

$$p_5 = P_5 / P_6 = \left|\frac{A_5}{B_6}\right|^2 \left|\Gamma - q_5\right|^2 \tag{2.17}$$

Where $q_3 = -\frac{B_3}{A_3}, q_4 = -\frac{B_4}{A_4}$, $and\ q_5 = -\frac{B_5}{A_5}$.

Finally, we can write:

$$\left|\Gamma - q_3\right| = \left|\frac{B_6}{A_3}\right| \sqrt{p_3} \tag{2.18}$$

$$\left|\Gamma - q_4\right| = \left|\frac{B_6}{A_4}\right| \sqrt{p_4} \tag{2.19}$$

$$\left|\Gamma - q_5\right| = \left|\frac{B_6}{A_5}\right| \sqrt{p_5} \tag{2.20}$$

Thus, we can find the reflection coefficient Γ of the DUT as the solution of these three equations, which is the intersection of three circles of centers q_i and of radius proportional to the square root of the detected powers. The centers of these three circles q_i are determined by the six-port characteristics and are independent of the reflection coefficient of the DUT. The magnitudes of q_i points should be at equal distance from the origin and the phase difference between two q_i points should be around 120˚(Engen, 1977). In general, the closer the magnitudes of q_i, and the bigger the difference between the phases of q_i, the higher will be the performance of the reflectometer (X. Xu et al., 2005). In practice, due to measurement errors and detector noises, the circles do not intersect in a point, and their intersection will comprise a triangular area, where Γ will be included. In such a case, the solution will be the intersection of the common chords, or radial centers (Engen, 1997). The determination of Γ can be also done by the intersection of only two circles, which would correspond to a five-port network (Engen, 1977). In such a case, there are two possible solutions for Γ, as the two circles intersect in a pair of points. When the device undertest (DUT) is a passive device, Γ should fall within the unit circle. Therefore, one of the two points is outside the unit circle, and we can easily choose between the two solutions.

From equation (2.3), and for the ports 3 to 6 matched to the power detectors which means there is no reflection from the power meter ($a_3 = a_4 = a_5 = a_6 = 0$), we can write (Fadhel M Ghannouchi & Mohammadi, 2009):

$$b_i = S_{i1}a_1 + S_{i2}a_2 \tag{2.21}$$

For i=2:

$$b_2 = S_{21}a_1 + S_{22}a_2 \tag{2.22}$$

$a_1 = \frac{b_2 - S_{22}a_2}{S_{21}}$; hence:

$$b_i = [S_{i2} - \frac{S_{i1}S_{22}}{S_{21}}]\, a_2 + \frac{S_{i1}}{S_{21}}b_2 \tag{2.23}$$

Comparing (2.23) with (2.5), we can write:

$$A_i = S_{i2} - \frac{S_{i1}S_{22}}{S_{21}} \tag{2.24}$$

$$B_i = \frac{S_{i1}}{S_{21}} \tag{2.25}$$

Thus,

$$q_i = -\frac{B_i}{A_i} = \frac{S_{i1}}{S_{i1}S_{22} - S_{i2}S_{21}} \qquad ; \text{i=3,...,6} \tag{2.26}$$

Therefore, the q_i-points of the six-port reflectometer can be directly calculated from the six-port scattering parameters by using (2.26).

2.5 The six-port correlator

The six-port junction used as correlator allows the measurement of the complex ratio of two microwave signals and will be used as the heart of the measurement system which will be built and described through this thesis. The six-port correlator has two input ports which are fed by microwave signals a_1 and a_2 and four output ports (P_3 to P_6) which are terminated by 4 power detectors. The unused port is connected to a matched load. The main advantage of using the complex six-port correlator is that we eliminate the need to use a reference power detector as in the case of the six-port reflectometer. In this case, all four power detectors are used to obtain four q_i points at equal distance from the origin, having a magnitude of 1 and a phase difference of 90˚ between them. As shown in Figure 2.6, the six-port correlator is built with one Wilkinson power divider and three 90-degree hybrids. The output waves b_3 to b_6 at ports 3 to port 6 which will arrive at the power detectors can be expressed as:

$$b_3 = -\frac{1}{2}(a_1 - ja_2) \tag{2.27}$$

$$b_4 = -\frac{1}{2}(-ja_1 + a_2) \tag{2.28}$$

$$b_5 = \frac{j}{2}(a_1 + a_2) \tag{2.29}$$

$$b_6 = \frac{1}{2}(-a_1 + a_2) \tag{2.30}$$

Therefore, the 6x6 S-matrix of the proposed six-port junction can be written as:

$$[S] = \frac{1}{2}\begin{bmatrix} 0 & 0 & -1 & j & j & -1 \\ 0 & 0 & j & -1 & j & +1 \\ -1 & j & 0 & 0 & 0 & 0 \\ j & -1 & 0 & 0 & 0 & 0 \\ j & j & 0 & 0 & 0 & 0 \\ -1 & +1 & 0 & 0 & 0 & 0 \end{bmatrix} \tag{2.31}$$

Hence, the S-parameters between the inputs and the 4 outputs of the six-port junction represent a theoretical value of - 6 dB.

Finally, we present the analysis and the design equations of the proposed six-port correlator in a similar manner to that done in the design of the six-port receiver reported in (Hammou et al., 2016) to find the I and Q components and also in the design of a six-port correlator consisting of four 90˚ hybrid couplers and a phase shifter (Haddadi, 2007) where an equivalent analysis is applied to the proposed six-port correlator in order to derive an analytical solution for the reflection coefficient.

Let the two microwave signals $a_1(t)$ and $a_2(t)$ at the inputs of the correlator in Figure 2.6 have amplitudes of A_1 and A_2 respectively and a phase shift of ϕ between them (Haddadi, 2007):

$$a_1(t) = A_1 e^{jwt} \tag{2.32}$$

$$a_2(t) = A_2 e^{j(wt+\phi)} \tag{2.33}$$

The waves $b_3(t)$ and $b_4(t)$ arriving at power detectors 3 and 4 at the output of the first hybrid coupler can be expressed as:

$$b_3(t) = -\frac{1}{2}(A_1 e^{jwt} + A_2 e^{j(wt+\phi-\pi/2)}) \tag{2.34}$$

$$b_4(t) = -\frac{1}{2}(A_1 e^{j(wt-\pi/2)} + A_2 e^{j(wt+\phi)}) \tag{2.35}$$

The detected powers P_3 and P_4 can then be determined as:

$$P_3 = Re\left(b_3(t)\ b_3^*(t)\right) = \frac{1}{4}\left(A_1^2 + A_2^2 + 2A_1A_2 sin\phi\right) \tag{2.36}$$

$$P_4 = Re\left(b_4(t)\ b_4^*(t)\right) = \frac{1}{4}\left(A_1^2 + A_2^2 - 2A_1A_2 sin\phi\right) \tag{2.37}$$

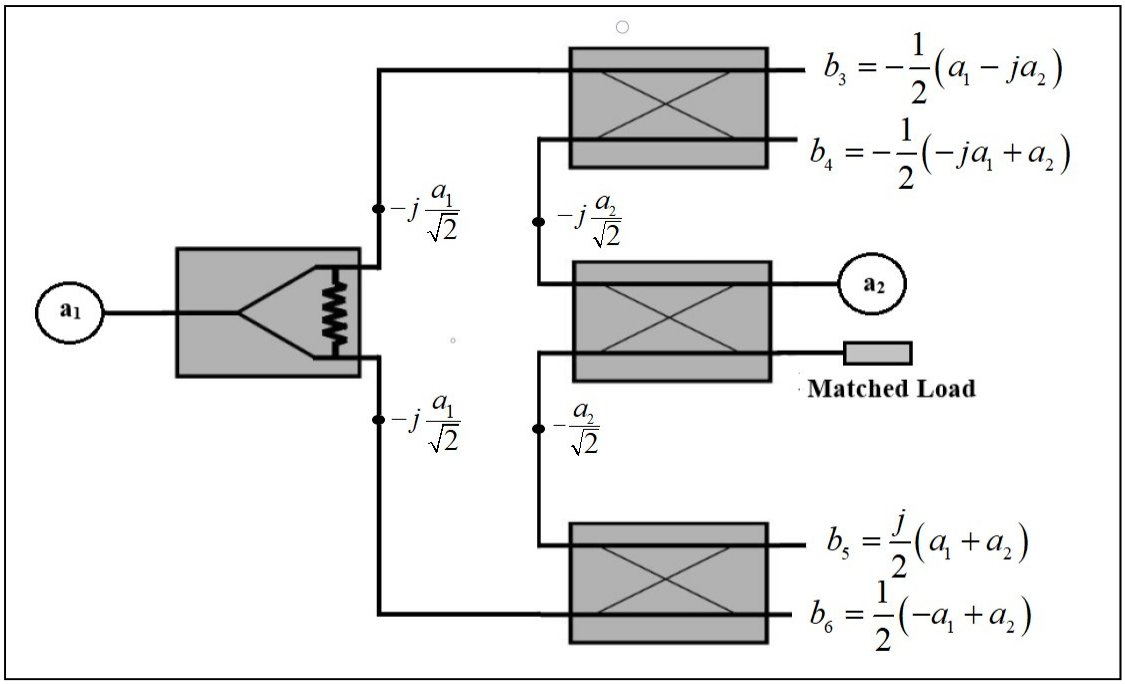

Figure 2.6 The six-port correlator circuit

Let's define the complex ratio Γ of the two signals $a_1(t)$ and $a_2(t)$ as:

$$\Gamma = \frac{A_2}{A_1} e^{j\phi} = I + j\,Q \tag{2.38}$$

Then, equations (2.36) and (2.37) can be written as:

$$P_3 = \frac{A_1^2}{4}(1 + |\Gamma|^2 + 2|\Gamma| sin\phi) \tag{2.39}$$

$$P_4 = \frac{A_1^2}{4}(1 + |\Gamma|^2 - 2|\Gamma| sin\phi) \tag{2.40}$$

Which can be written as:

$$\frac{4}{A_1^2} P_3 = \left(1 + I^2 + Q^2 + 2Q\right) = I^2 + (Q+1)^2 \tag{2.41}$$

$$\frac{4}{A_1^2} P_4 = \left(1 + I^2 + Q^2 - 2Q\right) = I^2 + (Q-1)^2 \tag{2.42}$$

It is clear that these are the equations of circles in the Γ plane having centers q_3= -j and q_4= +j.

In addition, the waves $b_5(t)$ and $b_6(t)$ arriving at power detectors 5 and 6 at the output of the third hybrid coupler can be expressed as:

$$b_5(t) = \frac{1}{2}(A_1 e^{j(wt+\pi/2)} + A_2 e^{j(wt+\phi+\pi/2)}) \tag{2.43}$$

$$b_6(t) = \frac{1}{2}(A_1 e^{j(wt+\pi)} + A_2 e^{j(wt+\phi)}) \tag{2.44}$$

In a similar way, we can easily demonstrate that the detected output powers P_5 and P_6 can be determined as:

$$P_5 = Re\left(b_5(t)\ b_5^*(t)\right) = \frac{1}{4}\left(A_1^2 + A_2^2 + 2A_1A_2\cos\phi\right) \tag{2.45}$$

$$P_6 = Re\left(b_6(t)\ b_6^*(t)\right) = \frac{1}{4}\left(A_1^2 + A_2^2 - 2A_1A_2\cos\phi\right) \tag{2.46}$$

This can be written as:

$$\frac{4}{A_1^2}P_5 = (I+1)^2 + Q^2 \tag{2.47}$$

$$\frac{4}{A_1^2}P_6 = (I-1)^2 + Q^2 \tag{2.48}$$

Obviously, these are the equations of circles in the Γ plane having centers $q_5 = -1$ and $q_6 = +1$.

It can be noted that the four detected output signals P_3 to P_6 are periodic of 2π and have the same amplitude and a phase shift of 90 degrees when the phase ϕ between the input signals is swept in a 0 to 360 degrees range.

Now, let's determine how to deduce the complex reflection coefficient Γ from the reading of the power detector outputs which can be used later to determine the reflection coefficient S_{11} and the transmission coefficient S_{21} of the six-port network analyzer.

Let's take the difference between the two equations (2.41) and (2.42), we will have:

$$\frac{4}{A_1^2}(P_3 - P_4) = (Q+1)^2 - (Q-1)^2 = 4Q \tag{2.49}$$

So that, we can deduce:

$$Q = \left(1/A_1^2\right)(P_3 - P_4) \tag{2.50}$$

In a similar manner, we can take the difference between the two equations (2.47) and (2.48), we will have:

$$\frac{4}{A_1^2}(P_5 - P_6) = (I+1)^2 - (I-1)^2 = 4I \tag{2.51}$$

This implies:

$$I = \left(1/A_1^2\right)(P_5 - P_6) \tag{2.52}$$

And the complex coefficient Γ can thus be written as:

$$\Gamma = I + jQ = \left(1/A_1^2\right)\left[(P_5 - P_6) + j(P_3 - P_4)\right] \tag{2.53}$$

Γ is equal to S_{11} or S_{21} depending on which correlator we are choosing; this will be explained in the next section.

2.6 The dual six-port network analyzer

The dual six-port network analyzer was first introduced in (Juroshek & Hoer, 1984) to measure the network parameters of a two-port system. Figure 2.7 shows the implementation of the proposed low cost 2-port vector network analyzer based on six port theory. The designed system consists of a source, one 90˚ hybrid coupler and one modified ring power divider and two six-port junctions. The output ports of the six-port junctions are terminated by diode detectors. “The advantages of using diodes are the simplicity of the system and the lower power requirements” (Juroshek& Hoer, 1984). The six-port junctions used as correlators in this configuration are used to measure the reflection coefficient S_{11} and the transmission coefficient S_{21} of a device under test (DUT). The reflection coefficient S_{11} can be determined from the four output power readings P_3...P_6 of the first six-port junction (Six-port junction 1). So, by reading the power of the output ports connected to the Schottky diodes, we can easily find the reflection coefficient of the device under test (DUT) by using equation (2.53).

In a similar manner, we can determine the transmission coefficient S_{21} from the 4 output power readings P_3', P_4', P_5' and P_6' of the second six-port junction (six-port junction 2) using the same equation. The output powers are measured using Schottky diodes which present a quadratic response for detected powers from about -15 dBm to 10 dBm in the operational frequency range with a maximum input power of 20 dB. Eventually, a simplified calibration method is used to get accurate measurement results and to reduce system imperfections. As will be shown later in this thesis, the system results after calibration show low deviations compared to expected theoretical results in the operating frequency range. As mentioned before, this circuit combines low cost, compactness and small size compared to a conventional network analyzer, which makes it a very promising device for out of laboratory applications such as applications in the biomedical non-destructive industry.

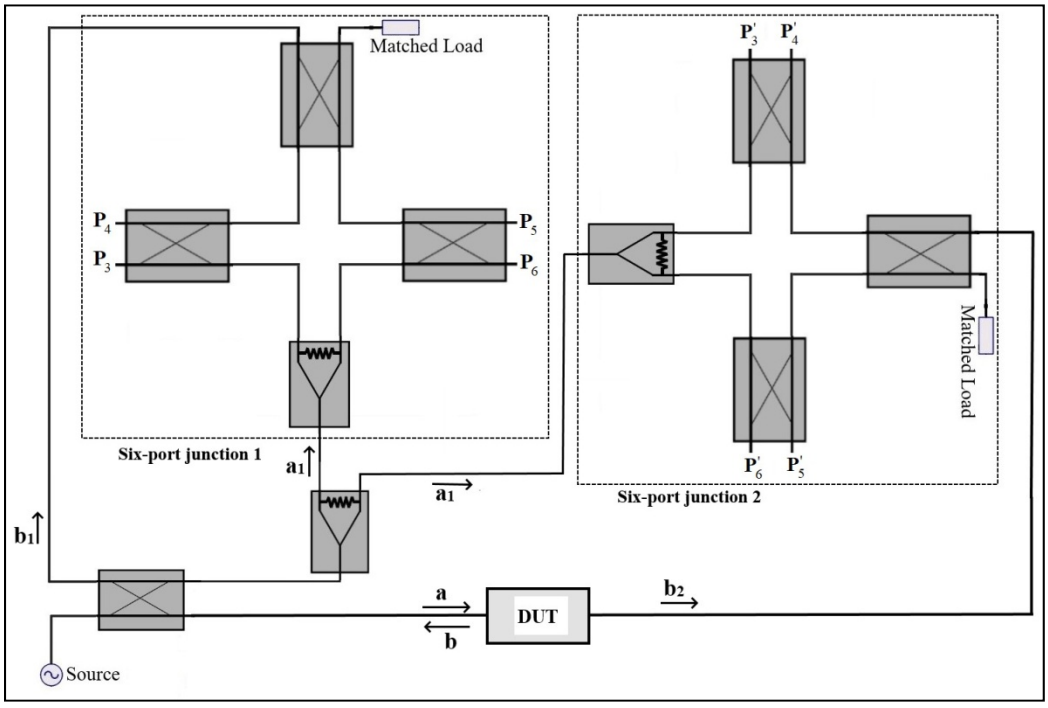

Figure 2.7 The proposed dual six-port network analyzer

CHAPTER 3

DESIGN OF WIDEBAND SIX-PORT COMPONENTS

3.1 Introduction

Power dividers and hybrid couplers are extremely useful microwave components whose principal function is to equally split the incident signal between the two outputs, with a certain required phase difference, while maintaining good matching at all ports and isolation between the output ports. These two components are the main components used in the proposed six-port architecture. In this chapter, a detailed analysis of these two components is presented in order to increase their operational bandwidth and performance since this will affect the overall six-port circuit performance.

3.2 Modified ring power divider

Power dividers are key components in the field of microwave engineering which are used in different applications including measurement systems as well as antenna distribution circuits, communication and radar systems. Many efforts have been recently made to design wideband power dividers by opportunely modifying the classical Wilkinson structure (Wilkinson, 1960). The most usual way to make this device wideband is by adding two or more sections to the conventional structure (Iqbal et al., 2016; Mishra et al., 2014; Ou & Chu, 2008; Y. Sun & Freundorfer, 2004) or by adding open-circuited stubs (Nadera et al., 2018; Chang et al., 2017; Pazoki et al., 2007). However, these structures add more circuit area to the conventional design. Other works, reported in the literature, have proposed broadband Wilkinson power dividers such as in (Nor et al., 2013) where double-sided parallel-strip line technique using similar structure at both the top and bottom layers with three isolation resistors at both layers was proposed. In (Ahmed & Abbosh, 2015), the proposed power divider using microstrip-to-slotline coupled structure and a top and bottom layer showed good performance over a 68.6 % bandwidth from 2.3 to 4.7 GHz. Another broadband power divider achieving good in-band responses across a 62 % fractional bandwidth was proposed in (S. S. Gao et al., 2013) by

arranging two open-circuited stubs and three coupled-line sections around the ring resonator. Moreover, a power divider composed of a pair of High-Low line (HLL) loaded at the outputs of the conventional Wilkinson power divider was proposed in (M. Kumar et al., 2018) to improve the performances. The equal power division is achieved with fractional bandwidth of 65% for 3.15 ± 0.2 dB. However, these power dividers require complex design configuration due to the use of different layers or coupled-line sections which makes the fabrication process more complicated. A compact ring power divider has been proposed in (Hammou et al., 2011). It introduced a circular layout with the addition of two half-wave transmission lines to connect the 100 Ω isolation resistor, converting the layout in a ring circuit of 1.5 λg length. The corresponding electric lengths θ_1 and $\theta 2$ are $\pi/2$ and π, respectively, and the normalized ring characteristic impedance z_{01} (which is equal to z_{02}) was found to be $\sqrt{2}$ (Hammou et al., 2011). The circuit has been rebuilt to operate at the center frequency of 3.12 GHz, as shown in Figure 3.1.

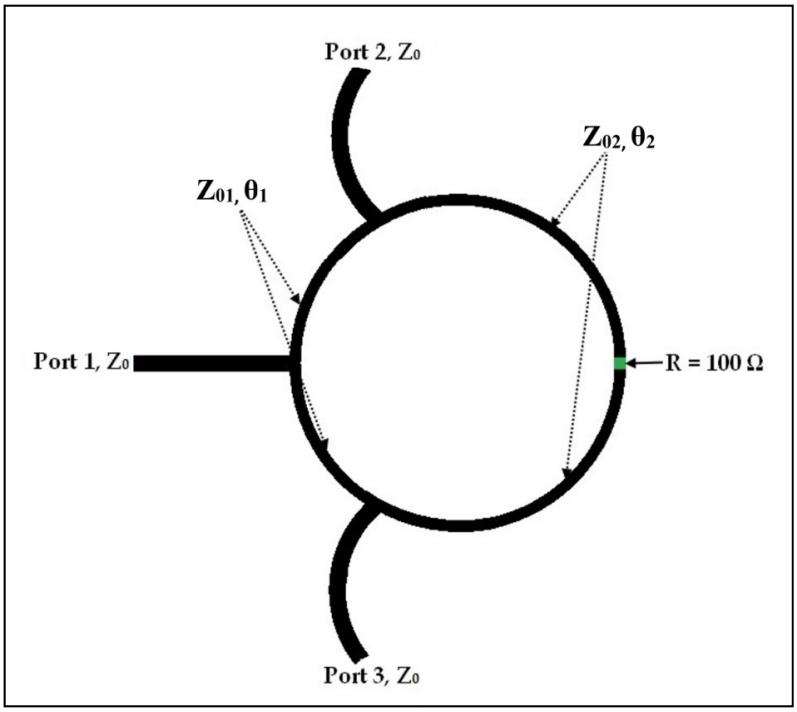

Figure 3.1 Layout of the conventional ring power divider

This circuit is offering very good performance over a wide bandwidth compared to the traditional Wilkinson power divider. In addition, this design had shown more stability and larger bandwidth than previous implementations among valid solutions. Furthermore, this circuit has a size reduction of about 20 % compared to the classical Wilkinson power divider and improved performances in terms of RF input/output matching and isolation between the output RF ports (Hammou et al., 2017). In order to improve its operational bandwidth, a modified ring power divider is proposed to cover the frequency bandwidth of 1.7 GHz to 4.6 GHz by adding an SIR to the old structure. The circuit in Figure 3.2 represents the layout of the proposed ring power divider. As it will be seen in the next sections, the simulation results show that the fractional bandwidth has a significant increase of 27.2 % compared to the old structure and this without affecting the circuit size since the added element is inside the ring structure.

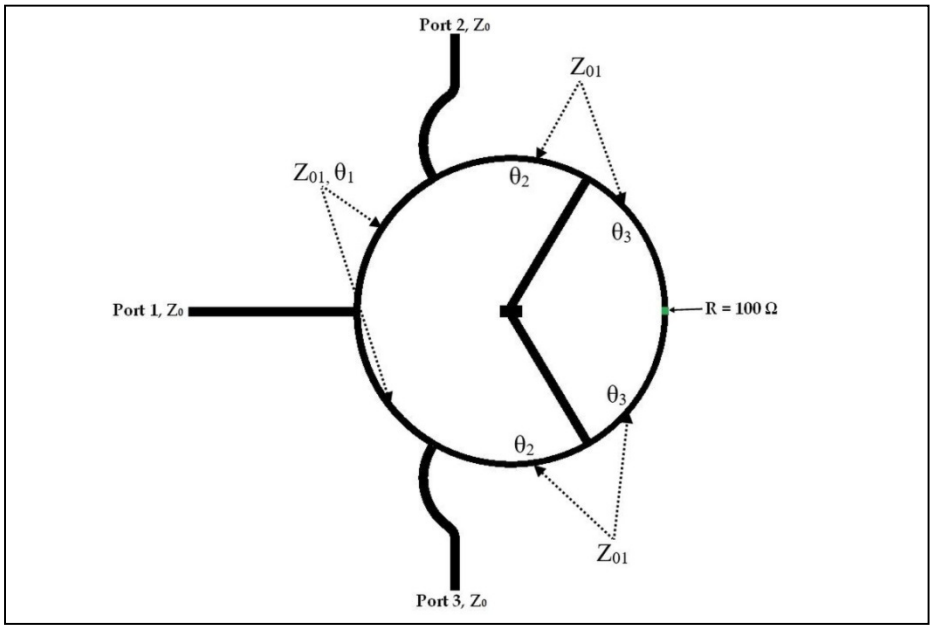

Figure 3.2 Layout of the proposed ring power divider

For this structure, a detailed even-odd mode analysis of the proposed ring power divider has been performed. To validate the theoretical analysis and simulations, a prototype is fabricated on a single layer substrate. The experimental results show that the proposed circuit is

broadband with a high factor amplitude balance over the considered bandwidth. The proposed ring power divider has the advantages of compact size and ease of fabrication which makes it very suitable for many wideband microwave applications.

3.2.1 Design and Simulations

The circuit diagram of the proposed wideband ring power divider is shown in Figure 3.3. It consists of six transmission lines of characteristic impedances (Z_{01}, Z_{02}, and Z_{03}), a Stepped-Impedance Resonator (SIR), and an isolation resistor R = 100 Ω.

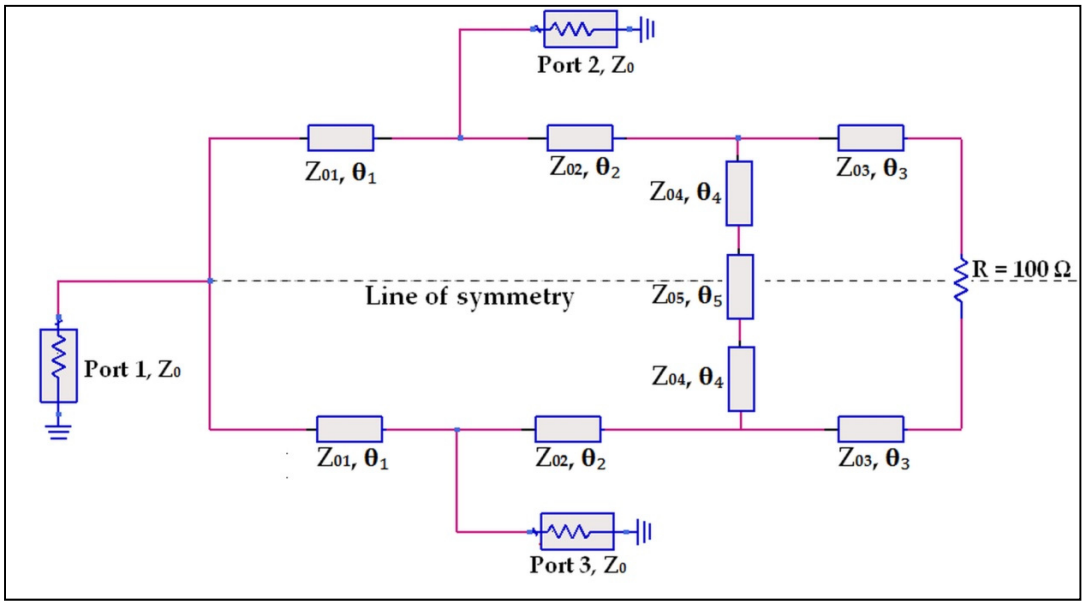

Figure 3.3 Proposed structure of the modified ring power divider

Microstrip resonators have been widely used in the design of microwave filters with wide stopband characteristics (Boutejdar et al., 2019). In addition, Stepped-impedance resonators (SIRs) have been found advantageous in the design of microstrip band-pass filters with good stopband performance (Hung et al., 2007; Kuo & Shih, 2003; Murmu et al., 2017). A typical SIR is used to modify the structure of the ring power divider and is built by joining three microstrip-line sections of different characteristic impedances Z_{04} and Z_{05} as shown in Figure 3.4. The microstrip line at the center has a characteristic impedance of Z_{05} with an electrical

length of θ_5 whereas the identical lines at the two sides both have a characteristic impedance of Z_{04} with an electrical length of θ_4.

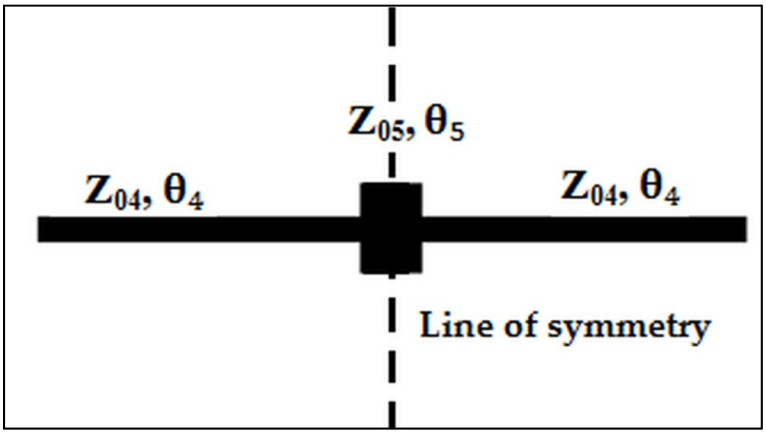

Figure 3.4 Stepped impedance resonator (SIR) used structure

As described in (Hung et al., 2007), the conditions for determining the resonance frequencies of a typical stepped impedance resonator (SIR) are given as:

$$K = \tan(\theta_5 / 2).\tan\theta_4 \ldots\ldots (for\ odd\ mode) \quad (3.1)$$

$$K\tan(\theta_5 / 2) = -\tan\theta_4 \ldots\ldots (for\ even\ mode) \quad (3.2)$$

Where K = Z_{04} / Z_{05} is the impedance ratio of the SIR.

Let's define the stepped percentage α of the SIR as $\alpha = 2\theta_4 / \theta_t$ where $\theta_t = (2\theta_4+\theta_5)$ is the total length of the SIR. Then, equations (3.1) and (3.2) can be expressed as:

$$K.\cot\left(\frac{\alpha.\theta_t}{2}\right) = \tan(\frac{(1-\alpha).\theta_t}{2}) \ldots..(for\ odd\ mode) \quad (3.3)$$

$$K.\cot\left(\frac{\alpha.\theta_t}{2}\right) = -\cot(\frac{(1-\alpha).\theta_t}{2}) \ldots..(for\ even\ mode) \quad (3.4)$$

Figure 3.5 shows the resonant electric length of the first spurious response mode with different impedance ratios K= 1, 1.5,2,3 as a parameter. “By properly choosing different combinations of α and K values, the first two resonant modes can be combined together to create a wide passband” (Hung et al., 2007).

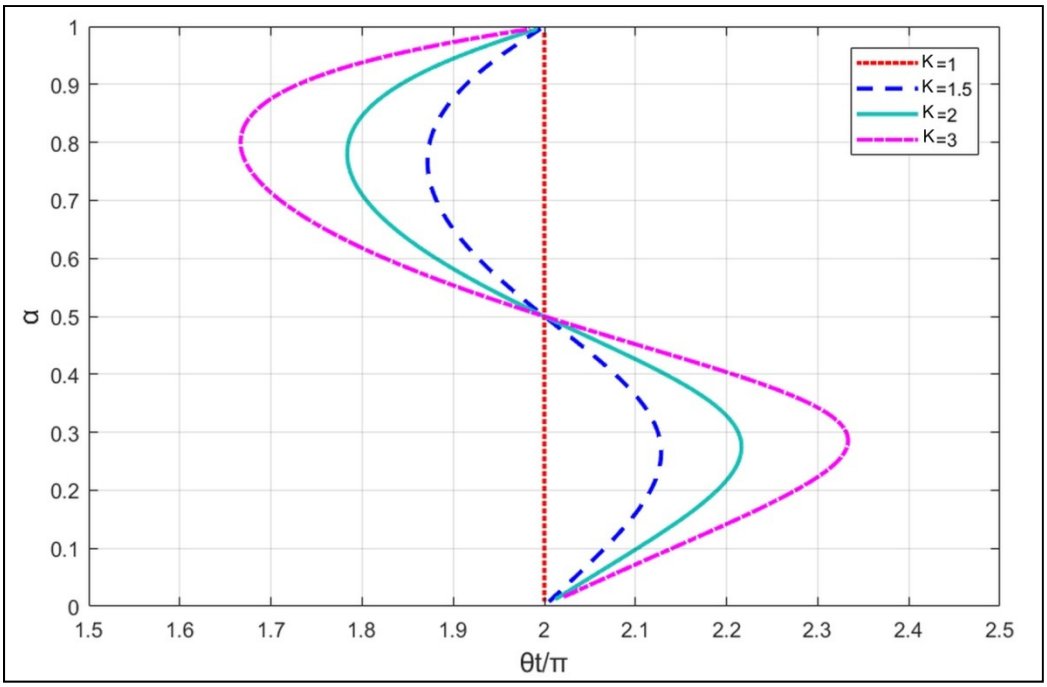

Figure 3.5 Resonant electric length θ_t versus stepped percentage α with different impedance ratios K

The structure of the proposed ring power divider is symmetric; thus, we can apply the even-odd mode analysis (Pozar, 2012) in order to analyze the divider parameters. In this study, the known parameters as defined in the previous analysis (Hammou et al., 2011) are the normalized characteristic impedances $z_{01} = z_{02} = z_{03} = z_{04} = \sqrt{2}$; and $\theta_1 = \pi/2$ and $(\theta_2 + \theta_3) = \pi$. The following analysis is performed in order to find the main characteristics of the added element to the old ring structure.

3.2.1.1 Even -mode analysis

In the even mode, ports 2 and 3 are excited by signals of the same magnitude and phase, which introduces a virtual open-circuit along the line of symmetry. By introducing the same voltages at the plane of symmetry, there is no current flow through the line of symmetry and the presence of open circuits allows for eliminating the resistance R in the equivalent circuit as shown in Figure 3.6. The calculation of the input impedance for the even-mode Z_{ine} viewed from port 2 corresponds to the equivalent impedances Z_{eq1e} and Z_{eq2e} connected in parallel.

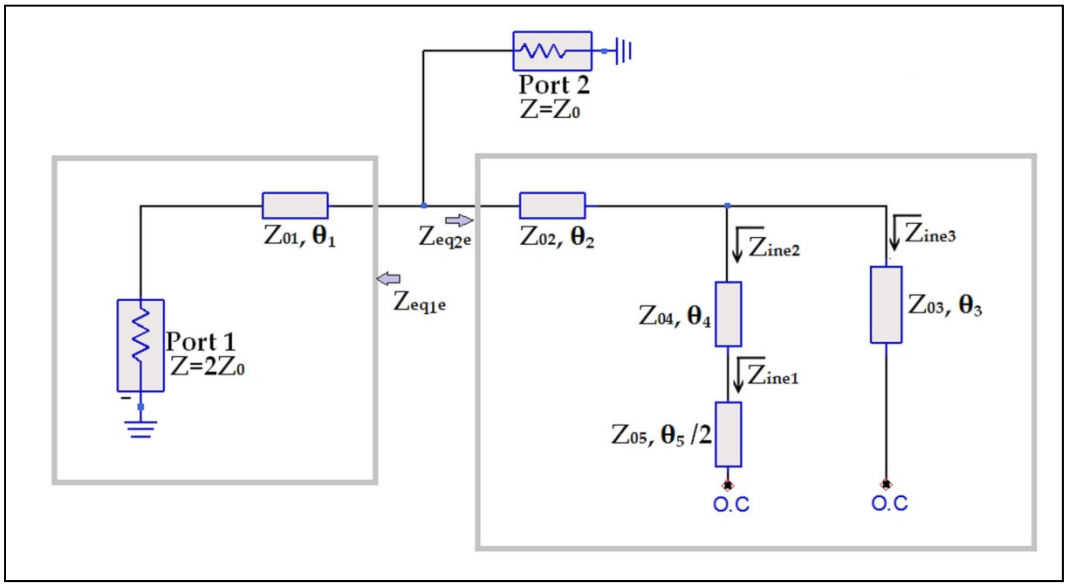

Figure 3.6 Equivalent circuit of the proposed ring divider for odd-mode

From the transmission line theory, we can easily calculate Z_{eq1e} as the input impedance of a quarter-wave transmission line terminated by $2Z_0$:

$$Z_{eq1e} = \frac{Z_{01}^{\ 2}}{2Z_0} = \frac{2Z_0^{\ 2}}{2Z_0} = Z_0 \tag{3.5}$$

Referring to Figure 3.6, the input impedances Z_{ine1} and Z_{ine2} can be expressed as follows

$$Z_{ine1} = -jZ_{05}cot\left(\frac{\theta_5}{2}\right) \tag{3.6}$$

$$Z_{ine2} = \frac{Z_{04}\left(Z_{ine1} + \mathrm{j} Z_{04}\, tan\theta_4\right)}{\left(Z_{04} + jZ_{ine1}\, tan\,\theta_4\right)} \tag{3.7}$$

$$Z_{ine2} = \frac{-j\,Z_{04}\left(Z_{05}\, cot\left(\theta_5 / 2\right) - Z_{04}\, tan\theta_4\right)}{Z_{04} + Z_{05}\ \cot\left(\theta_5/2\right) tan\,\theta_4} \tag{3.8}$$

In a similar way, the admittance Y_{ine3} can be expressed as the input admittance of an open-circuited transmission line.

$$Y_{ine3} = \frac{1}{Z_{ine3}} = j\,Y_{03} tan\,\theta_3 \tag{3.9}$$

Let Z_X be the parallel combination of these impedances Z_{ine2} and Z_{ine3}, then the equivalent admittance Y_X can be written as:

$$Y_X = Y_{ine3} + Y_{ine2} = j\left[Y_{03} tan\,\theta_3 + Y_{04} \frac{\left(Z_{04} + Z_{05}\ \cot\left(\theta_5/2\right) tan\,\theta_4\right)}{\left(Z_{05}\, cot\left(\theta_5 / 2\right) - Z_{04}\, tan\theta_4\right)} \right] \tag{3.10}$$

The equivalent impedance Z_{eq2e} can be expressed as the input impedance of a transmission line terminated by Z_X:

$$Z_{eq2e} = \frac{Z_{02}\left(Z_X + \mathrm{j} Z_{02}\, tan\theta_2\right)}{\left(Z_{02} + j\,Z_X tan\,\theta_2\right)} \tag{3.11}$$

Since the output is matched, the input admittance for the even-mode Y_{ine} viewed from port 2 should be equal to $Y_0 = 1/Z_0$:

$$Y_{ine} = \frac{1}{Z_{eq1e}} + \frac{1}{Z_{eq2e}} = \frac{1}{Z_0} \tag{3.12}$$

By replacing Z_{eq1e} and Z_{eq2e} in (3.12) with their values in (3.5) and (3.11), this will result in

$$\frac{\left(Z_{02} + j\,Z_X tan\,\theta_2\right)}{Z_{02}\left(Z_X + \mathrm{j} Z_{02}\, tan\theta_2\right)} \tag{3.13}$$

This yields to:

$$Y_X = -j\,Y_{02}\,tan\theta_2 \tag{3.14}$$

Comparing (3.10) and (3.14), and since $Y_{03} = Y_{02}$; we have

$$Y_{03}\left(tan\,\theta_3 + tan\,\theta_2\right) + Y_{04}\frac{\left(Z_{04} + Z_{05}\,\cot\left(\theta_5/2\right)\tan\theta_4\right)}{\left(Z_{05}\cot\left(\theta_5/2\right) - Z_{04}\,tan\theta_4\right)} = 0 \tag{3.15}$$

By using the trigonometric identity:

$$\left(tan\,\theta_3 + tan\,\theta_2\right) = \left(\tan\left(\theta_3 + \theta_2\right)\right)\left[1 - tan\theta_3\,tan\theta_2\right] \tag{3.16}$$

Then, since $\left(\theta_3 + \theta_2\right) = \pi$, we can simplify (3.15) to

$$Z_{04} + Z_{05}\,\cot\left(\theta_5/2\right)\tan\theta_4 = 0 \tag{3.17}$$

Which is the second resonance condition given by (3.2) for the even-mode resonance of a typical stepped-impedance resonator (Hung et al., 2007).

3.2.1.2 Odd -mode analysis

In the odd mode, ports 2 and 3 are excited by signals of the same amplitude but of opposite phases. The introduction of equal and contrary voltages implies a diverging current that can be represented by short circuits at the plane of symmetry which has the effect of introducing a virtual ground along the line of symmetry as shown in Figure 3.7. In this analysis, we can choose $\theta_2 = \theta_3 = \pi/2$ in order to have a symmetric design which will reduce the computational complexity. The calculation of the input impedance Z_{ino} viewed from port 2 is simplified and corresponds to Z_{eq1} and Z_{eq2} connected in parallel.

From the transmission line theory, we can easily calculate Z_{eq1} as the input impedance of a short-circuited line.

$$Z_{eq1} = jZ_{01}tan\theta_1 \tag{3.18}$$

Referring to Figure 3.7, the characteristic impedances Z_{ino1} and Z_{ino2} can be expressed as:

$$Z_{ino1} = jZ_{05}tan(\theta_5/2) \tag{3.19}$$

$$Z_{ino2} = Z_{04}\frac{(Z_{ino1} + jZ_{04}\,tan\theta_4)}{(Z_{04} + jZ_{ino1}\,tan\theta_4)} \tag{3.20}$$

$$Z_{ino2} = \frac{jZ_{04}\left(Z_{05}tan(\theta_5/2) + Z_{04}\,tan\theta_4\right)}{\left(Z_{04} - Z_{05}tan(\theta_5/2)tan\theta_4\right)} \tag{3.21}$$

$$Z_{ino3} = \frac{Z_{03}^{\ 2}}{(R/2)} = \frac{Z_{01}^{\ 2}}{(R/2)} \tag{3.22}$$

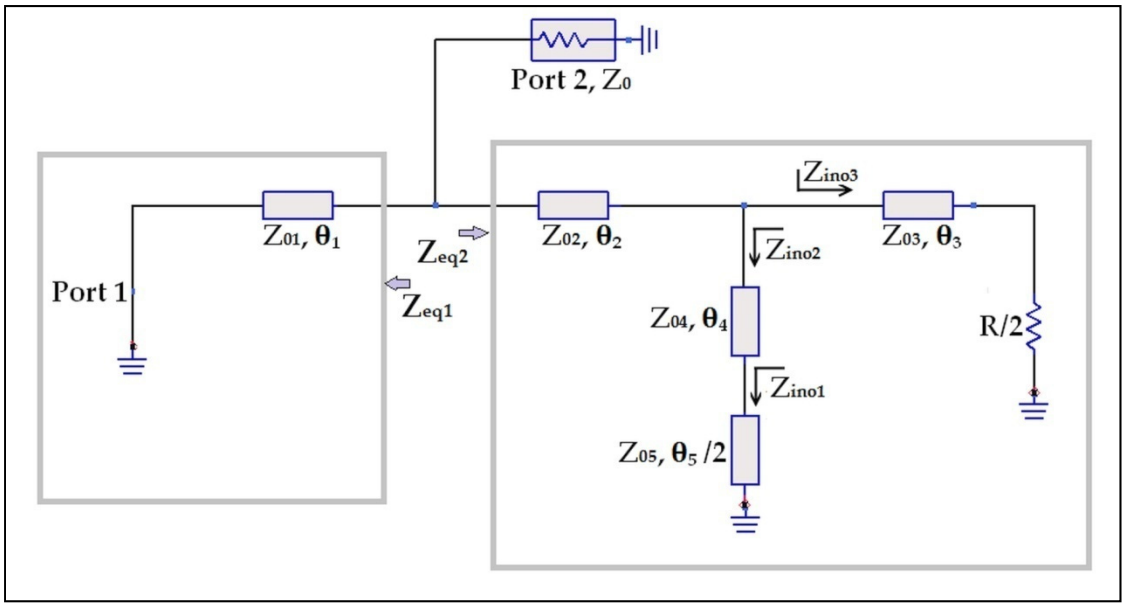

Figure 3.7 Equivalent circuit of the proposed ring divider for even-mode

The input impedance Z_{eq2} can be derived by using the quarter-wave transformer having characteristic impedance $Z_{02} = Z_{01}$, resulting in:

$$Z_{eq2} = Z_{01}{}^{2}\left(Y_{ino3} + Y_{ino2}\right) \tag{3.23}$$

$$Z_{eq2} = \frac{R}{2} - \frac{jZ_{01}^{2}\left(Z_{04} - Z_{05}tan\left(\theta_5/2\right)tan\theta_4\right)}{Z_{04}\left(Z_{04}\,tan\theta_4 + Z_{05}\,tan\left(\theta_5/2\right)\right)} \tag{3.24}$$

The input admittance Y_{ino} seen from port 2 must be matched to $Y_0 = 1/Z_0$.

$$Y_{ino} = \frac{1}{Z_{eq1}} + \frac{1}{Z_{eq2}} \tag{3.25}$$

$$Y_{ino} = \frac{1}{jZ_{01}tan\theta_1} + \frac{1}{\frac{R}{2} - \frac{jZ_{01}^{2}(Z_{04} - Z_{05}tan(\theta_5/2)\,tan\theta_4)}{Z_{04}\,(Z_{04}\,tan\theta_4 + Z_{05}\,tan\,(\theta_5/2))}} = \frac{1}{Z_0} \tag{3.26}$$

Since $\theta_1 = \pi/2$ and $Z_0 = R/2$; then after simplification, the matching condition in equation (3.26) becomes:

$$Z_{04} - Z_{05}tan(\theta_5/2)\,tan\theta_4 = 0 \tag{3.27}$$

Which is the first resonance condition given by (3.1) for the odd-mode resonance of a typical stepped-impedance resonator. Since the two conditions for even and odd mode resonance are satisfied, this proves that the added element is an SIR.

3.2.2 Stepped-impedance resonator design

The SIR is designed with fixed fundamental frequency, but different first spurious mode (f_{s1}) by choosing different combinations of K and α from Figure 3.5 and thereby the dimensions of the SIR can be determined. The impedance ratio K and the stepped percentage α are then tuned using electromagnetic (EM) simulation in order to consider step discontinuities (Hung et al., 2007).

It has been demonstrated that by changing the width ratio w_5/w_4 of the low-impedance (Z_{05}) line to the high-impedance (Z_{04}) line, which result in the modification of K, the position of the

transmission zeros can be adjusted. Furthermore, it is evident that by incrementing the width ratio w_5/w_4, the resonance frequency is changed (Murmu et al., 2017).

A parametric study is conducted to evaluate the effect of SIR's characteristic impedance ratio on the bandwidth of the proposed power divider. Figure 3.8 shows the effect of variation of K on the transmission S-parameter magnitude of the proposed power divider.

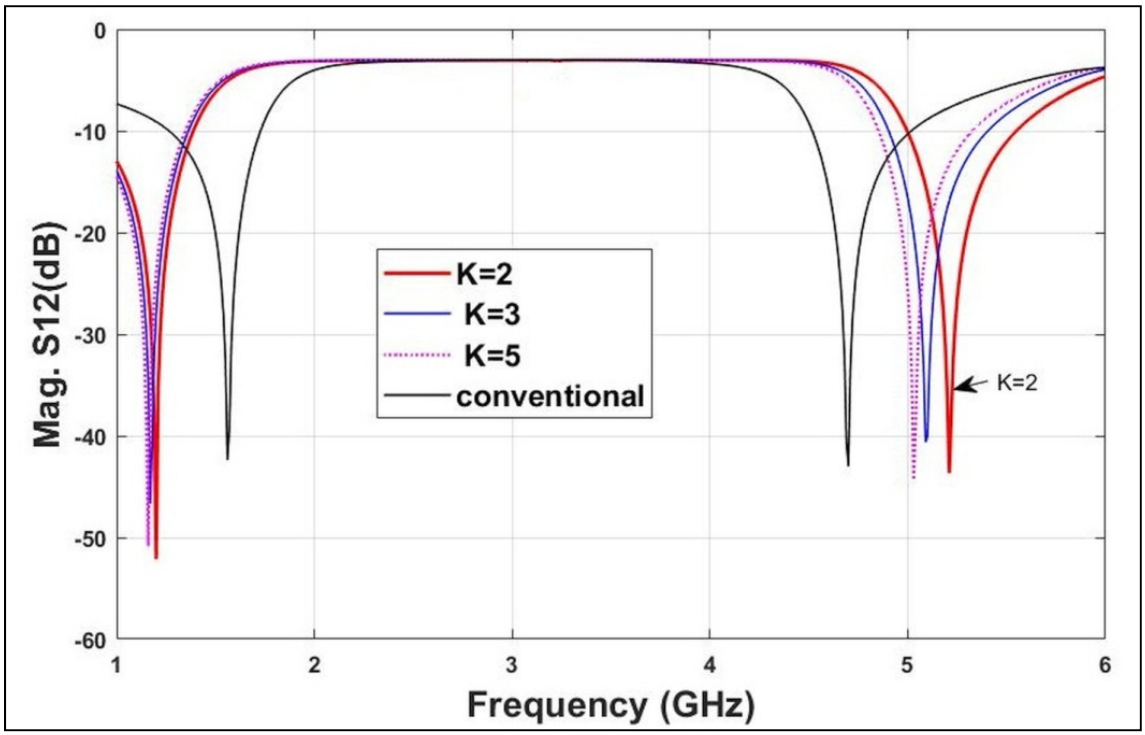

Figure 3.8 Transmission S-parameter of proposed power divider with the variation of K

It can be seen from Figure 3.8, that when K increases, there is almost no effect on the lower transmission zero; however, the second transmission zero is shifted to a lower frequency. The simulation results are also compared to the case of the conventional ring power divider (without SIR). It is noticed that for K =2, we get the wider bandwidth with two transmission zeros situated at 1.2 GHz and 5.21 GHz with -52 dB and -44 dB attenuation values respectively.

Following the above guidelines, the optimized parameters of K = 2 and $\alpha = 0.95$ can be used in order to get a wide bandwidth from 1.7 GHz to 4.6 GHz of the proposed divider. As a result, the stepped impedance resonator can be designed to have the characteristic impedances Z_{04} =

40 Ω and Z_{05} =20 Ω, and the electrical lengths θ_4 and θ_5 are set to 84.5˚ and 7.8˚ respectively. This can be used in order to calculate the dimensions of the Stepped Impedance Resonator (SIR) cell. The microstrip widths and lengths corresponding to characteristic impedances Z_0, Z_{01}, Z_{04} and Z_{05} are shown in Table 3.1. The radius of the ring is 15 mm.

Table 3.1 Dimensions of the proposed ring power divider

Characteristic Impedance	**Z_0**	**Z_{01}**	**Z_{04}**	**Z_{05}**
Width (mm)	0.76	0.44	0.89	2.2
Length (mm)	18.8	23	30	1.3

3.2.3 Simulation results

Figure 3.9 and Figure 3.10 show the EM simulation results of the conventional and proposed ring power divider respectively obtained by using the Advanced Design System (ADS) software. As can be observed from these figures, the conventional ring structure (Hammou et al., 2011) has a fractional bandwidth of 63 % ranging from 2.14 GHz to 4.11 GHz (S_{11} < - 10 dB), while simulations of the proposed ring structure show that the fractional bandwidth has increased up to 90.2 % producing therefore a remarkable bandwidth enhancement of 27.2 % as mentioned in section 1. By comparing the results of the two ring power dividers, we can notice that the proposed ring power divider has an insertion loss, which is between - 3.04 dB and -3.58 dB over the whole band (1.74 – 4.6 GHz) with quasi-null amplitude imbalance (S_{21}=S_{31}) while the conventional power divider has an insertion loss between -3.06 dB and - 3.61 dB over a narrower band (2.14 – 4.11 GHz). In addition, it is obvious that the proposed divider has better return loss and better isolation between the output ports, which are lower than -10 dB in the whole band (1.74 – 4.6 GHz) providing thus a significant wide bandwidth contribution compared to the previous reported ring divider which operates from 2.14 GHz to 4.11 GHz as can be clearly seen from Figure 3.9 and Figure 3.10.

Compared with other wideband power dividers present in the literature such as in (Ahmed & Abbosh, 2015; S. S. Gao et al., 2013), it is obvious that apart from its simpler structure, the proposed ring power divider has better performance over a wider operational bandwidth. It is to be noted that the power dividers developed in (Ahmed & Abbosh, 2015; S. S. Gao et al., 2013) have a fractional bandwidth of 68.6 % and 62 % respectively.

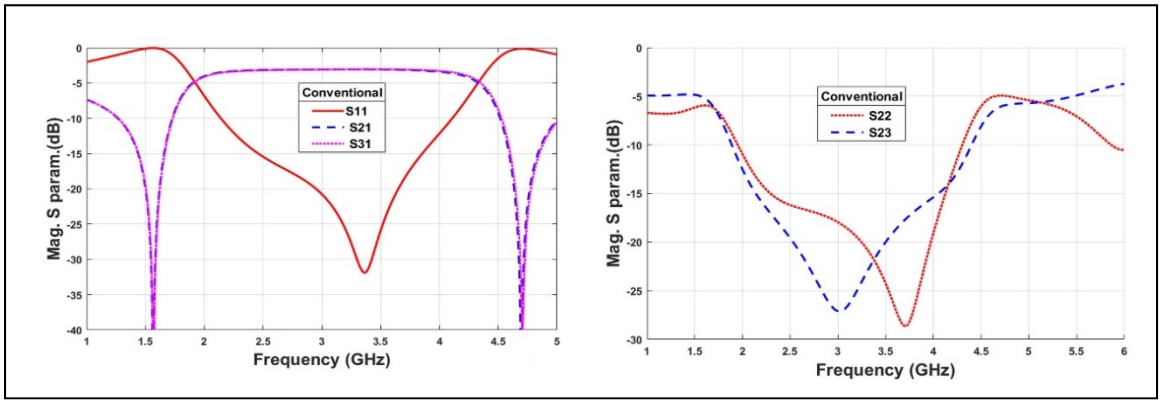

Figure 3.9 Simulated S-parameters of the conventional power divider: (a) S_{11}, S_{21} & S_{31} and (b) S_{22} & S_{23}

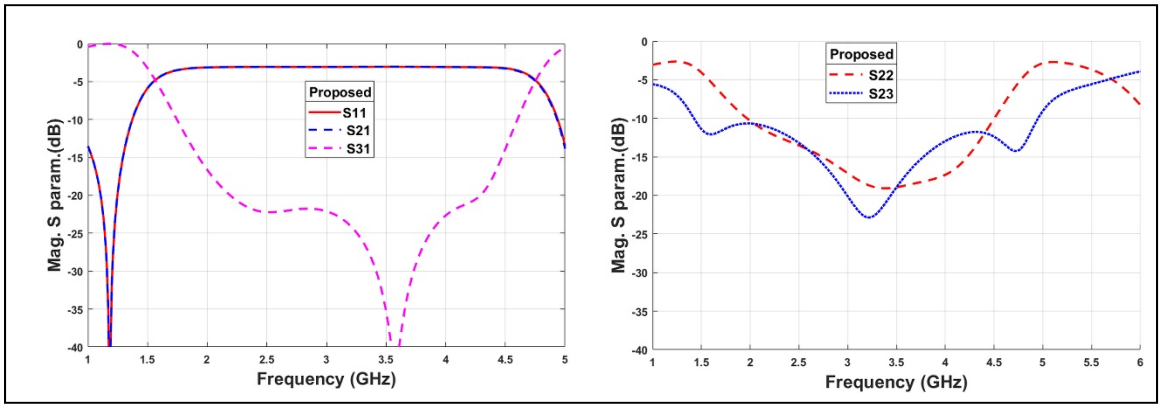

Figure 3.10 Simulated S-parameters of the proposed power divider: (a) S_{11}, S_{21} & S_{31} and (b) S_{22} & S_{23}

3.2.4 Fabrication and measurement results

For verification of the theoretical results, the proposed power divider has been fabricated on a Rogers RT/Duroid 6002 substrate whose dielectric constant is 2.93, loss tangent of 0.0013 and

its thickness 0.254 mm. It operates at the center frequency of 3.17 GHz and has a large bandwidth (1.7- 4.64 GHz) as expected. The fabricated ring power divider is shown in Figure 3.11 and it occupies a small surface area of 5.1 cm × 5.5 cm.

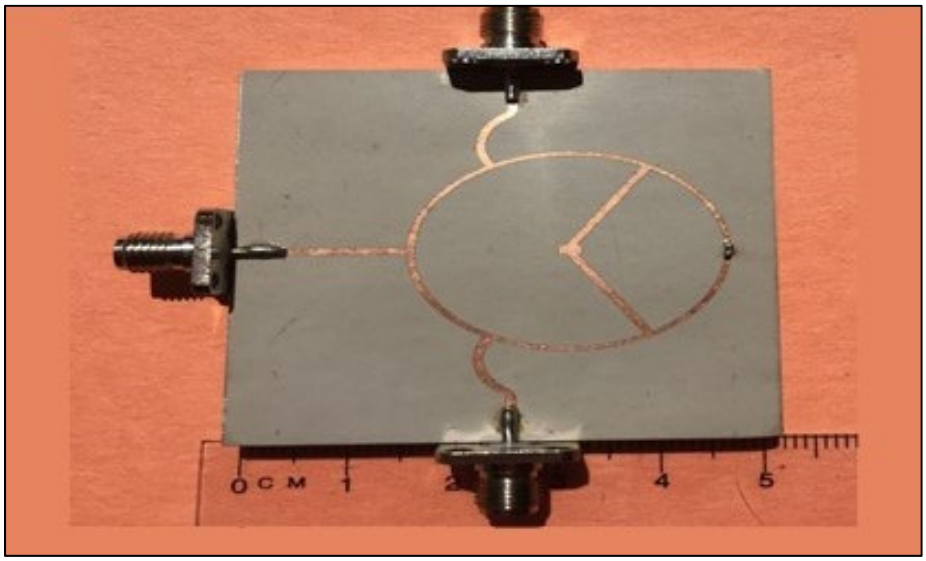

Figure 3.11 Photograph of the fabricated ring power divider

The S-parameter measurements were accomplished using the Agilent E8362B vector network analyzer over the frequency range from 1 to 6 GHz. The EM simulations and measured S-parameter results of the proposed power divider are shown in Figure 3.12 and Figure 3.13.

The measurement results show that the proposed power divider has an insertion loss variation of 0.74 dB ranging from - 3.36 dB to - 4.1 dB between 1.74 GHz and 4.64 GHz. The measured return loss is better than -10 dB from 1.6 GHz to 4.71 GHz. The output return loss is better than -10 dB from 1.7 GHz to 4.64 GHz. The isolation between the outputs is better than -10 dB between 1.42 GHz to 5.21 GHz. It can be concluded by comparing the measurement and EM simulation results that there is good agreement over the whole band of interest.

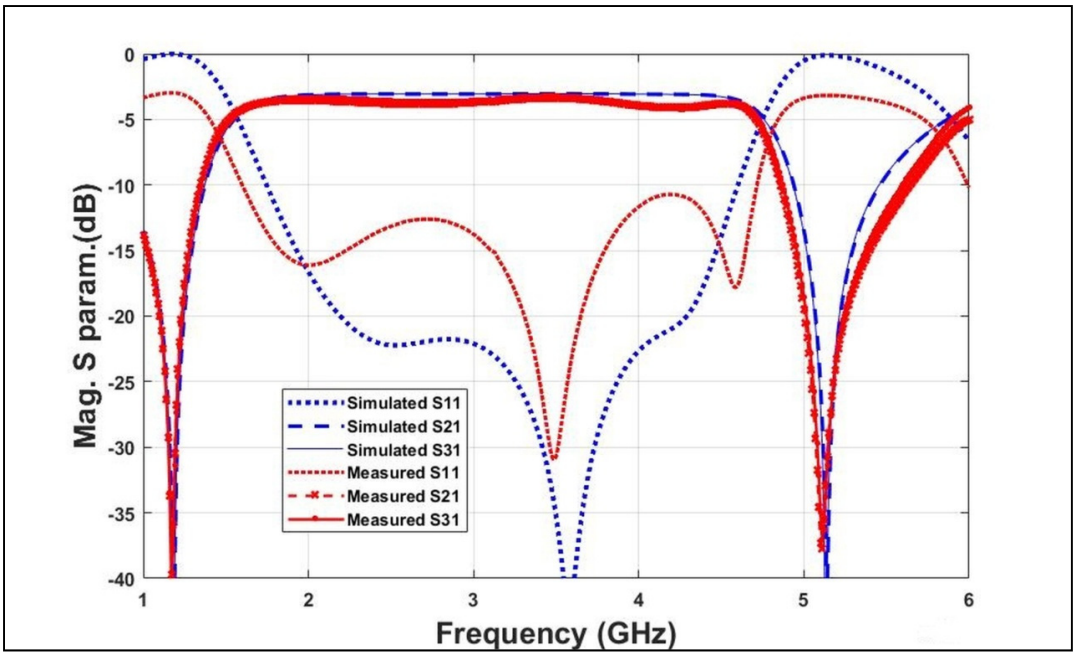

Figure 3.12 Simulated and measured input return loss and insertion loss of the proposed divider

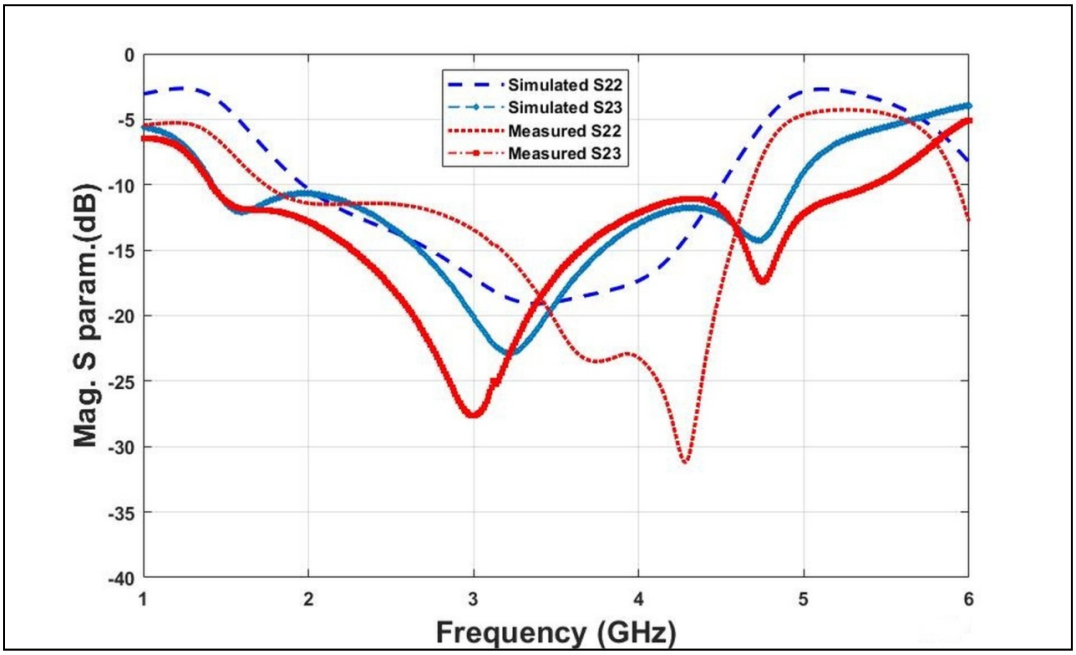

Figure 3.13 Simulated and measured output return loss and isolation of the proposed divider

The measured amplitude and phase imbalances between outputs of the proposed divider are shown in Figure 3.14. These results show that the proposed power divider has a maximum amplitude imbalance of 0.21 dB in the whole band from 1.7 GHz to 4.64 GHz which implies that the power is divided evenly between the 2 outputs. In addition, the two outputs are in-phase in the whole band with a tolerance of less than 2.5 degrees over the whole bandwidth of interest which proves the good phase performance of the fabricated power divider.

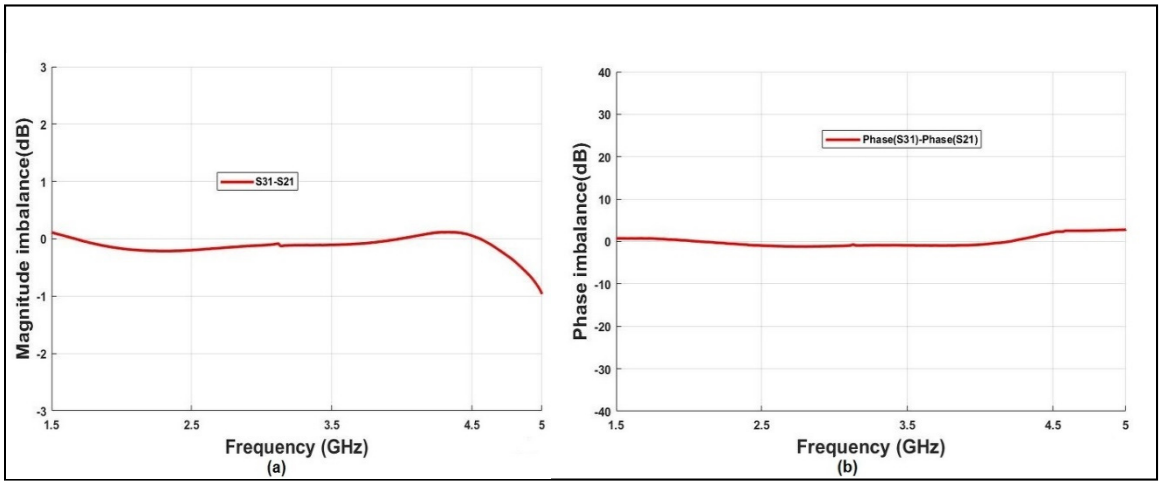

Figure 3.14 Measured outputs imbalance of the proposed power divider: (a) Magnitude and (b) Phase

3.3 Quadrature Hybrid Coupler

Quadrature hybrids, also known as branch-line hybrids, are used to split the input signal into 2 outputs with a 90° phase difference between them. In practice, the bandwidth of a branch-line coupler is restricted to about 10–20 % (Pozar, 2012) which makes it unsuitable for many wideband applications. In order to improve its bandwidth, different techniques have been used in the literature such as coupled transmission lines (Chen et al., 2017) or by using open circuited series stubs (Arriola et al., 2011; Johnosono et al., 2006) or lumped distributed elements (Chun & Hong, 2006) or by cascading multiple sections (Kim et al., 2015; Tang et al., 2006; Yoon & Min, 2017). The coupler reported in (Chen et al., 2017) was composed of two elliptical microstrip lines by using a multilayer architecture involving broadside slot

coupling. However, the measurement results of this coupler indicated that the coupling is 3 ± 1 dB, and the phase deviation was 90° ± 5° across the band of 1.1–2.1 GHz, where the phase errors were associated to the manufacturing process. Another reported work proposed an hybrid coupler with four open-circuited λ/4 microstrip coupled lines in suspended line structures (Arriola et al., 2011) operating at 5.9 GHz with an insertion loss better than 3.6 dB.

As known, the most common technique used for designing wideband microstrip branch line couplers is by cascading two or more sections. In (Yoon & Min, 2017), a two-section wideband hybrid coupler having 55% fractional bandwidth operating at the center frequency of 1.9 GHz has been reported. Another two-section microstrip line coupler operating in the frequency band of 1.71 - 2.7 GHz has been reported in (Kim et al., 2015).

Moreover, a 90-degree hybrid coupler using cascaded sections with different open stubs and lumped distributed elements was reported in (Chun & Hong, 2006) with a 56 % fractional bandwidth (FBW) at the center frequency of 2 GHz. However, the need to use high-impedance transmission lines in multi-section hybrid couplers makes the fabrication process difficult to realize due to manufacturing limitations. In (Tang et al., 2006), a wideband hybrid coupler has been designed by using a four-section topology with a defected ground. To overcome the limitation of high-impedance transmission line in terms of very narrow line widths, a defected ground structure (DGS) has been introduced. The proposed structure had 40% fractional bandwidth at the center frequency of 2.4 GHz. However, using defected ground structures may cause unwanted radiation problems which has non-desirable effects on the overall performance of the coupler. In this thesis, the proposed design approach of a two-section branch-line coupler will be presented. In order to ensure easy and cost-effective fabrication, the design of the proposed wideband hybrid coupler is optimized to be built on a single-layer board.

3.3.1 Design and Simulations

The circuit diagram of the proposed wideband two-section coupler is shown in Figure 3.15. It includes two sections with three sets of transmission lines having characteristic

impedances Z_{01}, Z_{02} and Z_{03}. All the transmission lines used have a length of λ/4 at the operating frequency.

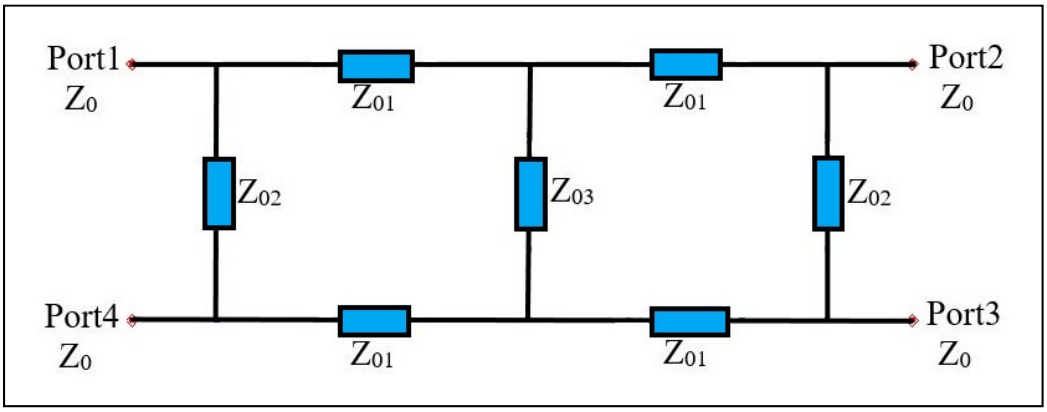

Figure 3.15 Circuit diagram of the two sections quadrature coupler

In order to design this coupler with an impedance transformation ratio r and an output power ratio k^2, we use the same analysis as in (S. Kumar et al., 1995) to determine the characteristic impedances Z_{01} and Z_{02}:

$$Z_{01}^2 = Z_0 Z_{03}\sqrt{r-\left(\frac{r}{t}\right)^2} \tag{3.28}$$

$$Z_{02} = Z_0\frac{\sqrt{r(t^2-r)}}{(t-1)} \tag{3.29}$$

Where t defined as: $t = r\sqrt{(1+k^2)}$.

In our design, since the input and output ports have the same characteristic impedance Z_0, the impedance transformation r = 1. In addition, for an equal power distribution (k=1), we have $t^2 = 2.r^2$. Note that Z_{01} and Z_{03} can be selected to be different. However, $Z_{01} = Z_{03}$ provides the maximum bandwidth and best performance (S. Kumar et al., 1995). In this case, we can calculate the characteristic impedances directly from (3.28) and (3.29) which gives $Z_{01} = Z_{03} = 35.35\ \Omega$ and $Z_{02} = 120.7\ \Omega$. It is to be noted that the shape of the circuits rounded in our design to ensure better S-parameter performances (Hannachi et al., 2013).

Based on the above theoretical analysis, compact two-section 90-degree coupler with a rounded structure is designed to operate at 3 GHz. Figure 3.16 shows the layout of this 90-degree coupler made up of microstrip single layer technology on a Rogers RT/Duroid 6002 substrate.

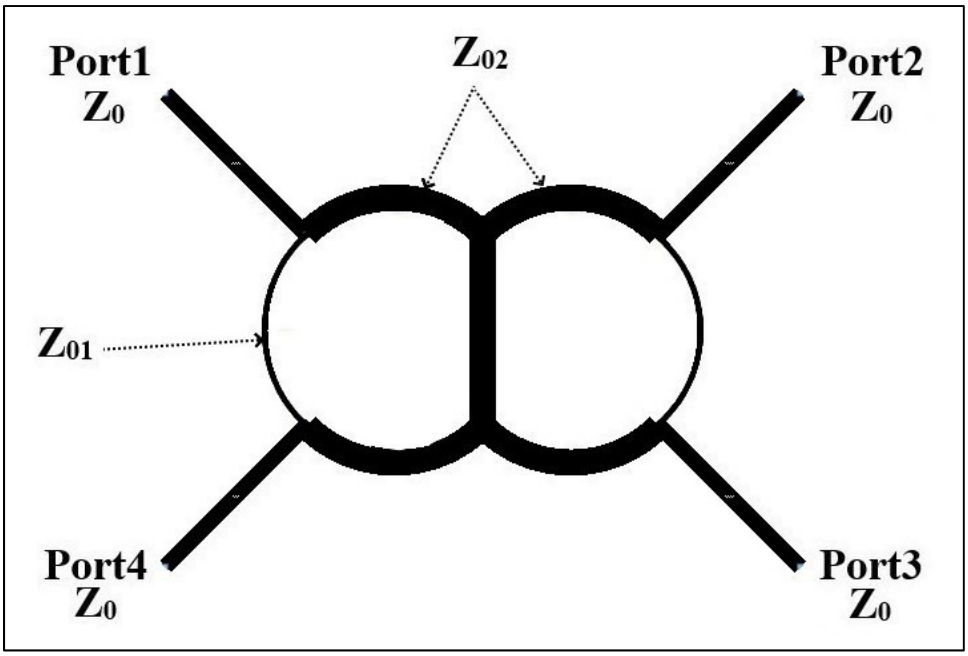

Figure 3.16 Layout of the two-section 3-dB quadrature coupler

The EM simulation results obtained by using the Advanced Design System (ADS) software presented in Figure 3.17 show the wideband characteristics of this coupler. From these results, we can notice that the reflection coefficient S_{11} as well as the isolation between port 1 and 4 are lower than -50 dB at 3 GHz. The input reflection coefficient S_{11} is under -10 dB between 2.3 GHz and 3.96 GHz which means a wide operational bandwidth of the proposed coupler. In addition, the insertion loss is -3.09 dB from 2.8 GHz to 3.5 GHz with quasi null amplitude imbalance. The magnitude imbalance is less than ± 1 dB between 2.6 GHz and 3.7 GHz. The isolation between the input and the isolated port $|S_{41}|$ is below -15dB between 2.46 GHz and 3.77 GHz. Besides, the phase difference between the two output ports is 90° ± 1° from 2.5 GHz and 3.8 GHz as is clearly shown in Figure 3.18.

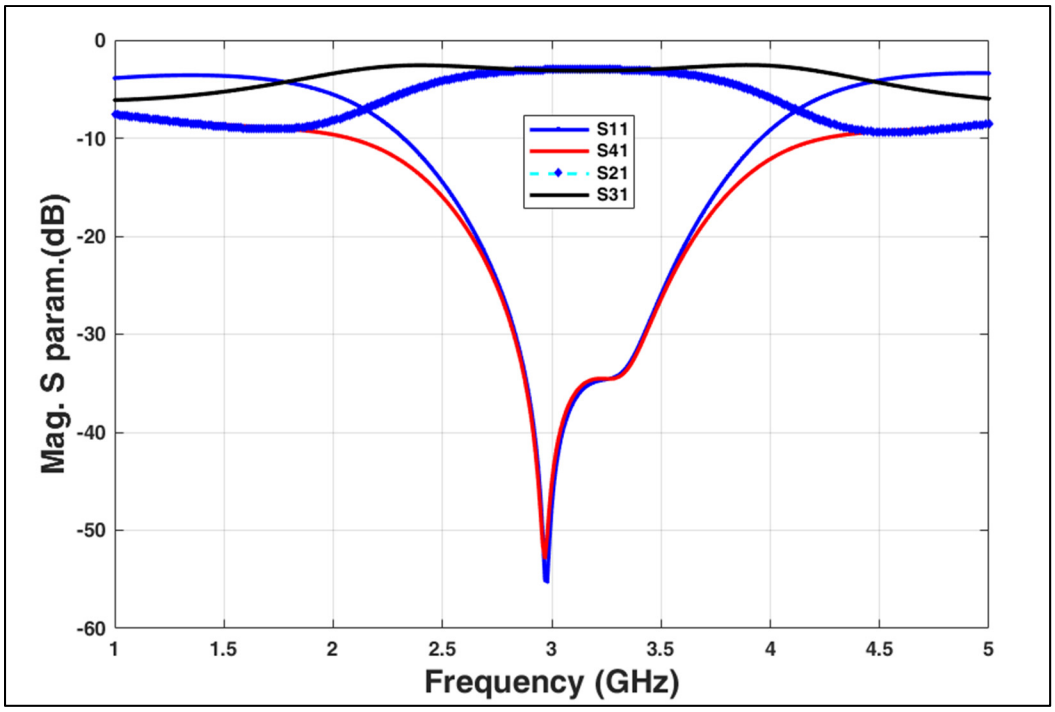

Figure 3.17 Simulated S-parameters of the proposed 3-dB quadrature coupler

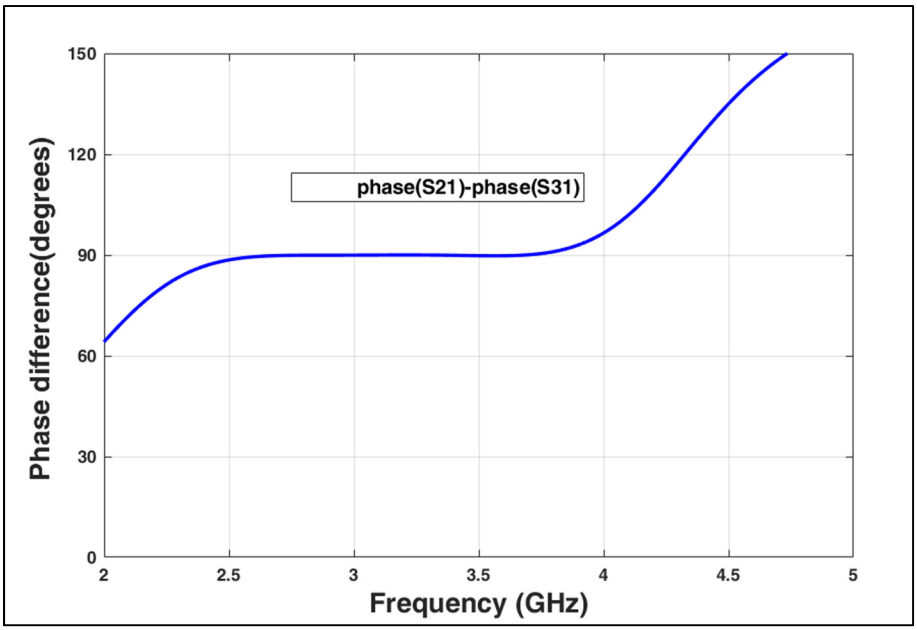

Figure 3.18 Simulated output phase difference of the proposed 3-dB quadrature coupler

3.4 Conclusion

In this chapter, we have designed a modified ring power divider to cover the frequency bandwidth of 1.7 GHz to 4.6 GHz by adding an SIR to the old structure to improve its operational bandwidth. A detailed even-odd mode analysis of the proposed ring power divider has been performed. To validate the theoretical analysis and simulations, a prototype is fabricated on a single layer substrate. The experimental results show that the proposed circuit is broadband with a high factor amplitude balance over the considered bandwidth. The proposed ring power divider has the advantages of compact size and ease of fabrication which makes it very suitable for many wideband microwave applications. In addition, a compact two-section 90-degree coupler with a rounded structure is designed and simulated. The simulation results of the proposed coupler show good performance between 2.6 GHz and 3.7 GHz. The good results obtained indicate that these two devices are good candidates for integration into the proposed six-port junction.

CHAPTER 4

DESIGN OF WIDEBAND SIX-PORT REFLECTOMETER

4.1 Introduction

After presenting the main components used to design the six-port measurement system, the six-port reflectometer will be described in this chapter. To evaluate its wideband performance, the proposed six-port reflectometer is then tested by measuring the reflection coefficient of different DUTs over a large frequency band. The measured results are then corrected by a proper calibration method to have optimal results. Compared to conventional six-port calibration methods, the proposed calibration process is relatively simple and allows accurate reflection coefficient measurements. The designed six-port reflectometer operating at 3 GHz is then fabricated in microstrip technology on a Rogers RT/Duroid 6002 substrate whose dielectric constant is 2.93, loss tangent of 0.0013 and having a thickness of 0.508 mm. The next section describes the six-port architecture design and simulations. The measurement results presented in Section 4.2 are compared with those obtained by simulation to show the validity of the proposed system. Then, the proposed six-port reflectometer is used to measure different loads. A simple calibration method is then developed in section 4.4 to consider the imperfections of the proposed system and to do further corrections of the measured results. After calibration, the proposed six-port reflectometer can measure the phase and magnitude of the complex reflection coefficient of any DUT with good accuracy.

4.2 Six-port junction design

As mentioned in chapter 2, the six-port junction is made up of a ring power divider and three identical 90-degree hybrid couplers. In this design, all four power detectors are used so that we eliminate the need to use a reference power detector. To simplify the fabrication process and minimize the cost, the six-port circuit is designed on a single-layer rather than a multi-layer PCB. The layout implementation of the proposed six-port junction, which is accomplished in momentum ADS at a center frequency of 3 GHz is shown in Figure 4.1. In this layout, port 1

and port 2 are the input ports connected to the source and the DUT respectively, ports 3 to 6 are connected to diode detectors and the unused port 7 is matched to a load termination. The microstrip transmission lines used to connect the components are quarter-wavelength and half-wavelength long. All the transmission lines used are designed to have a characteristic impedance $Z_0 = 50\ \Omega$. The choice of a rounded shape for the branch line couplers was found to be more beneficial in terms of getting better coupling, return loss, and isolation over a wide band of frequencies ensuring better S-parameter performances (Hannachi et al., 2013).

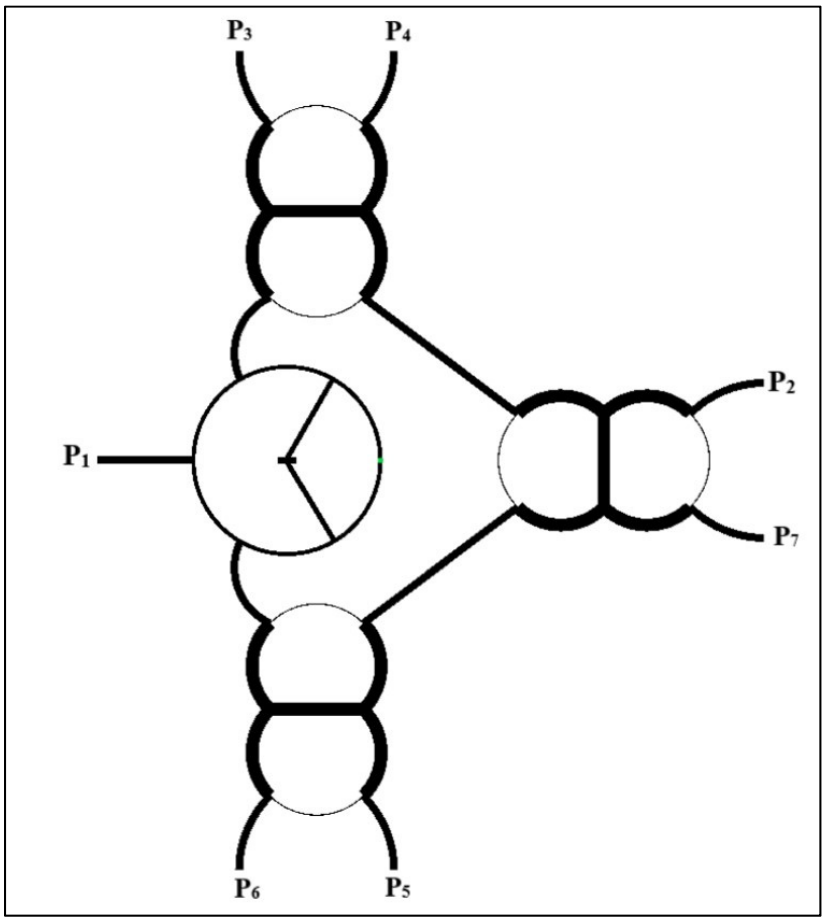

Figure 4.1 Layout of the proposed six-port junction

4.2.1 Momentum simulations

Figures 4.2 and 4.3 show the EM simulation S-parameter magnitude results of the proposed six-port junction. It can be noted that the return loss S_{11} of the input port 1 is lower than -30 dB between 2.82 and 3.45 GHz and is lower than -20 dB over the entire operating frequency band from 2.44 to 3.65 GHz. Following the theoretical analysis discussed in chapter 2, the insertion loss of the six-port should be equal to - 6 dB in the ideal case. The simulated insertion losses with respect to input port 1 are identical and equal to -6.1 dB from 2.8 to 3.5 GHz, which is close to the ideal case of -6 dB. In addition, the simulated insertion loss is -6.1 ± 1 dB in the frequency range 2.55– 3.7 GHz. Moreover, the return loss S_{22} of the input port 2 is lower than -30 dB from 2.83 to 3.5 GHz and is lower than -20 dB across the frequency band from 2.66 to 3.65 GHz. The simulated insertion loss with respect to input port 2 is - 6.1 dB ± 1 dB in the frequency range 2.66– 3.6 GHz. It can be observed also that the isolation between the two input ports S_{21} is lower than -20 dB in the frequency range 2.54–3.85 GHz.

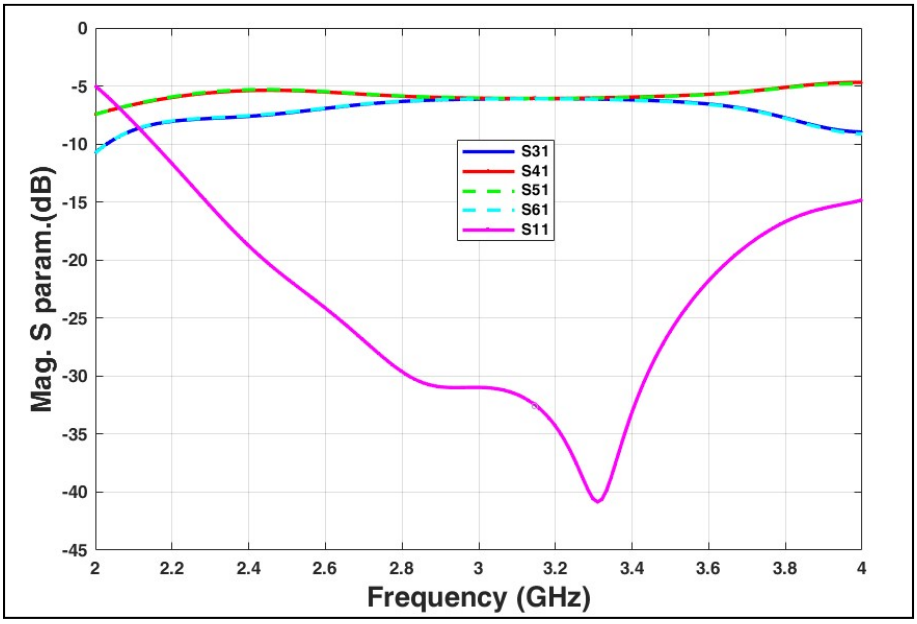

Figure 4.2 Magnitude transmission S-parameters and return loss of input port 1

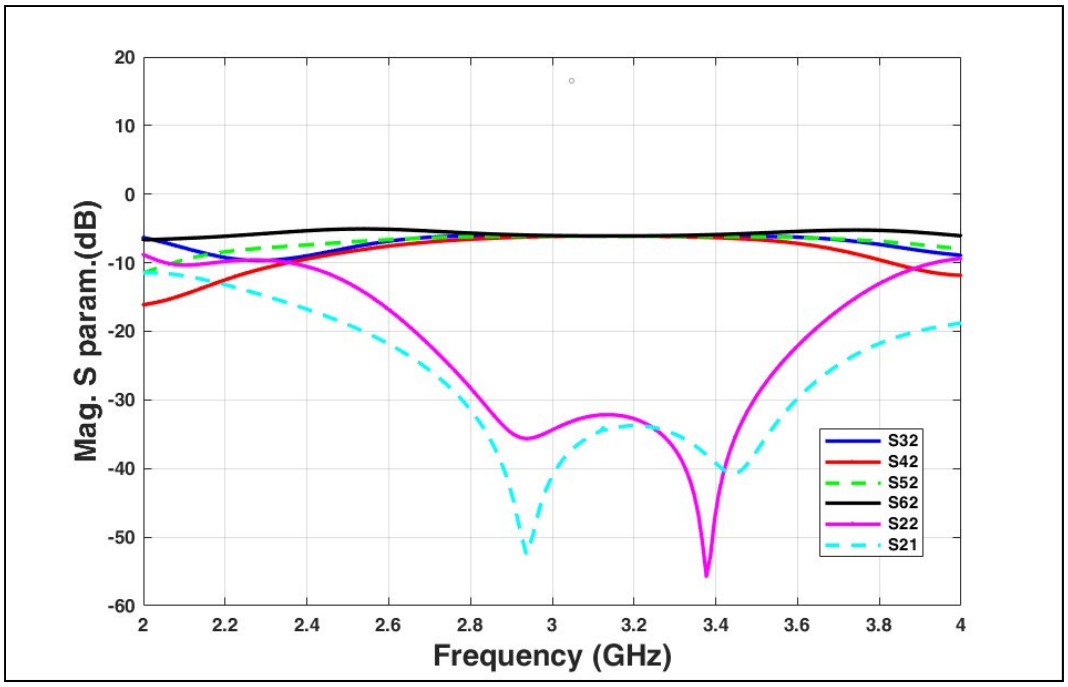

Figure 4.3 Magnitude transmission S-parameters, isolation and return loss of input port 2

Figure 4.4 shows the EM simulation phase response of the transmission S-parameters between input port 1 and the output ports of the proposed six-port junction. It can be noted that similarly to the good S-parameter magnitude performance, the phase performance is excellent over the entire frequency band of interest 2.6– 3.8 GHz. The phases of S_{31} and S_{61} are equal and there is a 90° ± 1° phase shift between them and the phases of S_{41} and S_{51} in the frequency range 2.6– 3.8 GHz which agrees with the theoretical analysis of the six-port junction in chapter 2.

To further study the operation of the wideband six-port reflectometer, the position of the q_i points is an important factor for good performance. Normally, a very good circuit performance is obtained when the q_i points are at equal distance from the origin of the complex plane and angularly separated by 360° divided by their number (Hammou et al., 2016). In the ideal case where port 1 and port 2 are isolated, the equivalent q_i points can be written as (X. Xu et al., 2005):

$$q_i = \frac{S_{i1}}{S_{i2}} \qquad i = 3,4,5,6 \tag{4.1}$$

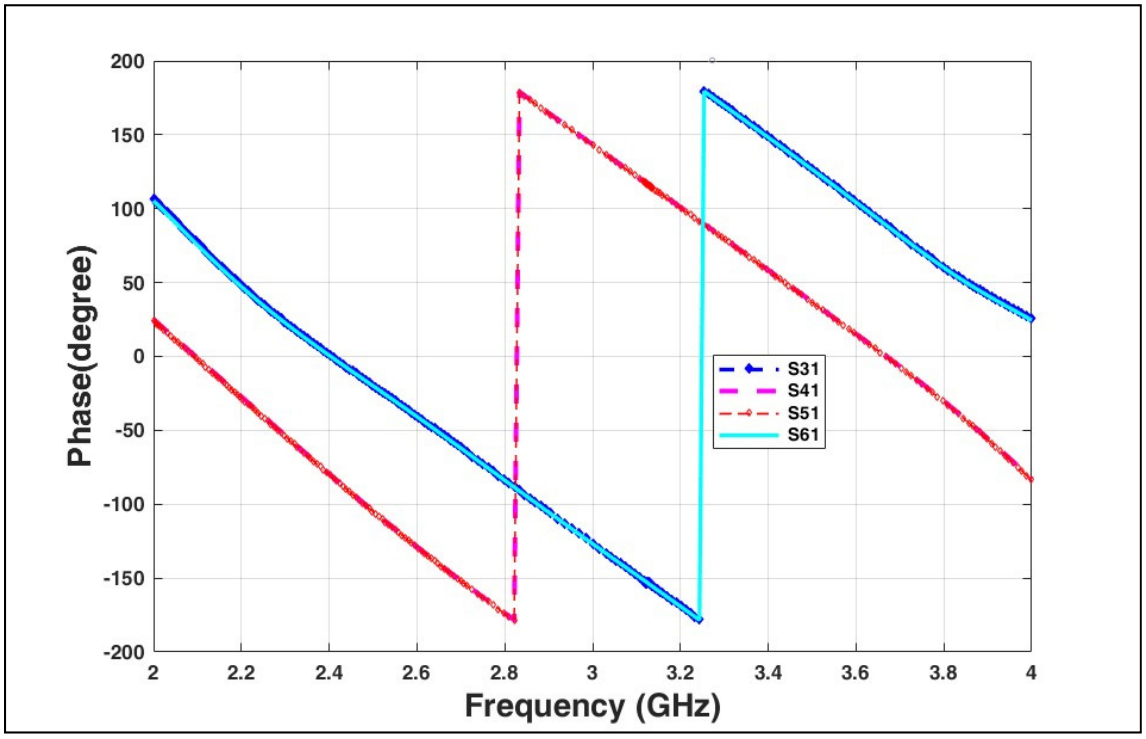

Figure 4.4 EM Simulation of the transmission phase response of the six-port junction

According to the theoretical analysis done in chapter 2, the centers of output power circles of the proposed six-port junction are as follows: q_3= -j, q_4= +j, q_5= -1 and q_6= +1 for the ideal case. The plot of the q_i-points based on the EM-simulation results in ADS of the proposed six-port circuit in the frequency band 2–4 GHz is shown in Figure 4.5. As can be noticed, the magnitudes of the q_i points are near to 1, while the phase difference is not far away from 90° between two consecutive q_i points. These results are consistent with the theoretical expectations, showing that the proposed six-port junction presents high performance over a wide frequency band of operation.

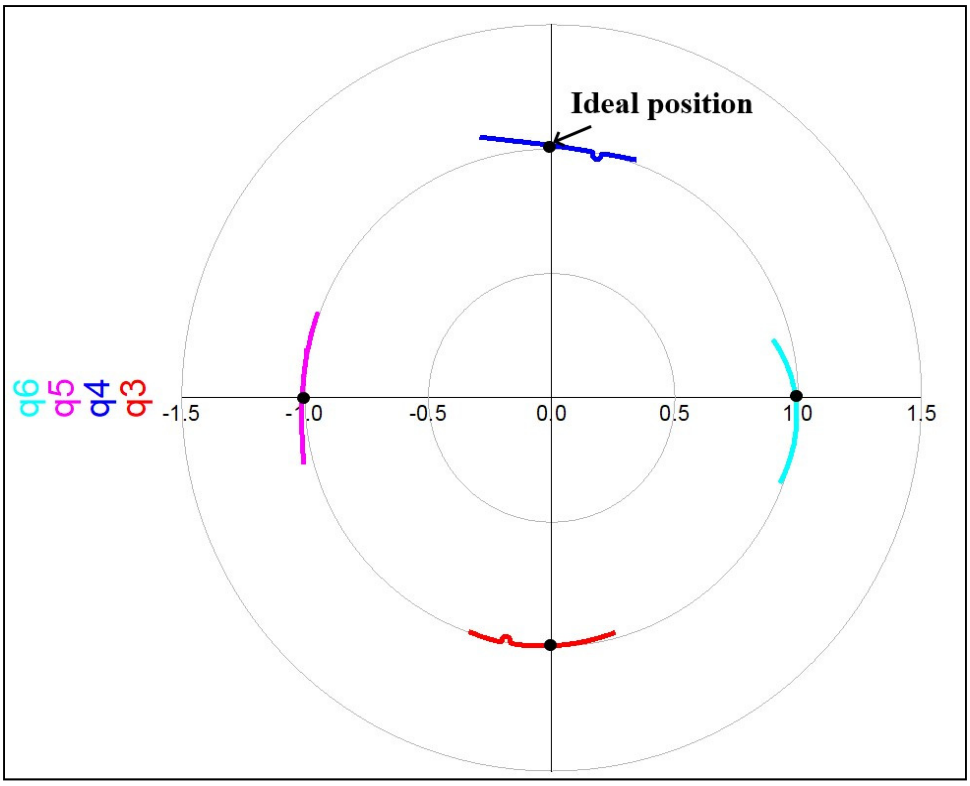

Figure 4.5 Simulation results of q_i-points of the proposed six-port circuit

4.2.2 Harmonic Balance Simulation

To demonstrate the excellent performance of the six-port junction, a harmonic balance simulation is accomplished using ADS as shown in Figure 4.6. At the output of the diode detectors D_1 to D_4, the DC output voltages with respect to the phase shift between the two input signals can therefore be obtained. The output voltage of the Schottky diodes used for power detection operating in the square-law region is proportional to the square of their input voltage so that we can write:

$$V_i = K_i.|b_i|^2 \quad (where\ i = 3,\ 4,\ 5,\ 6) \tag{4.2}$$

Where K_i is a constant. In addition, if the diode detectors are identical, we can write $K_i = K$.

By using the theoretical analysis in chapter 2, the complex reflection coefficient Γ of the six-port correlator can be obtained by reading the power signals at the output of the power detectors D_1 to D_4.

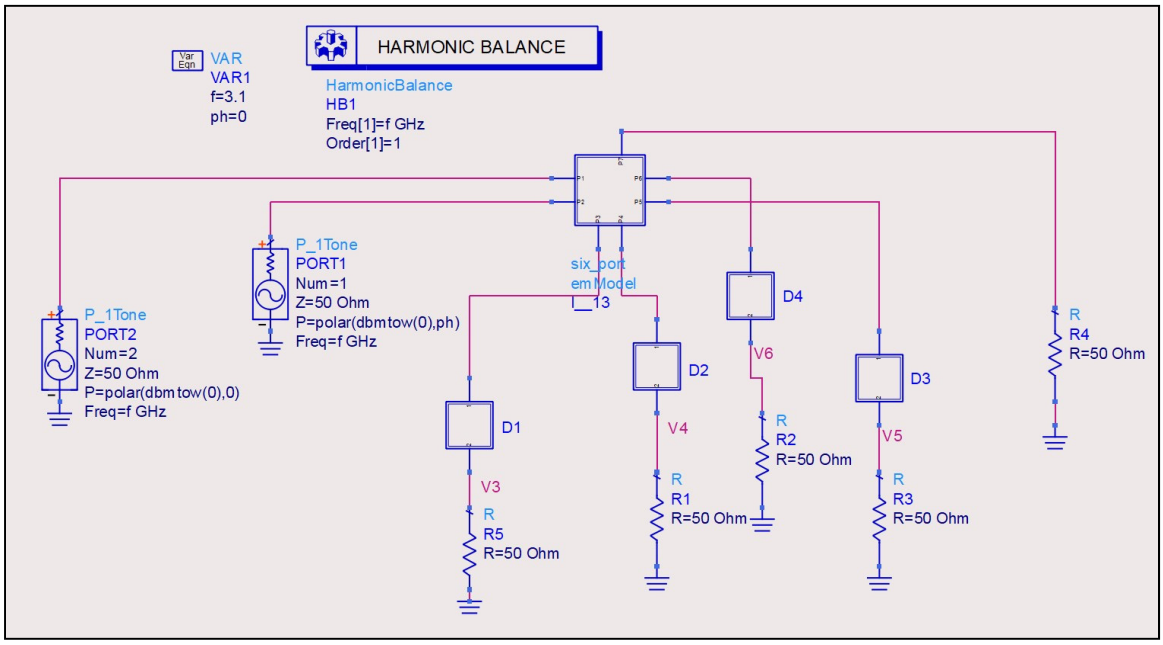

Figure 4.6 Schematic diagram for six-port harmonic simulation

In addition, the magnitude voltage differences (V_5-V_6) and (V_3-V_4) at the outputs are related to I and Q signals, respectively. In fact, the detected signals V_3 to V_6 at the output of the six-port correlator can be written as:

$$V_3 = \frac{K.A_1^2}{4}(1+|\Gamma|^2+2|\Gamma|sin\phi) \tag{4.3}$$

$$V_4 = \frac{K.A_1^2}{4}(1+|\Gamma|^2-2|\Gamma|sin\phi) \tag{4.4}$$

$$V_5 = \frac{K.A_1^2}{4}\left(1+|\Gamma|^2+2|\Gamma|\cos\phi\right) \tag{4.5}$$

$$V_6 = \frac{K.A_1^2}{4}\left(1+|\Gamma|^2-2|\Gamma|\cos\phi\right) \tag{4.6}$$

The phase between the two input signals is swept from 0 to 360° and the two input levels are fixed to 0 dBm. The six-port output voltage magnitudes V_3 to V_6 versus the phase shift between the inputs can therefore be obtained. It can be noted that a 90° phase difference exists between the four sinusoidal outputs having similar amplitudes, which is required for good performance of the six-port junction as is clearly shown in Figure 4.7.

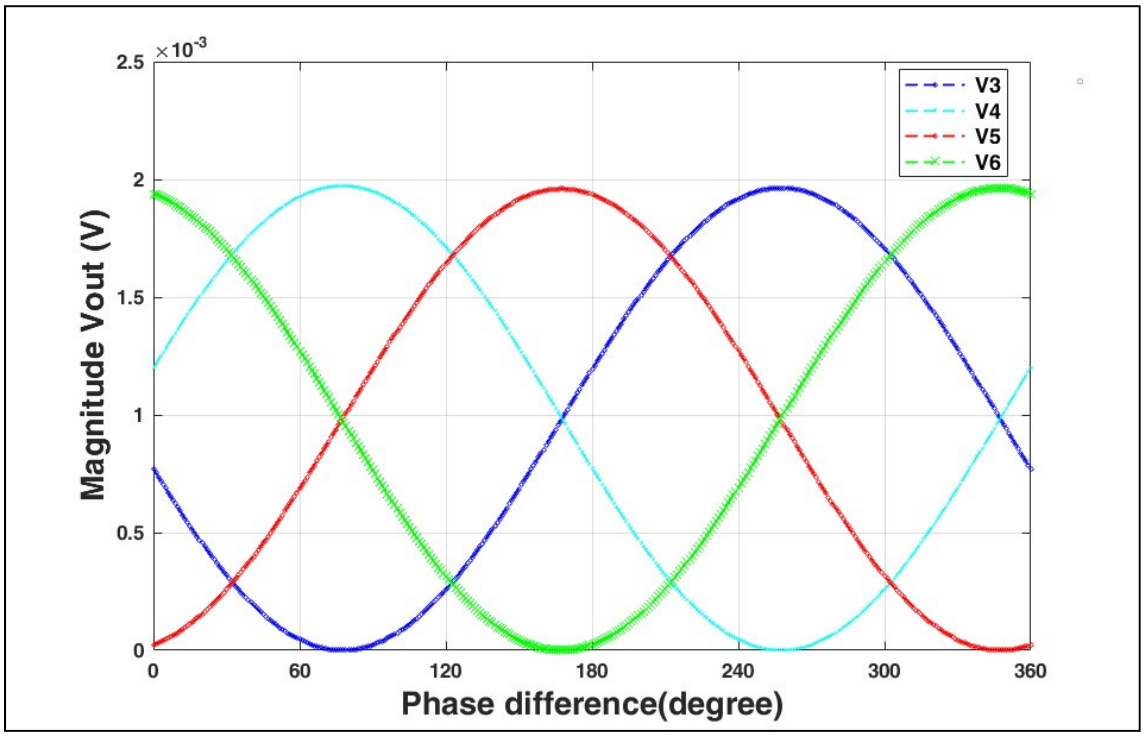

Figure 4.7 Harmonic balance simulation results of |Vout| versus RF input phase difference

By taking the difference between the detected output voltages, the I and Q signals can be written as:

$$I = V_5 - V_6 = K.A_1^2.\cos\phi \tag{4.7}$$

$$Q = V_3 - V_4 = K.A_1^2.\sin\phi \tag{4.8}$$

These signals are the in-phase and quadrature components of the complex reflection coefficient Γ ($\Gamma = I + jQ$). Figure 4.8 shows the I and Q signals in relation with the phase difference

between the input ports. As it can be noticed, the I and Q signals have identical amplitude and a 90-degree shift between them as expected which ensures a very good operation of the proposed six-port correlator.

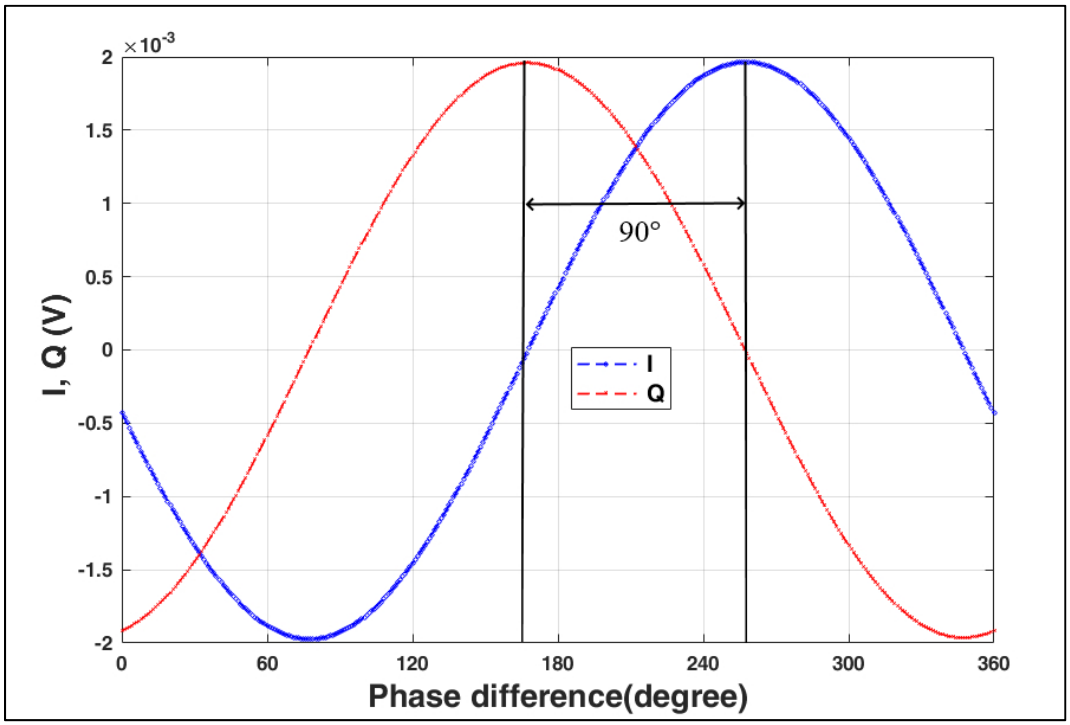

Figure 4.8 I and Q signals versus RF input phase difference

4.2.3 Measurement results

For verification of the theoretical results, the proposed six-port circuit has been fabricated on a Rogers RT/Duroid 6002 substrate whose dielectric constant is 2.93, loss tangent of 0.0013 and its thickness 0.508 mm. It operates at the center frequency of 3 GHz and has a large bandwidth as expected. The proposed six-port junction is then fabricated using the microstrip single layer technology at the center frequency of 3 GHz. The fabricated six-port junction occupies an overall surface area of 11 cm x 13.6 cm. The wideband operation of this system depends on the operating band of the hybrid couplers as well as the modified ring power divider, which are the main components of the circuit. The fabricated six-port circuit is shown

in Figure 4.9 with SMA connectors placed at all ports. The S-parameter measurements were accomplished using the Agilent E8362B vector network analyzer (VNA) over the frequency range from 1 to 5 GHz. The VNA was calibrated using Agilent calibration kit before any S-parameter measurements are performed to get accurate results.

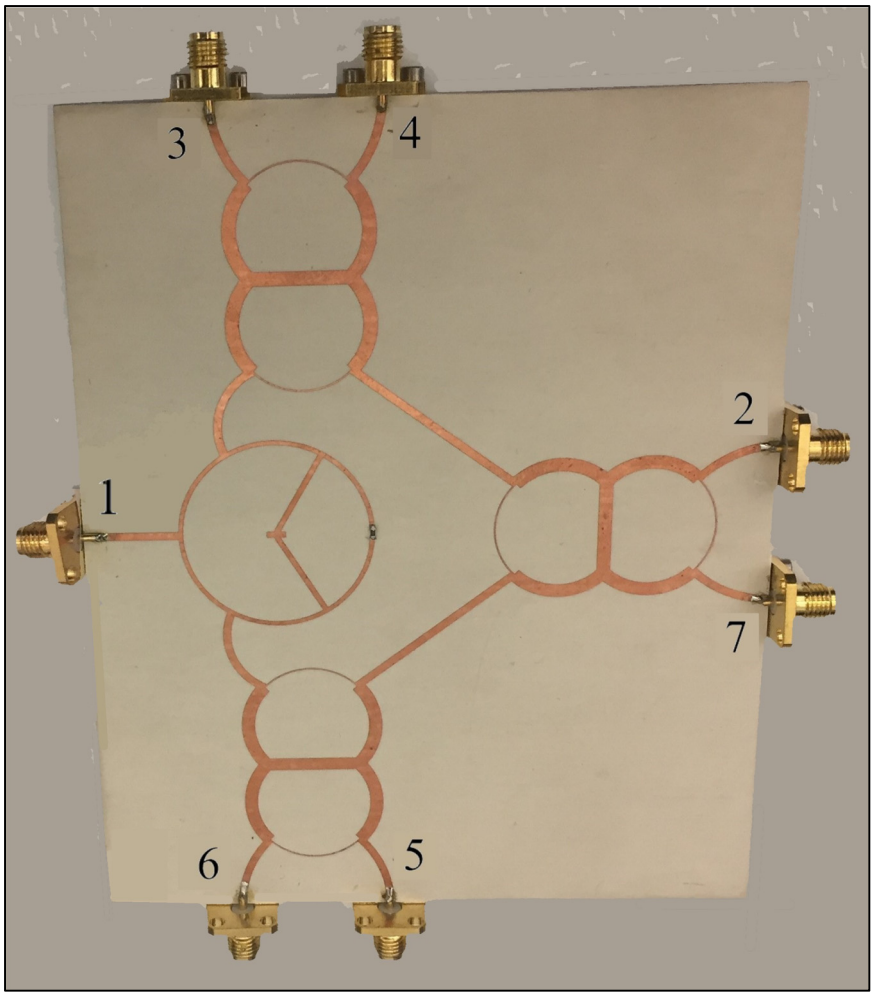

Figure 4.9 Photograph of the fabricated six-port junction

Figure 4.10 shows measured transmission parameters related to input port 1 as well as the return loss and isolation. The measured return loss S_{11} versus frequency is better than -17 dB in the frequency band 2.2–3.67 GHz. The transmission coefficients with respect to port 1 are -6.3 dB which is near the theoretical value of -6 dB and represent a quasi-null amplitude imbalance in the frequency band 2.7–3.3 GHz and a good amplitude response of -6.3 ± 1 dB

from 2.2 to 3.55 GHz. In addition, the return loss related to port 2 (S_{22}) is better than -20 dB at the center frequency of 3 GHz and less than -15 dB in the 2.3– 3.7 GHz and the isolation is less than -15 dB from 2.3 to 4.4 GHz. These results show that there is a very good agreement between the simulated and measured S-parameter results which ensures a good performance of the six-port junction.

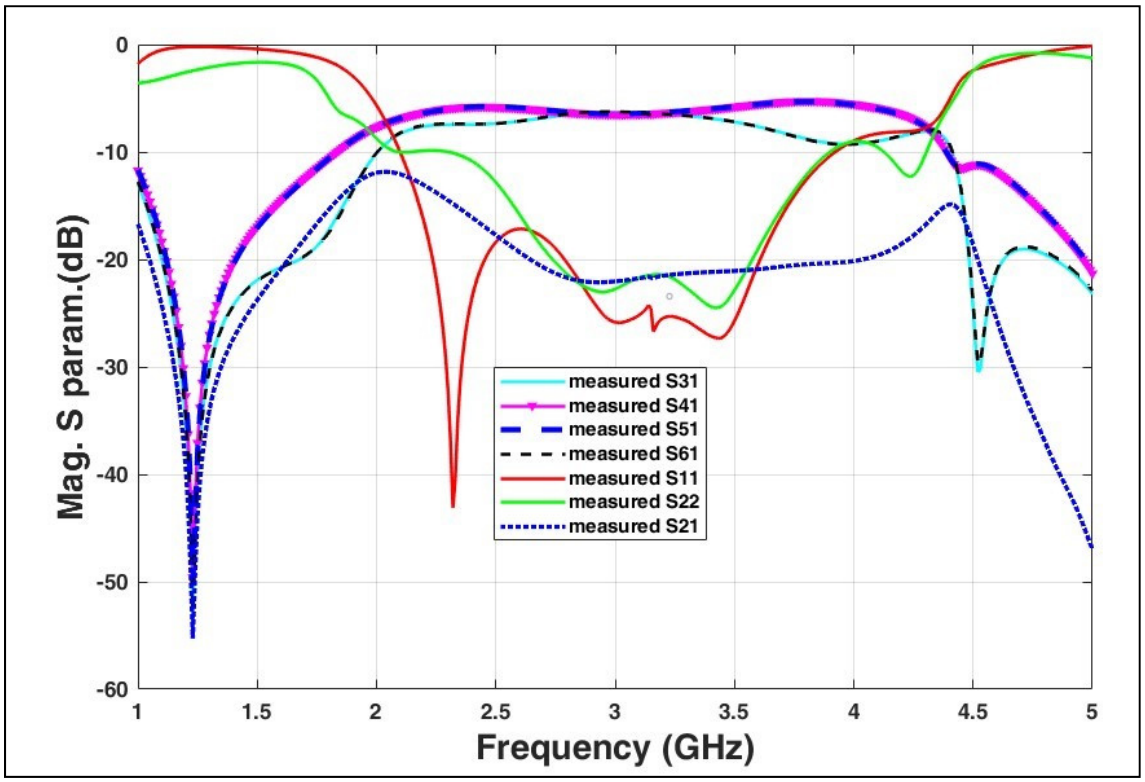

Figure 4.10 Measured magnitude S-parameters of the proposed six-port junction

In addition, Figure 4.11 shows the measured phase response of transmission S-parameters related to port 1 which present a good linearity over the whole frequency band of interest. It can be noted that the phases of (S_{31}) and (S_{61}) are equal and there is 90° ± 4° out of phase between them and the phases of (S_{41}) and (S_{51}) over a wide band from 2.4 to 3.6 GHz which indicates a very good agreement between the measured and simulation results.

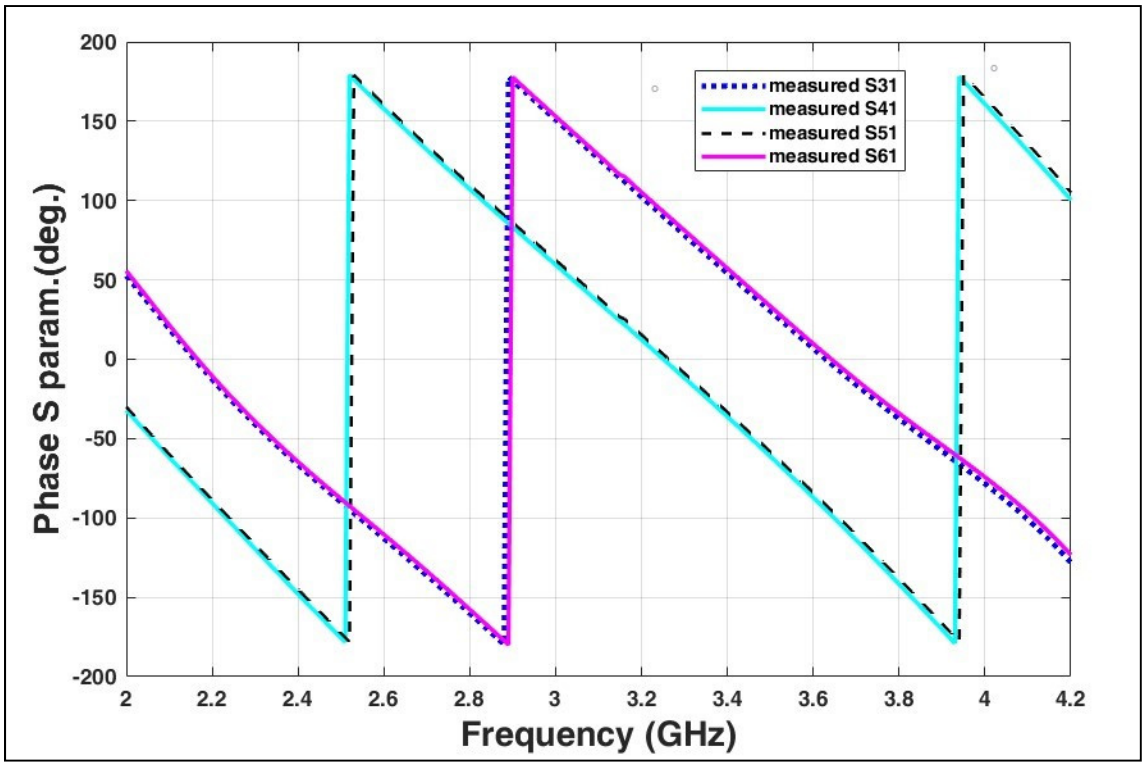

Figure 4.11 Measured S-parameters transmission phases of the proposed Six-port junction

The plot of the centers of the power circles (q_i points) based on the S-parameter measurement results of the proposed six-port junction is shown in Figure 4.12. As in the simulation case, the magnitudes of the q_i points are very close to 1, while the phase difference is close to 90° between two consecutive qi points which proves high precision location of the measured q_i points. The obtained results are in good agreement with the simulations results.

Table 4.1 compares the proposed six-port junction design with some designs present in the literature, in terms of bandwidth, insertion loss, return loss, number of layers and design complexity.

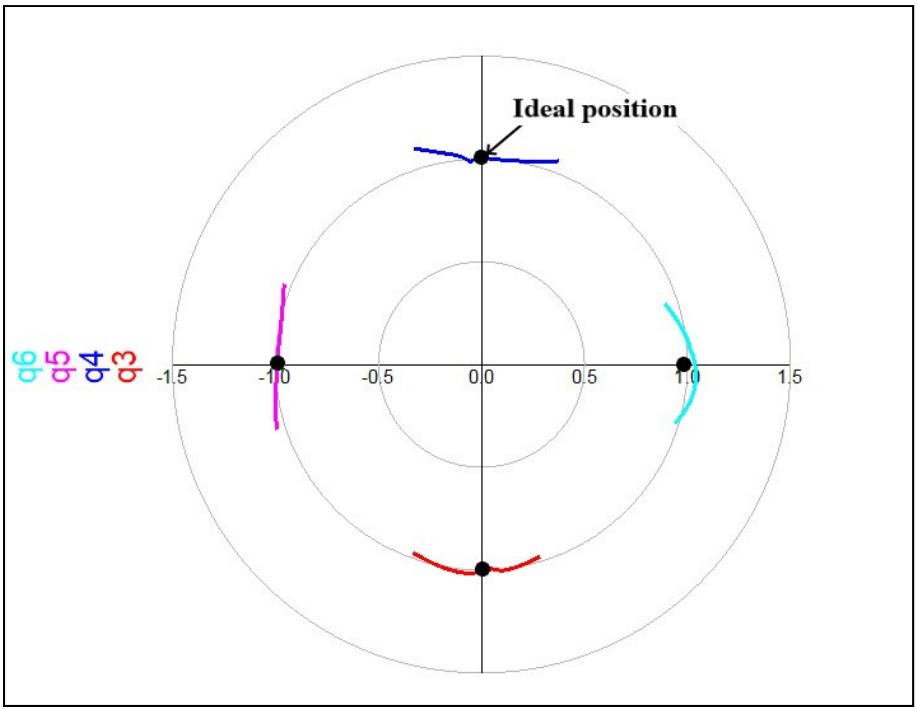

Figure 4.12 Measurement results q_i points distributions of the proposed six-port circuit

Table 4.1 Comparison of performance of different Six-port junctions in the literature

Reference	Bandwidth	Fractional Bandwidth	Return Loss	Insertion loss	layers/Design complexity
(Fang et al., 2011)	2.2 - 2.6 GHz	16.7 %	< -10 dB	- 6.7 ± 2.3dB	Single /High
(Kamil Staszek et al., 2016)	2.5-3.5 GHz	33.3 %	< -20 dB	- 6.0 ± 5 dB	Multilayer/ High
(Lee et al., 2016)	2.34 - 3 GHz	24.7 %	< -20 dB	- 6.0 ± 3.4 dB	Single/ High
(S. Sun et al., 2017)	1.6-2.6 GHz	47.6%	< -10 dB	- 8.1 ± 1.6 dB	Single/ High
(Ibrahim et al., 2016)	5.5 - 8 GHz	37%	< -10 dB	- 7.0 ± 2 dB	Single/Low
Our work	2.2 - 3.55 GHz	47%	< -17 dB	- 6.3 ± 1 dB	Single/Low

As it is known, low complexity, good performance and uncomplicated design are important factors in the design process of six-port junctions. While most of the designs present in the literature suffer from increased design complexity, the proposed six-port junction is relatively simpler compared to other six-port systems. For example, the design presented in (Kamil Staszek et al., 2016) consists of the use of four single-section coupled-line directional couplers in a stripline technology which is more difficult (and more expensive) to fabricate than microstrip. The six-port correlator presented in (S. Sun et al., 2017) is formed of a three-section power divider and three filtering couplers. The used power divider was composed of three sections of coupled lines and three isolation resistors, and the couplers consisted of three two-line and four three-line coupled lines. Since "coupled-line coupler with tight coupling level is difficult to be fabricated due to the narrow coupling gap" (L. Gao et al., 2019), this makes the design very complicated and adds an extra level of difficulty on the fabrication. In contrast, our proposed six-port design is much simpler and exhibits better amplitude imbalance and better return loss over a wider operational bandwidth compared to other designs in Table 4.1. Considering both return loss and insertion loss, under same operational bandwidth, our proposed six-port design outweighs all other designs in terms of better performance and low complex design and fabrication constraints. In particular, the proposed six-port design has better overall performance in terms of insertion and return loss compared to the six-port design presented in (S. Sun et al., 2017) having almost the same bandwidth. Therefore, the proposed six-port junction provides better S-parameter results than most of the previous existing six-port systems in the literature and this by maintaining the design complexity low.

4.3 Six-port reflectometer design

As mentioned in chapter 2, the six-port reflectometer is made up of a six-port junction composed of a ring power divider and three identical 90-degree hybrid couplers and an additional circuit needed to feed the six-port network. In this design, four q_i points equidistant from the origin having a magnitude of one and an argument difference of 90˚ between them are obtained. The six-port reflectometer diagram shown in Figure 4.13 comprises the six-port correlator whose main function is to determine the complex ratio of the two signals a_1 and a_2

from power readings and an additional circuit. The microwave source and the device under test (DUT) are connected to the six-port junction unit through the additional circuit formed by a 90-degree hybrid and a ring power divider to deduce the complex reflection coefficient Γ of a device under test (DUT). The additional circuit's function is to separate the incident and reflected signals from DUT so that it can be easy to get the ratio between them. The microwave source signal delivered to the DUT through the directional coupler reflects back to enter port 2 of the six-port junction. In addition, the incident signal continues through the ring power divider which is used to feed port 1 of the six-port junction through one output port while the other output is terminated by a power detector used to keep track of the level of the source power and used as a reference port. Therefore, the reflection coefficient is found as the complex ratio $\Gamma = b_1/a_1$ by using the same analysis given in chapter 2 which can thus be written as:

$$\Gamma = \frac{\left[\left(P_5 - P_6\right) + j\ \left(P_3 - P_4\right)\right]}{P_{ref}} \tag{4.9}$$

Where the power values P_{ref}, P_3, P_4, P_5 and P_6 are measured by the power detectors connected at the output ports. It is to be noted that A_1^2 in equation 2.53 is replaced by P_{ref}. The diode detectors are chosen to be identical and operating in the square-law region.

To validate our work, the designed six-port correlator model is used in advanced Design System (ADS) momentum to obtain the reflection coefficient of a device under test (DUT) as shown in Figure 4.14. For the DUT, a 3 dB attenuator connected to port 2 can be used. The source signal connected to port 1 can be used to feed the six-port junction using an additional circuit composed of an ideal 90-degree hybrid and a Wilkinson power divider. The output ports are connected to 50 Ω terminations. The source goes through a branch line coupler to a DUT where the signal is reflected. The source signal continues through a Wilkinson power divider to feed port 1 of the six-port correlator. This allows getting the reflection coefficient Γ of the DUT ($\Gamma = \frac{b}{a} = \frac{b_1}{a_1}$). It is to be noted that a_1 and b_1 are the two inputs to the six-port correlator whose function is to get the ratio between these two complex input signals from power readings at the output ports.

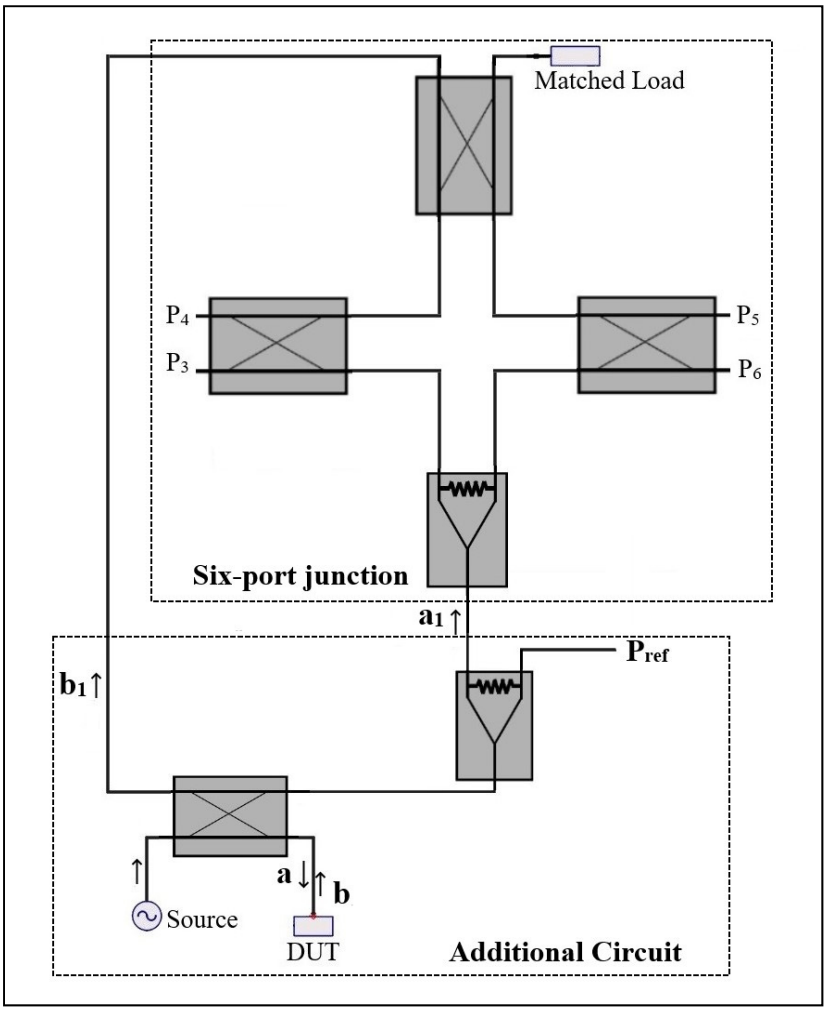

Figure 4.13 Block diagram of the proposed six-port reflectometer

By using power detectors operating in the square-law region, and according to the schematic simulation in Figure 4.14, we have $P_{ref} = |S_{21}|^2, P_3 = |S_{31}|^2,\ \ P_4 = |S_{41}|^2,\ P_5 = |S_{51}|^2,\ P_6 = |S_{61}|^2$ so that equation 4.9 can be written as:

$$\Gamma = \frac{\left[\left(|S_{51}|^2 - |S_{61}|^2\right) + j\ \left(|S_{31}|^2 - |S_{41}|^2\right)\right]}{|S_{21}|^2} \qquad (4.10)$$

Where S_{21} to S_{61} are the transmission S-parameters related to port 1 which are got by simulation and used to get the reflection coefficient Γ of the 3 dB attenuator used as a device under test.

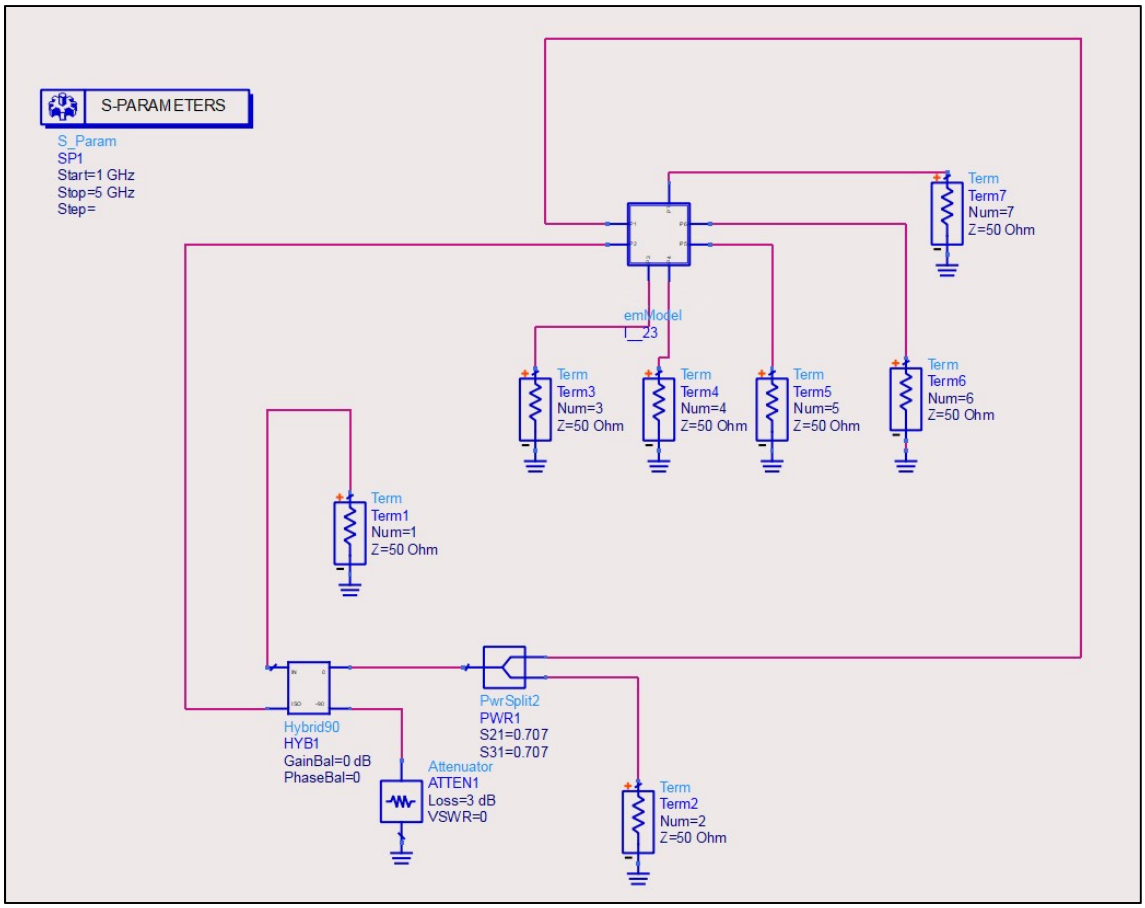

Figure 4.14 Schematic diagram of the designed six-port reflectometer with ideal additional circuit

Since the attenuator is terminated by a short circuit, the reflected signal should be – 6 dB. The simulation results of the calculated reflection coefficient Γ obtained using ADS is shown in Figure 4.15. It can be noted that the reflection coefficient is close to the theoretical expected value of – 6 dB in the frequency range 2.7—3.8 GHz which demonstrate the good operation of the six-port junction.

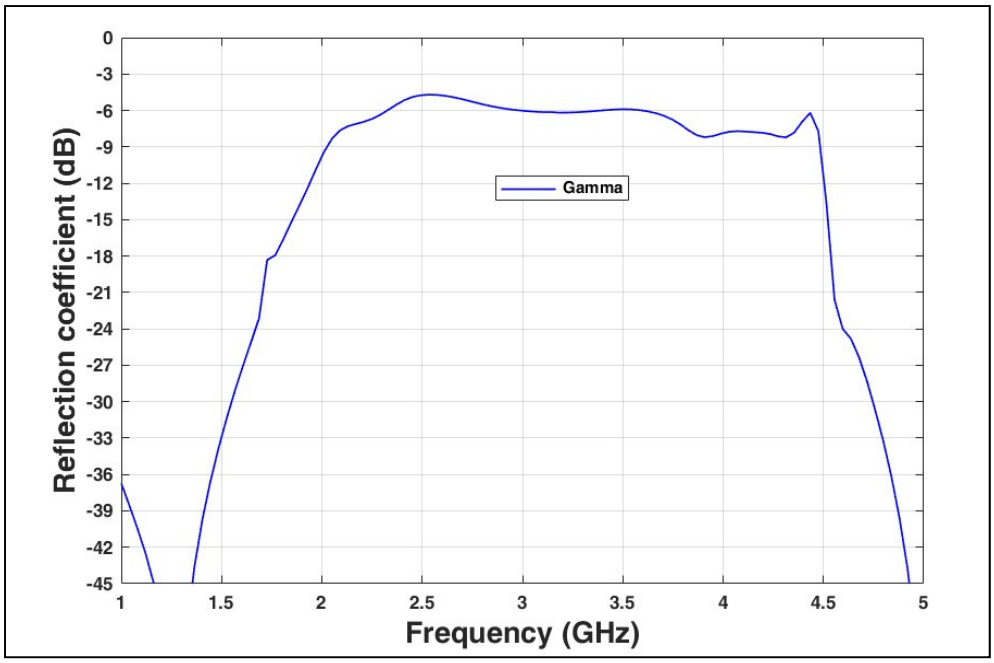

Figure 4.15 Simulation results of calculated reflection coefficient for a 3 dB attenuator as DUT

Since the six-port junction was fabricated, the additional circuit needed to complete the six-port reflectometer is then designed in momentum ADS in order to be fabricated. This additional circuit is composed of a branch line coupler and a ring power divider, and its layout is shown in Figure 4.16.

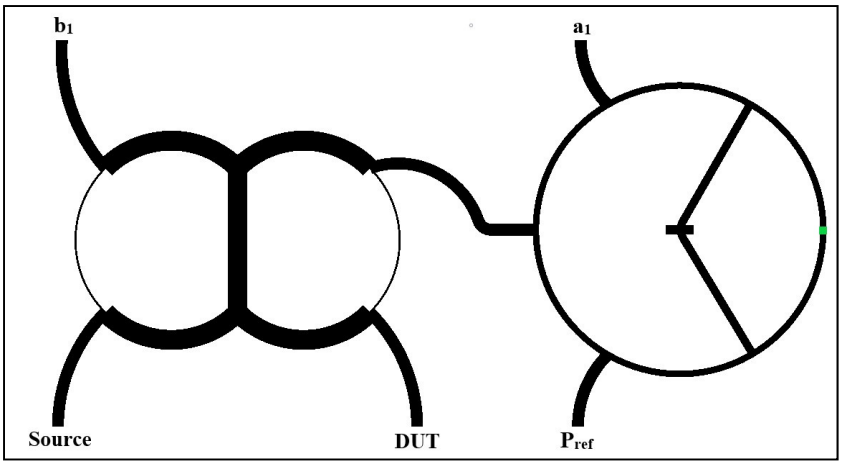

Figure 4.16 Layout of the additional circuit used to complete the six-port reflectometer

4.3.1 Six-port circuit validation

To further validate the six-port reflectometer correct operation, a test circuit is used in Advanced Design System (ADS) where the six-port junction is connected to the additional circuit described in the previous section. For the device under test (DUT), a 2 dB attenuator has been used, which is connected to port 2, and the single-tone source signal is connected to port 1. The output ports are terminated with 50 Ω loads as shown in Figure 4.17.

In this simulation, the ideal components used in the previous simulation are replaced with our developed components forming the additional circuit used to feed the six-port circuit. The six-port junction is represented by the momentum model and the additional circuit by its touchstone "SnP" component, where the number of ports is five, exported from momentum S-parameter results. The simulation results show that the reflection coefficient Γ is near the expected value of -4 dB over a wide frequency range. In fact, the signal going to the attenuator is totally reflected by the short-circuit so that we will have ideally S_{11} = - 4 dB. The value of S_{11} obtained from the simulation is around -4 ± 1 dB with small deviation between 2.65 and 3.4 dB as is shown in Figure 4.18.

These good results demonstrate the excellent performance of the six-port reflectometer design. The next step will be the manufacturing of the additional circuit needed to complete the reflectometer design. After the complete measurement system is manufactured, the system needs to be calibrated to give accurate results.

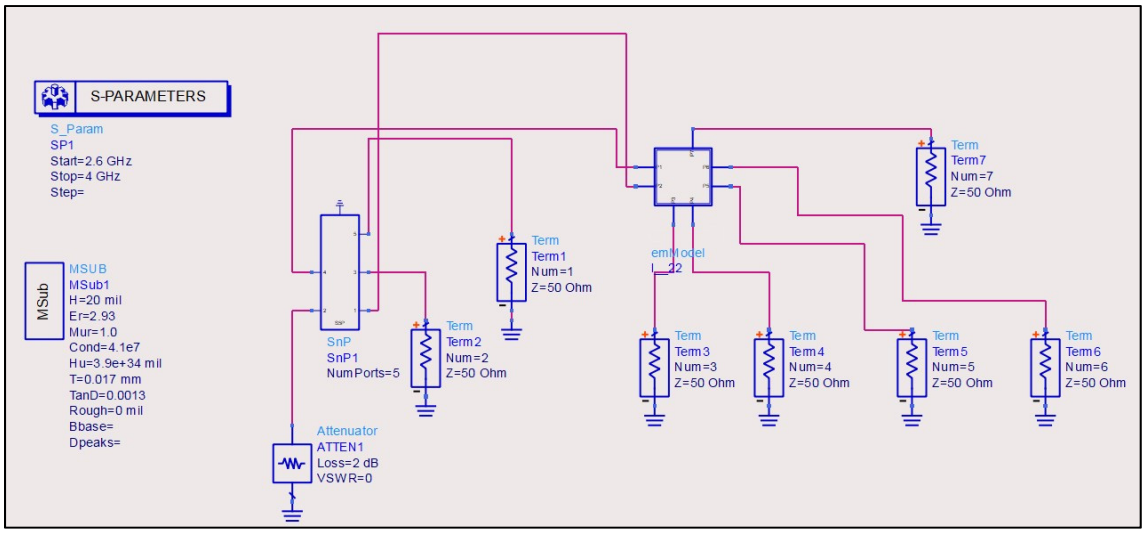

Figure 4.17 Schematic diagram of the proposed six-port reflectometer with a 2 dB attenuator as DUT

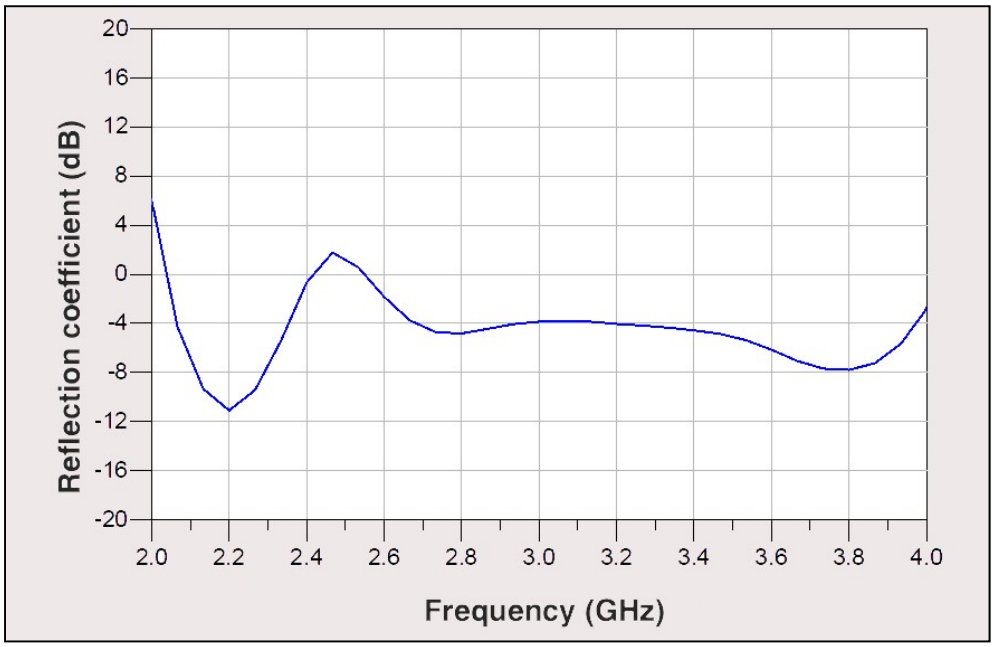

Figure 4.18 EM Simulation results of computed reflection coefficient for a 2 dB attenuator as DUT

4.3.2 Six-port reflectometer fabrication

In order to complete the Six-port reflectometer structure, the additional circuit has been fabricated on a Rogers RT/Duroid 6002 substrate to operate at the center frequency of 3 GHz. The complete structure of the six-port reflectometer is shown in Figure 4.19. As mentioned earlier, the overall six-port junction occupies the surface area of 11 cm x13.6 cm, whereas the additional circuit has the surface area 4.1 cm x 9 cm.

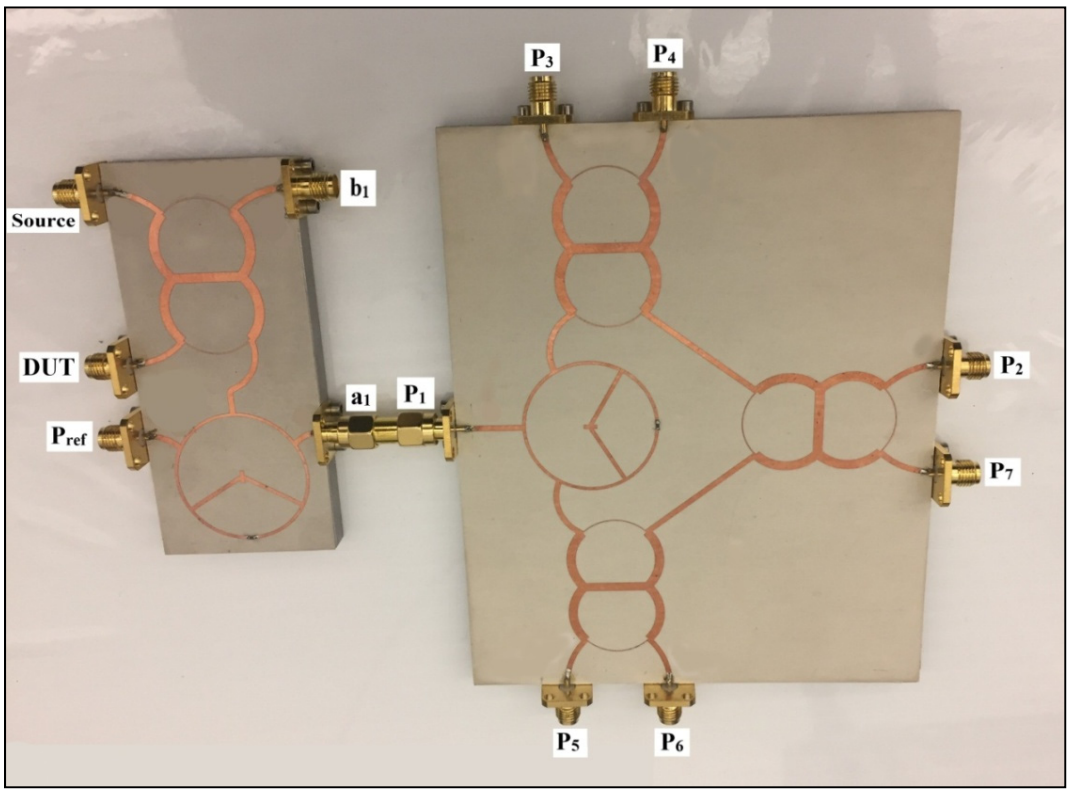

Figure 4.19 Fabricated six-port reflectometer including the additional circuit

Referring to Figure 4.19, the reflection coefficient of the DUT is found by the ratio of the two signals b_1 and a_1 as explained earlier where b_1 is to be connected to port 2 of the six-port junction. The output ports are connected to four identical power detectors and unused port 7 connected to a matched load. The reference output port P_{ref} is used to monitor the input signal and is also connected to a power detector. This will allow to find the reflection coefficient

through real time measurements by the detected output powers. The power detectors used are Pasternack zero bias Schottky detectors PE8014 which can operate in the frequency range 10 MHz - 26.5 GHz. The Zero Biased power detectors used are shown in Figure 4.20.

Figure 4.20 Schottky power detectors used in the six-port reflectometer

Many loads can be easily available in the lab and used as device under test (DUT) such as 75 Ω resistors, open, short, match, 3 dB or 6 dB attenuators as shown in Figure 4.21.

Figure 4.21 Photograph of different loads available as DUT

4.3.3 Six-port Measurement setup

At this stage, the reflection coefficient measurement of different loads can be done in practice, which intends to validate all the theoretical and simulation results. To do this, a generator is sending a signal on the device under test and the reflected signal is measured. The connection cables used in the reflectometer are high-quality low-loss radio frequency cables over which the incident signal and the reflected signal propagate, and the power detectors are connected to output ports as shown in Figure 4.22.

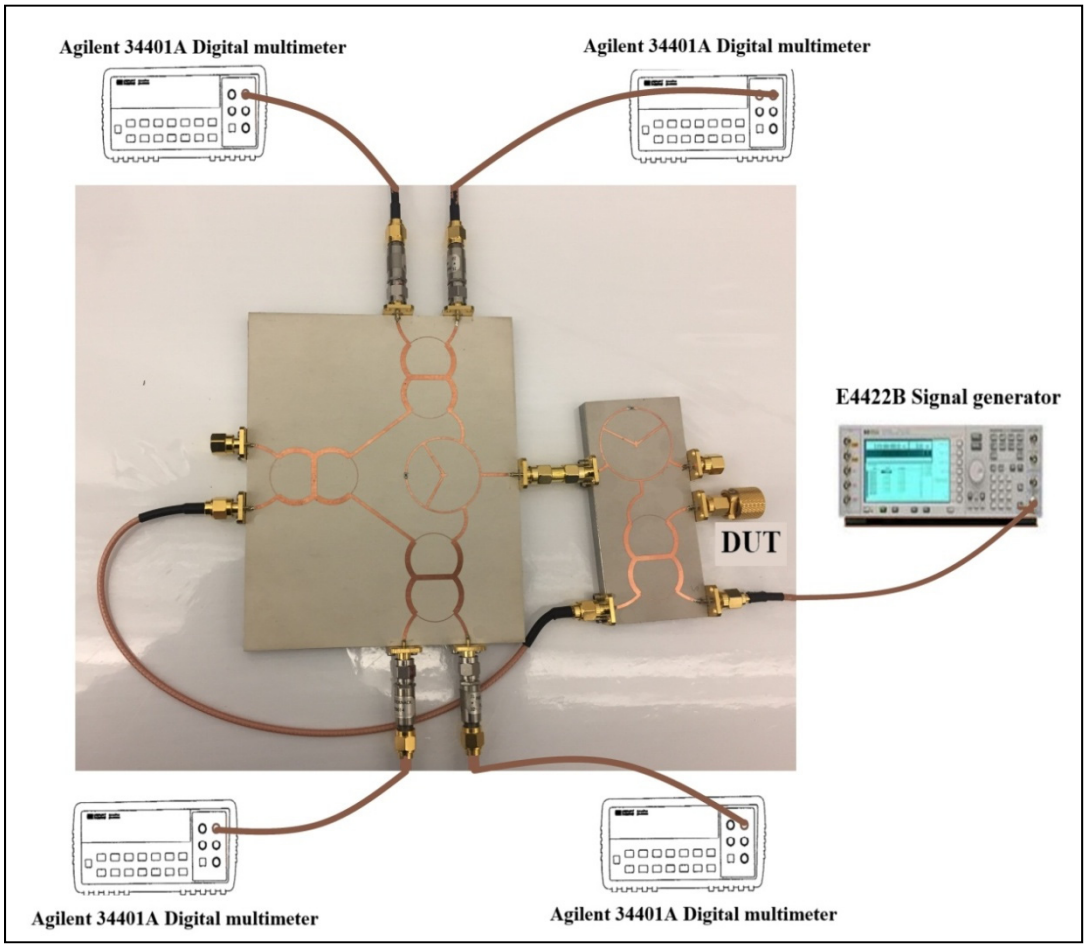

Figure 4.22 Measurement setup block diagram of the six-port reflectometer

The calibration process allows taking into account system imperfections as well as losses in the connection cables to make the necessary corrections. The results of reflection coefficient measurements are discussed in the next section where a comparison is made between corrected and uncorrected data of the reflection coefficient of different devices under test and this through a large frequency bandwidth of interest.

4.4 Calibration and Reflection Coefficient Measurements

To calibrate our six-port reflectometer, because of its similarity in reading the reflection coefficient Γ to a commercial vector network analyzer (VNA), we adapted, for simplicity, the conventional three-term error model for one-port calibration, normally used to calibrate traditional network analyzers (Bianco et al., 1978; Zeier et al., 2017) to the proposed six-port reflectometer

This model deals with measurement errors which are essentially the result of undesired systematic errors such as the directivity (e_{00}), port match (e_{11}), and reflection tracking error ($e_{10}.e_{01}$). These errors can be removed by using a virtual error correction box which represents the general calibration equations needed to obtain the actual S-parameters from the measured parameters. The measured reflection coefficient S_{11} is corrected by the application of three-term error correction model for one port as shown in Fig. 4.23.

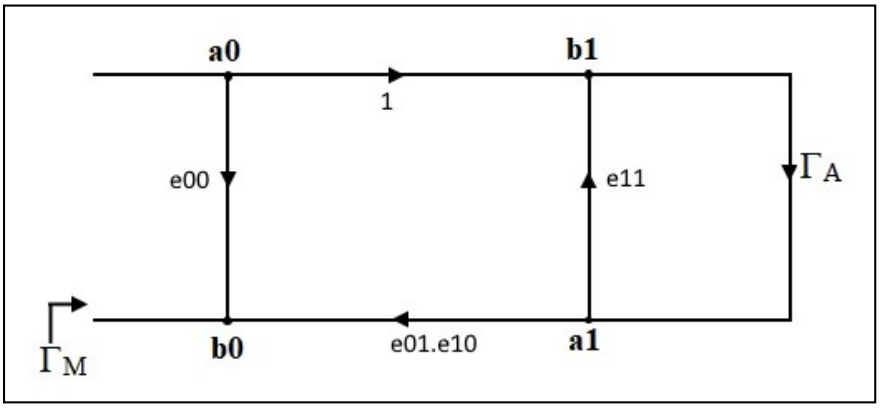

Figure 4.23 Three-term error model for one-port calibration

From the flow graph, we can determine the relation between the measured reflection coefficient Γ_M and the corrected (or actual) reflection coefficient Γ_A.

$$\Gamma_M = \frac{b_0}{a_0} = e_{00} + \frac{(e_{01}e_{10})\Gamma_A}{1 - e_{11}\Gamma_A} \tag{4.11}$$

This can be written as:

$$e_{00} + \Gamma_A \Gamma_M e_{11} - \Gamma_A \Delta = \Gamma_M \tag{4.12}$$

Where $\Delta = e_{00}e_{11} - e_{01}e_{10}$.

By using three measurements with three known standards, we can write three equations from (4.11) with 3 unknowns. The three standards measured are: open ($\Gamma_A = 1$), short ($\Gamma_A = -1$) and match ($\Gamma_A = 0$).

$$e_{00} + \Gamma_{mstd1} e_{11} - \Delta = \Gamma_{mstd1} \tag{4.13}$$

$$e_{00} - \Gamma_{mstd2} e_{11} + \Delta = \Gamma_{mstd2} \tag{4.14}$$

$$e_{00} = \Gamma_{mstd3} \tag{4.15}$$

These equations are used for the one port calibration by measuring the reflection coefficient for three standards (Open, Short and Load) at the reference plane. The three unknown error terms can then be deduced by resolving these equations. The three reflection coefficients Γ_{mstd1}, Γ_{mstd2} and Γ_{mstd3} are the measurement results for the reflection coefficient when applying the three standards (Open, short and load) to the DUT. While the first error term e_{00} is found directly from equation (4.14), the second error term can be found by adding (4.13) and (4.14), which imply:

$$e_{11} = \frac{\Gamma_{mstd1} + \Gamma_{mstd2} - 2\Gamma_{mstd3}}{\Gamma_{mstd1} - \Gamma_{mstd2}} \tag{4.16}$$

By subtracting (4.13) from (4.15), we can find the third error term after some manipulation:

$$e_{01}e_{10} = (\Gamma_{mstd3} - \Gamma_{mstd1})(e_{11} - 1) \tag{4.17}$$

At the end of the calibration process, the actual or corrected reflection coefficient can be deduced from equation (4.11) in function of the three error terms and the measured reflection coefficient.

$$\Gamma_A = \frac{(\Gamma_M - e_{00})}{e_{11}(\Gamma_M - e_{00}) + e_{01}e_{10}} \tag{4.18}$$

As mentioned, the three measurement standards are the result of making three measurements when applying our three known standards over the frequency range of interest. Then, we can find the three error unknown terms which are used later to correct the measurement reflection coefficient of any unknown DUT directly by using equation 4.18.

In order to verify the one-port calibration steps when applied to the proposed six-port reflectometer, there are 3 steps to complete the calibration process. The first step will be the calibration of diode power detectors. The second step will be to apply the three well-known standards as DUTs and get the three error terms. Once the error terms are known, the last step will be to calculate the corrected complex reflection coefficient as explained above.

4.4.1 Power detectors calibration

The six-port reflectometer in Figure 4.21 is used to measure different loads connected as device under tests. Prior to make any measurements, the diode detectors used need to be calibrated to have accurate results. The calibration consists of sweeping the input power level of the detectors in the range from -18 to 10 dBm in equidistant power steps and the output power levels are recorded. Then, an interpolation is used to have the correct power level by using the transfer functions plotted at different frequencies. After the calibration step, the calculated input power should be equal to the actual power that is present at ports 3 to port 6 of the circuit in Figure 4.22. The plotted transfer function curves of the identical power detectors in the frequency range of 2.4 - 4.0 GHz are shown in Figure 4.24.

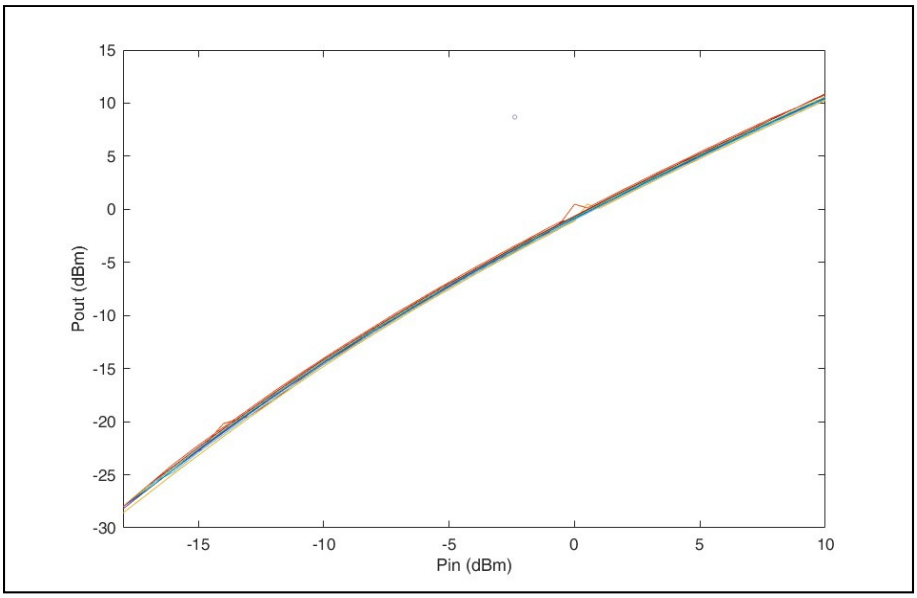

Figure 4.24 Output power versus Input power of the used diode detectors

After the diode detectors are calibrated, the test circuit is ready to be used to find the corrected reflection coefficients of the different loads using one-port error correction model.

4.4.2 One-port error model

The proposed six-port reflectometer is used to measure the magnitude and phase of the complex reflection coefficient. The measured S_{11} parameter is corrected by the one port error model(M. Zeier, 2018). used to calibrate VNAs as shown in Figure 4.25. In this section, the 3 known standards (open, short and load) are used as DUTs to find the three error terms of the error box model.

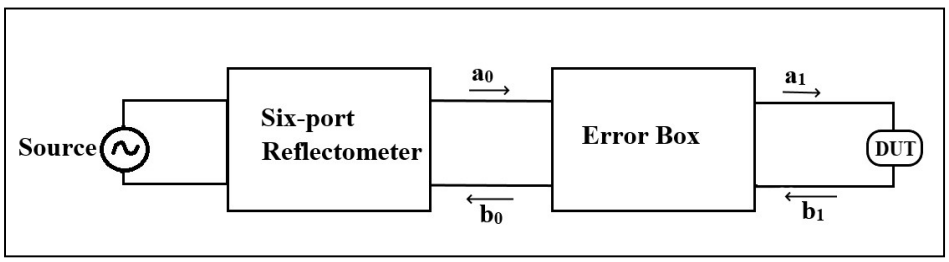

Figure 4.25 Basic error model for the six-port reflectometer

At each frequency, the proposed six-port reflectometer in figure 4.22 is used to calculate the measured standards Γ_{mstd1}, Γ_{mstd2} and Γ_{mstd3} by using equation 4.9 with the power readings P_3 to P_6 and P_{ref}. The measured results of the reflection coefficient of the 3 standards (open, short and match) are shown in Table 4.2.

Table 4.2 Results of measured standards (open, short, match)

Frequency	***Γ*mstd1 (open)**	***Γ*mstd2 (short)**	***Γ*mstd3 (match)**
2.40E+09	0.7698-0.0397j	0.2572-1.1783j	0.363-0.4498j
2.50E+09	1.1047+0.0304j	-0.8044-1.8414j	0.3355-0.4617j
2.60E+09	1.2545+0.0164j	-1.014-0.8017j	0.2385-0.3379j
2.70E+09	1.135-0.1138j	-0.9377-0.2621j	0.1199-0.2349j
2.80E+09	0.9578-0.27j	-0.9389+0.0659j	0.0343-0.142j
2.90E+09	0.8707-0.4189j	-0.9209+0.3861j	0.0028-0.0499j
3.00E+09	0.8303-0.5811j	-0.7694+0.6691j	0.0158+0.0152j
3.10E+09	0.7304-0.7223j	-0.5477+0.8505j	0.0394+0.0363j
3.20E+09	0.5496-0.8375j	-0.3466+0.9326j	0.0489+0.021j
3.30E+09	0.3168-0.9584j	-0.1589+0.9696j	0.0473-0.0092j
3.40E+09	0.0615-1.0745j	0.0754+0.9615j	0.0484-0.0529j
3.50E+09	-0.1722-1.1218j	0.3485+0.8843j	0.0488-0.1305j
3.60E+09	-0.3878-1.0505j	0.5703+0.6875j	0.015-0.2219j
3.70E+09	-0.7469-0.8832j	0.6455+0.3866j	-0.0443-0.257j
3.80E+09	-1.3957-0.7093j	0.6083+0.1251j	-0.06-0.2509j
3.90E+09	-1.1097-0.3043j	0.6188-0.0047j	-0.0002-0.2676j
4.00E+09	-0.5132-0.285j	0.8251-0.1486j	0.0794-0.4319j

These results will be used to calculate the three error terms of the error box at each frequency. The three complex error terms which will fully describe the error box used for error correction are shown in Table 4.3.

Table 4.3 Calculated three error terms for one-port calibration

Frequency	e_{00}	e_{11}	$e_{01}.e_{10}$
2.40E+09	0.363-0.4498j	-0.1336-0.3244j	0.328+0.5968j
2.50E+09	0.3355-0.4617j	-0.3314-0.14j	0.9552+0.7629j
2.60E+09	0.2385-0.3379j	-0.1077-0.0094j	1.122+0.402j
2.70E+09	0.1199-0.2349j	-0.0172+0.0465j	1.0382+0.0759j
2.80E+09	0.0343-0.142j	-0.0326+0.0364j	0.949-0.1657j
2.90E+09	0.0028-0.0499j	-0.0399+0.0195j	0.8953-0.4006j
3.00E+09	0.0158+0.0152j	-0.0061+0.0313j	0.8008-0.6254j
3.10E+09	0.0394+0.0363j	0.0111+0.057j	0.6401-0.7897j
3.20E+09	0.0489+0.021j	0.0001+0.0594j	0.4497-0.8882j
3.30E+09	0.0473-0.0092j	-0.0069+0.0345j	0.2386-0.965j
3.40E+09	0.0484-0.0529j	0.0033+0.0197j	-0.0071-1.0184j
3.50E+09	0.0488-0.1305j	-0.0205+0.0338j	-0.2591-1.0041j
3.60E+09	0.015-0.2219j	-0.0727+0.0477j	-0.4716-0.8697j
3.70E+09	-0.0443-0.257j	-0.0013-0.0114j	-0.6963-0.635j
3.80E+09	-0.06-0.2509j	0.2985-0.0832j	-0.8989-0.4327j
3.90E+09	-0.0002-0.2676j	0.2535-0.1748j	-0.8218-0.2213j
4.00E+09	0.0794-0.4319j	-0.1456-0.3066j	-0.7239-0.0134j

4.4.3 Corrected reflection coefficient

Once the error terms are known, we can easily find the corrected reflection coefficient of any device under test by using equation 4.18. For experimental validation, three different devices under test (R=75 Ω, 3 dB attenuator, 6 dB attenuator) have been used to test the calibration procedure when applied to the proposed six-port reflectometer. The attenuators are terminated with short-circuits, therefore corresponding S_{11} are - 6 dB and - 12 dB, respectively. In addition, the theoretical value of S_{11} when connecting a 75 Ω load is -14 dB. The measured reflection coefficient is found by incrementing the frequency by steps of 0.1 GHz in the

frequency range 2.4 GHz to 4 GHz while maintaining the amplitude source signal level to 13 dBm. The measured results of the complex reflection coefficient are found directly from power readings by applying equation 4.9 in the 2.4– 4 GHz frequency range. The measured reflection coefficients in polar form are shown in Table 4.4 where the phases are expressed in degrees.

Table 4.4 Measured results of the reflection coefficient for three different loads

Frequency.	**Γm_1 (DUT = 75 Ω)**	**Γm_2 (DUT = 3 dB att. + short)**	**Γm_3 (DUT = 6 dB att. + short)**
2.40E+09	0.5605∠-37.00	0.8288∠-75.74	0.6717∠-66.45
2.50E+09	0.6083∠-32.24	0.9762∠-100.72	0.6837∠-82.48
2.60E+09	0.5277∠-29.3	0.6608∠-122.44	0.4463∠-96.22
2.70E+09	0.3932∠-33.57	0.482∠-146.89	0.2887∠-118.97
2.80E+09	0.2823∠-37.87	0.4494∠-173.80	0.2273∠-154.35
2.90E+09	0.2219∠-35.30	0.4809∠160.68	0.2299∠166.91
3.00E+09	0.2084∠-31.65	0.5081∠138.69	0.2533∠136.73
3.10E+09	0.2068∠-35.36	0.5121∠121.52	0.2635∠116.62
3.20E+09	0.2101∠-47.86	0.4984∠109.16	0.254∠104.02
3.30E+09	0.2239∠-64.62	0.4823∠97.58	0.2343∠92.70
3.40E+09	0.2623∠-79.47	0.46∠82.89	0.209∠75.79
3.50E+09	0.3312∠-90.47	0.4213∠63.24	0.1695∠46.38
3.60E+09	0.4034∠-101.28	0.3579∠39.41	0.1416∠0.45
3.70E+09	0.4291∠-115.75	0.3148∠12.59	0.1626∠-35.14
3.80E+09	0.4216∠-127.02	0.33∠-9.01	0.2102∠-44.87
3.90E+09	0.3584∠-122.41	0.4061∠-21.02	0.2966∠-45.36
4.00E+09	0.4184∠-100.27	0.6549∠-37.76	0.5266∠-55.92

The ideal values of the reflection coefficient magnitude for the three DUTs used are 0.2, 0.5 and 0.25. As can be noticed, the measured values are acceptable around the center frequency. However, they need to be corrected as we move away from the center frequency. Next, equation 4.18 is applied to the measured results to evaluate the calibration method. The

corrected values of the reflection coefficients (in polar form) at the frequency range 2.4– 4 GHz are shown in Table 4.5 below.

Table 4.5 Corrected results of the reflection coefficient for 3 different loads

Frequency	**Γ_{C1} (DUT = 75 Ω)**	**Γ_{C2} (DUT =3 dB att. + short)**	**Γ_{C3} (DUT = 6 dB att. + short)**
2.40E+09	**0.2142∠4.44**	**0.5279∠-174.44**	**0.2689∠-174.13**
2.50E+09	**0.1965∠-0.38**	**0.4931∠179.52**	**0.2463∠179.51**
2.60E+09	**0.2012∠0**	**0.504∠180**	**0.2529∠0**
2.70E+09	**0.2005∠0.11**	**0.501∠179.95**	**0.2509∠179.88**
2.80E+09	**0.1994∠0.09**	**0.5007∠-179.85**	**0.2512∠0**
2.90E+09	**0.2001∠-0.06**	**0.5018∠179.98**	**0.2512∠179.93**
3.00E+09	**0.201∠-0.03**	**0.5008∠179.99**	**0.2509∠179.93**
3.10E+09	**0.1988∠-0.2**	**0.4992∠179.94**	**0.2506∠179.89**
3.20E+09	**0.2001∠-0.06**	**0.5001∠179.84**	**0.2524∠179.93**
3.30E+09	**0.2004∠0.06**	**0.5017∠-179.97**	**0.2515∠179.98**
3.40E+09	**0.2003∠-0.09**	**0.502∠179.99**	**0.2518∠-179.89**
3.50E+09	**0.2004∠0.23**	**0.5021∠-179.92**	**0.2516∠-179.86**
3.60E+09	**0.2025∠0.45**	**0.5061∠-179.69**	**0.2544∠-179.59**
3.70E+09	**0.204∠-0.11**	**0.5082∠179.89**	**0.2558∠179.87**
3.80E+09	**0.1998∠0.8**	**0.5005∠-179.45**	**0.2508∠-179.29**
3.90E+09	**0.2172∠2.3**	**0.5313∠-177.79**	**0.2712∠-177.38**
4.00E+09	**0.2232∠4.93**	**0.5541∠-172.96**	**0.2835∠-172.91**

These results reveal the excellent performance of the calibration process used. In order to better clarify the good performance of the one-port calibration method, the corrected results compared to the measured results for the three chosen DUTs are shown in Figure 4.26.

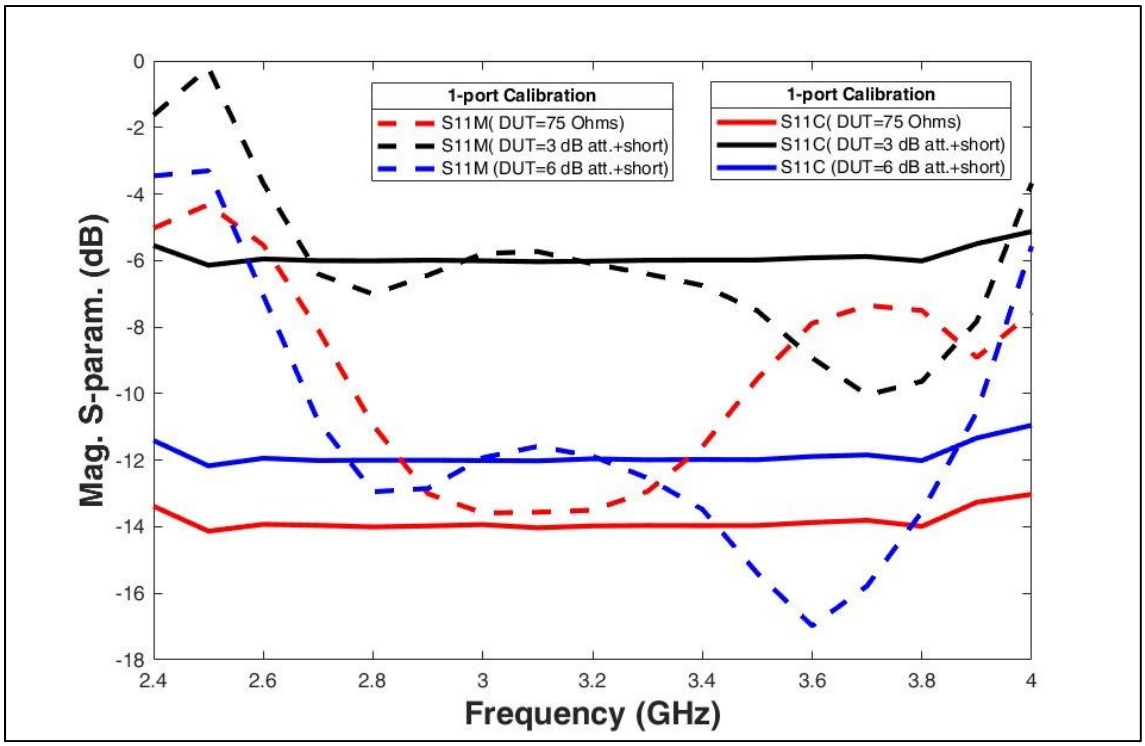

Figure 4.26 Measured and corrected reflection coefficient S_{11} for three different loads

As can be noticed, there is a great improvement in the corrected results of the reflection coefficient of different DUTs compared to measured results which proves that the calibration process works perfectly from 2.6 to 3.8 GHz to remove any hardware imperfections from the six-port reflectometer.

4.5 Conclusion

A low-cost six-port reflectometer has been designed and fabricated on a single-layer microstrip technology in order to find the complex reflection coefficient. The circuit uses enhanced components to broaden the bandwidth. The advantage of using the direct analytical method for obtaining the reflection coefficient is the great simplification in mathematical concepts compared to the conventional use of the six-port traditional method using a graphical method where the reflection coefficient was obtained by the intersection of three circles. The proposed six-port reflectometer is then calibrated to obtain high-precision real-time measurements. In

addition, the calibration process, which uses the three-term error model for one-port calibration is so simple to use and relatively fast compared with the complicated methods used on the past. The calibration method, although it looks like the usual calibration of a conventional VNA, shows that the six-port measurement circuit can be used easily without the need of operators with high amount of expertise in microwave measurements. In the past the calibration methods were very cumbersome, mainly because the classical six-port complicated mathematical equations were used. After calibration, the obtained measurement results with this specific circuit were accurate over a large frequency band from 2.6 GHz to 3.8 GHz.

CHAPTER 5

DESIGN OF WIDEBAND SIX-PORT NETWORK ANALYZER

5.1 Introduction

While six-port reflectometers can provide the reflection coefficient of a DUT, six-port network analyzers (SPNAs) are required to measure both reflection and transmission coefficients. The main advantage of the six-port technique is its ability to produce portable, low-cost, easily fabricated measurement systems that can be adapted to any frequency range. However, the calibration techniques reported in the literature are somewhat complicated due to the complexity of the used calibration algorithms involving long matrix calculations (De Sousa & Huyart, 2003; Woods, 1980).

This chapter presents a low-cost and portable dual six-port network analyzer (SPNA) for measuring the complex reflection and transmission coefficients of an unknown DUT. The SPNA consists of an RF source, an additional circuit and two six-port junctions with power detectors connected at the output ports.

A simplified approach of a full two-port calibration method based on two-port error correction, normally used for two-port calibration of industrial network analyzers (Rumiantsev & Ridler, 2008), with only four standards is presented. The measured and corrected complex reflection and transmission coefficients S_{11} and S_{21} (both magnitude and phase) obtained from the different tests performed are evaluated and compared to demonstrate the validity of the calibration method. In addition, the proposed SPNA's performance is so high so that the obtained measurement results are close to expected values as will be seen in section 5.4 which validates the proposed calibration approach.

5.2 Proposed Six-port Network Analyzer System

A block diagram of the dual six-port network analyzer is shown in Figure 5.1. It is built by two six-port junctions with power detectors to be connected at output ports and an additional circuit for power distribution which is formed by one 90-degree coupler and one ring power divider.

The microwave source signal is connected through the quadrature hybrid coupler to the measurement port associated with the DUT. A power divider ensures an equal distribution of the excitation signal to feed port 1 of the two six-port junctions simultaneously (P_1 and P_1'). Some portion of the incident power is reflected from the DUT to enter the second input port (P_2) of the first six-port junction while the other portion is transmitted to feed input port 2 (P_2') of the second six-port junction.

Therefore, the first six-port junction is used to find the reflection coefficient S_{11} while the second six-port junction is used to find the transmission coefficient S_{21}. Each six-port junction is terminated by four diode detectors on the output ports. The eight power readings at the output of the diode detectors are then collected to extract the quantities $(\Gamma_1 = b_1/a_1)$ and $(\Gamma_2 = b_2/a)$ of the DUT.

Since the outputs of the power divider feeding the 2 six-port junctions are equal $(a_1 = a_1')$, the system provides the measured complex transmission coefficient $(S_{21} = b_2/\sqrt{2}.a_1)$ through the four power detectors of the second six-port junction P'_1, P'_2, P'_3 and P'_4. In addition, the first six-port junction provides the complex reflection coefficient $(S_{11} = b_1/a_1)$ through the four power detectors P_1, P_2, P_3 and P_4.

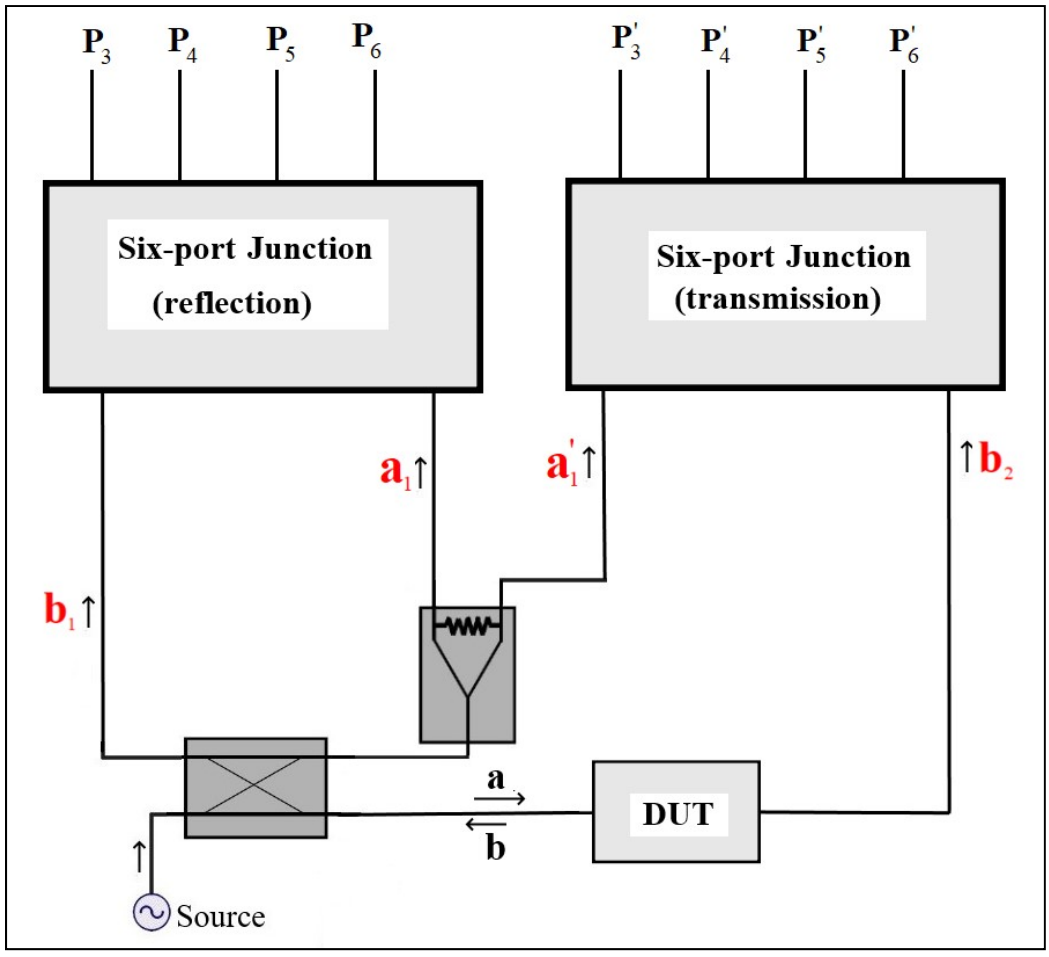

Figure 5.1 The complete dual six-port measurement system

5.3 Six-port Network Analyzer System Validation

A system simulation is used to validate the correct operation of the designed six-port network analyzer in Advanced Design System (ADS) in order to obtain both the transmission and the reflection coefficients of a device under test (DUT) as shown in Figure 5.2. In this simulation, momentum models for the two six-port junctions as well as for the additional circuit composed of a 90-degree hybrid and a Wilkinson power divider are used. The output ports are connected to 50 Ω terminations. The incident source signal going into the additional circuit is fed equally into the input ports (P_1, P_1') of the two six-port junctions. The reflected signal from the DUT is fed into Port 2 of the first six-port junction, and the transmitted signal is fed into port 2 of the second six-port junction. This allows getting both the reflection coefficient Γ and the

transmission coefficient Γ_1 directly from S-parameter simulations in Figure 5.2. By using power detectors operating in the square-law region, we have the powers at the output of the diode detectors as follows:

$$P_{ref} = 2 \mid S_{21} \mid^2, P_3 = \mid S_{31} \mid^2,\ P_4 = \mid S_{41} \mid^2,\ P_5 = \mid S_{51} \mid^2,\ P_6 = \mid S_{61} \mid^2 \tag{5.1}$$

It is to be noted that the values of the output powers in equation 5.1 correspond to the S-parameter simulation of Figure 5.2. So that equation 4.9 can yield to:

$$\Gamma = \frac{\left[\left(\left|S_{5,1}\right|^2 - \left|S_{6,1}\right|^2\right) + j\ \left(\left|S_{3,1}\right|^2 - \left|S_{4,1}\right|^2\right)\right]}{2 \cdot \left|S_{2,1}\right|^2} \tag{5.2}$$

In a similar manner, the powers at the output ports of the second port junction can be written as

$$P_3' = \mid S_{8,1} \mid^2, P_4' = \mid S_{9,1} \mid^2,\ P_5' = \mid S_{10,1} \mid^2,\ P_6' = \mid S_{11,1} \mid^2 \tag{5.3}$$

So that equation 4.8 can yield to:

$$\Gamma_1 = \frac{\left[\left(\left|S_{10,1}\right|^2 - \left|S_{11,1}\right|^2\right) + j\ \left(\left|S_{8,1}\right|^2 - \left|S_{9,1}\right|^2\right)\right]}{2 \cdot \left|S_{2,1}\right|^2} \tag{5.4}$$

Where $S_{8,1}$, $S_{9,1}$, $S_{10,1}$, $S_{11,1}$ are the transmission coefficients from port 1 to the output ports of the second six-port junction as presented in Figure 5.2. These equations allow computing the reflection and transmission coefficients from S-parameter simulations of any DUT by using the proposed six-port network analyzer.

As shown in Figure 5.3, the magnitude of the reflection coefficient $|S_{11}|$ deduced from the simulated scattering parameters is less than -15 dB between 2.8 GHz and 3.5 GHz. In addition, the transmission coefficient's magnitude $|S_{21}|$ is near the expected value of -2 dB with a very small variation from 2.8 to 3.5 GHz. Moreover, the transmission coefficient is -2 ± 0.6 dB over a large frequency band from 2.7 GHz to 3.8 GHz.

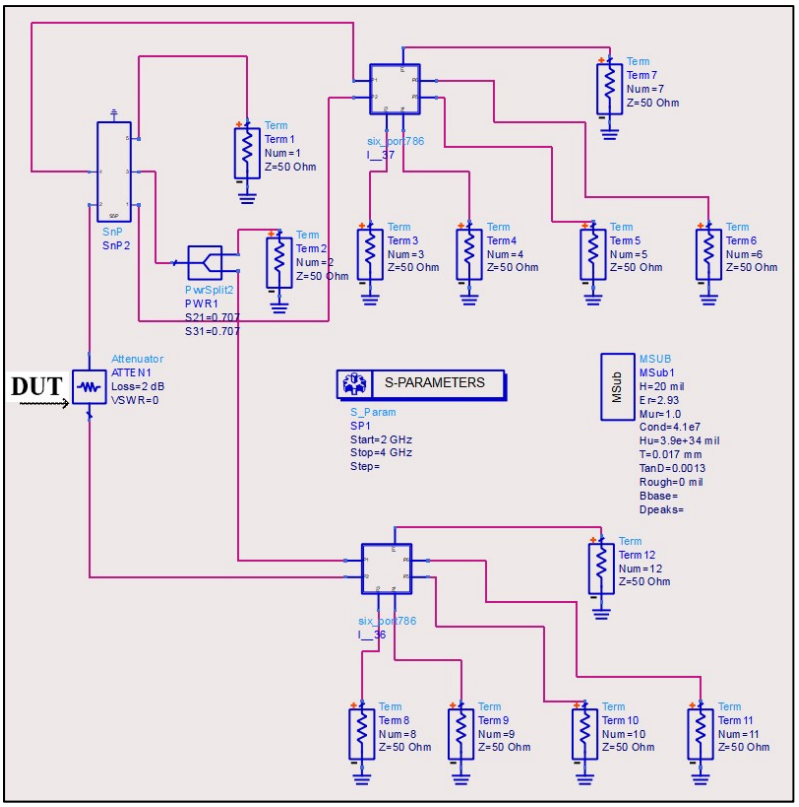

Figure 5.2 Simulation of the proposed six-port network analyzer with a 2 dB attenuator as DUT

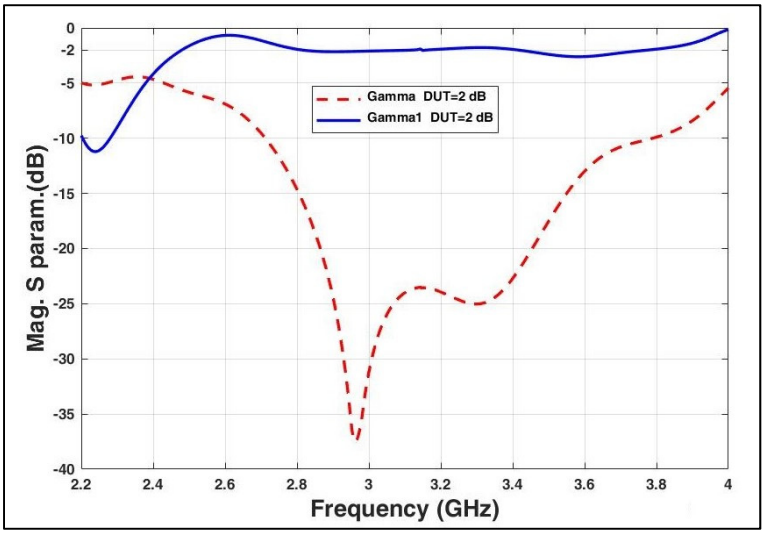

Figure 5.3 EM Simulation results of reflection and transmission coefficients for a 2 dB attenuator as DUT

Next, the designed six-port network analyzer is tested with two other DUTs in order to measure the complex reflection and transmission coefficients. Figure 5.4 shows the obtained reflection and transmission coefficients for 3 dB and 5 dB attenuators as DUTs placed in the schematic diagram in Figure 5.2. It can be noticed that the reflection and transmission coefficients show accurate results for a wide band from 2.8 GHz to 3.6 GHz for the 2 DUTs used. These results show the good performance of the proposed six-port network analyzer structure as a measurement system.

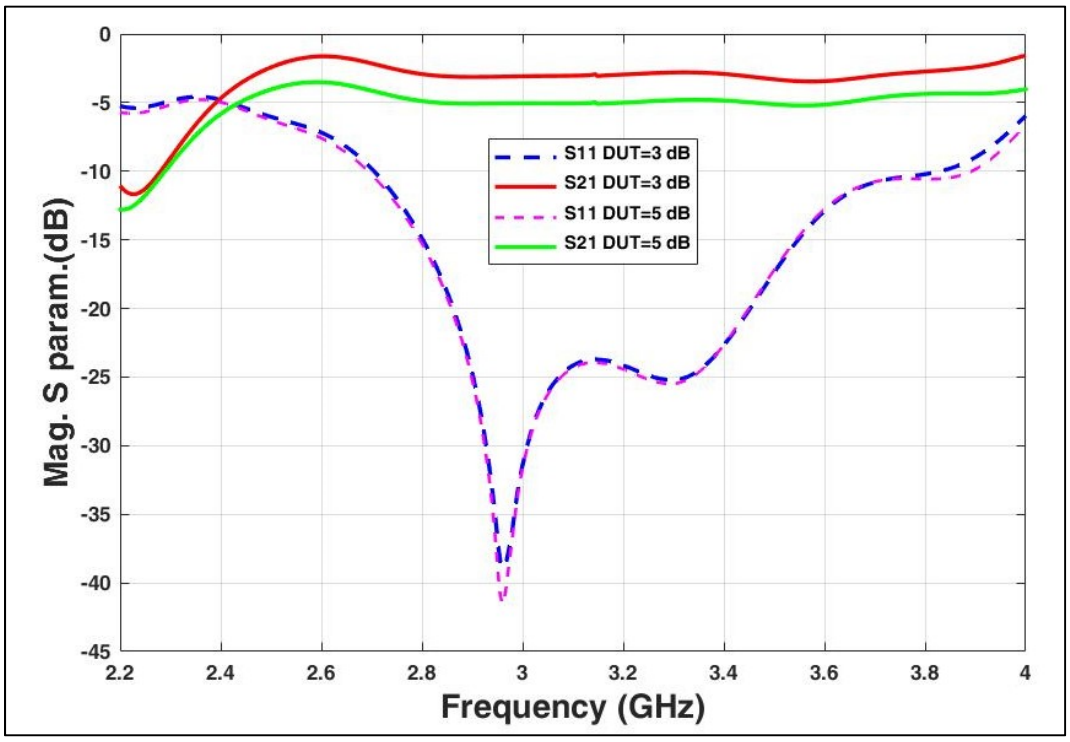

Figure 5.4 EM Simulation results of reflection and transmission coefficients for 2 attenuators as DUT

5.4 Six-port network analyzer experimental setup

The entire structure of the proposed six-port network analyzer (SPNA) includes the fabrication of the two six-port junctions and the additional circuit. Since one six-port junction and the additional circuit are already fabricated and have been used to build the six-port reflectometer, the second six-port junction is then fabricated using the microstrip single layer technology at

the center frequency of 3 GHz in order to complete the six-port network analyzer structure. The proposed SPNA experimental setup with the microwave source coming from an E4422B signal generator is shown in Figure 5.5. The additional circuit is used to extract incident and reflected waves and to feed the two six-port junctions from the source signal. The incident signal coming from the source goes through a quadrature coupler and then is distributed evenly by the ring power divider to feed the 2 input ports of the first and second six-port junction (a_1 and a'_1). The quadrature directional coupler can extract the reflected wave from the DUT which goes back to port 2 of the first six-port junction while the transmitted wave continues to port 2 of the second six-port junction. Thus, the second six-port junction which is fed with the transmitted signal and part of the source signal allows to find the transmission S-parameter (S_{21}). Likewise, the first six-port junction allows us to get the reflection coefficient (S_{11}) of the DUT. Since we have only four power detectors available, these power detectors are placed at the output of the each six-port junction simultaneously, in order to get the power readings of each junction separately while unused ports are terminated by matched loads as shown in Figure 5.5.

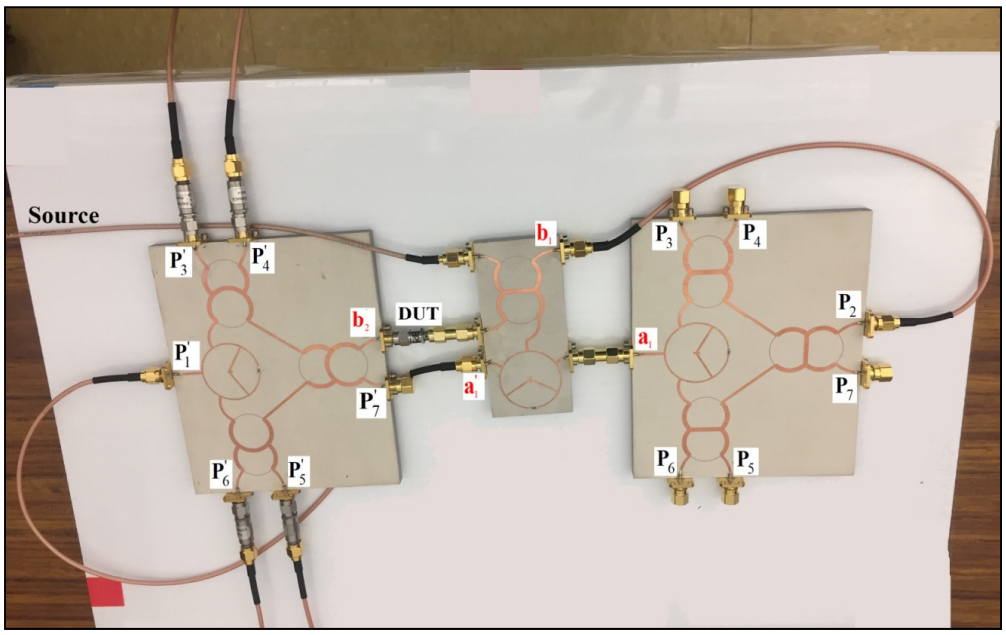

Figure 5.5 The entire structure of the proposed six-port network analyzer experimental setup

To this end, different loads can be used as DUTs in the experimental setup to deduce the complex reflection and transmission parameters from eight power readings. To do this, the microwave generator is sending a signal on the source input of the additional circuit and the Schottky power detectors PE8014 are connected to output ports 3 to 6 of the two six-port junctions simultaneously to get the output powers. The outputs of the power detectors are connected to Agilent 3440A digital multimeters in order to display the output powers as in the case of six-port reflectometer.

Now that the complete six-port network analyzer has been built, the experimental measurements are ready to be done. But since errors mainly caused by the imperfections of the six-port components and the transmission lines considerably influence the measurement results, the proposed SPNA requires calibration before performing any measurement tests as in the case of typical microwave measurement instruments in the laboratory.

5.5 Six-port network analyzer calibration

Among many calibration methods, the well-known network analyzer error correction model, based on the two-port error box network can be used in order to obtain the correct device parameters (Ferrero & Pisani, 1991). The same error correction model is applied to the proposed six-port network analyzer where the two-port calibration method uses the same standards as for one-port calibration with the addition of an extra standard known as Thru that is used to find the insertion loss S_{21}.

The block diagram of the six-port network analyzer calibration system (Ferrero & Pisani, 1991) is shown in Figure 5.6 where two virtual error correction boxes are placed one for port 1 and the other for port 2.

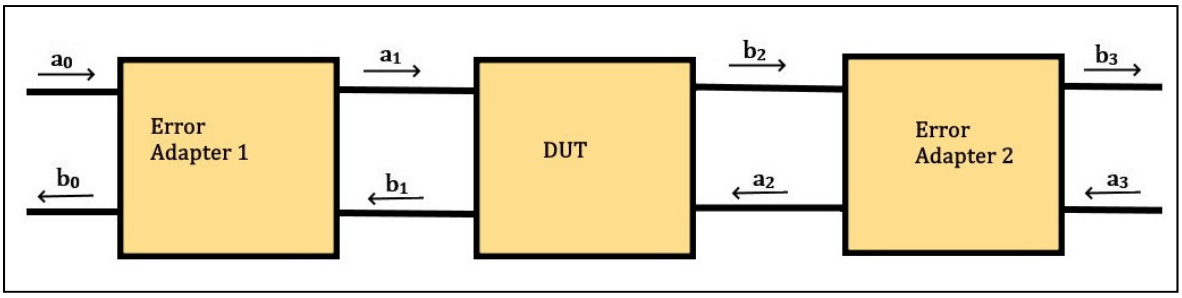

Figure 5.6 Block diagram of the six-port network analyzer calibration

Initially introduced for commercial vector network analyzers, this error model became the standard model for the description of systematic measurement errors of two-port vector network analyzers (VNAs) and is implemented in all current measurement industrial instruments (Rumiantsev & Ridler, 2008). By using the signal-flow graph of the system error model (Rumiantsev & Ridler, 2008) as shown in Figure 5.7, the equations needed for the error correction of the two-port six-port network analyzer can be derived.

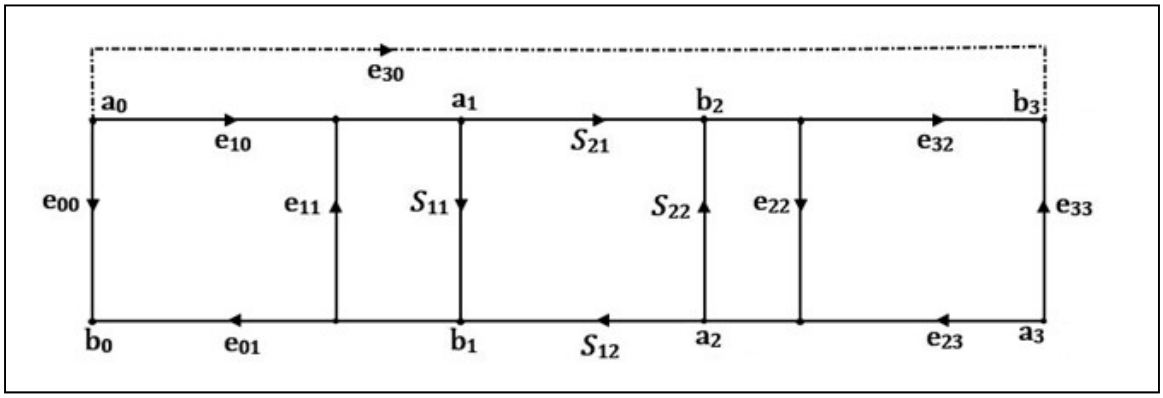

Figure 5.7 System error model for 2-port calibration (Rumiantsev & Ridler, 2008)

Using Mason's rule, we can easily find the measured S-parameters S_{11M} and S_{21M} from the flow graph in Fig. 5-7 by setting $a_3 = 0$ (matched load).

$$S_{11M} = \frac{b_0}{a_0}\bigg|_{a_3=0} = e_{00} + \frac{e_{01}.e_{10}(S_{11} - e_{22}\Delta_S)}{(1 - e_{11}.S_{11} - e_{22}.S_{22} + e_{11}.e_{22}.\Delta_S)} \tag{5.5}$$

$$S_{21M} = \left.\frac{b_3}{a_0}\right|_{a_3=0} = e_{30} + \frac{e_{10}.e_{32}.S_{21}}{1 - e_{11}.S_{11} - e_{22}.S_{22} + e_{11}.e_{22}.\Delta_S} \tag{5.6}$$

Where $\Delta_S = S_{11}.S_{22} - S_{12}.S_{21}$.

In a similar manner, we can find S_{12M} and S_{22M} by setting for the reverse mode by setting $a_0 = 0$ (matched source). Then, equations (5.5) and (5.6) can be solved to get the values of the corrected S-parameters S_{11}(or S_{11C}) and S_{21}(or S_{21C}).

$$S_{11} = \frac{\left(\frac{S_{11M} - e_{00}}{e_{01}.e_{10}}\right)\left[1 + \left(\frac{S_{22M} - e_{00}}{e_{01}.e_{10}}\right).e_{11}\right] - e_{22}.\left(\frac{S_{21M} - e_{30}}{e_{10}.e_{32}}\right).\left(\frac{S_{12M} - e_{30}}{e_{10}.e_{32}}\right)}{D} \tag{5.7}$$

$$S_{21} = \frac{\left(\frac{S_{21M} - e_{30}}{e_{10}.e_{32}}\right)\left[1 + \left(\frac{S_{22M} - e_{00}}{e_{01}.e_{10}}\right).(e_{11} - e_{22})\right]}{D} \tag{5.8}$$

Where

$$D = \left[1 + \left(\frac{S_{11M} - e_{00}}{e_{10}.e_{01}}\right).e_{11}\right]\left[1 + \left(\frac{S_{22M} - e_{00}}{e_{10}.e_{01}}\right).e_{11}\right] - \left(\frac{S_{21M} - e_{30}}{e_{10}.e_{32}}\right)\left(\frac{S_{12M} - e_{30}}{e_{10}.e_{32}}\right).e_{22}^2 \tag{5.9}$$

In this analysis, we assume that the forward and reverse models are the same which means the error boxes have the same error terms in forward and reverse calibration. However, the DUT must be manually reversed to measure the reverse S-parameters S_{12} and S_{22} (Henze et al., 2014).

The two-port calibration process is realized in 3 steps. The first step is to calibrate Port 1 with standards (Open, Short and Match) to obtain the error terms for port 1 e_{00}, e_{11} and $e_{01}e_{10}$ as in the case of the six-port reflectometer. Then, matched terminations (Z_0) are connected to Ports 1 and port 2 to find the crosstalk error e_{30} from port 1 to port 2. The third step will be to connect Port1 directly with Port 2 using the Thru standard to calculate the transmitted signal and find the error terms e_{22} and $e_{10}.e_{32}$.

The ideal response for Thru standard has the following scattering matrix (Woods, 1980):

$$[S]=\begin{bmatrix}0 & 1\\ 1 & 0\end{bmatrix} \tag{5.10}$$

For the Thru standard in forward mode, we set a_3=0 as shown in Figure 5.8 so that the signal-flow graph for the error correction model can be simplified to derive the equations for S_{11M} and S_{21M} from which the error correction terms e_{22} and $e_{10}.e_{32}$ can be found.

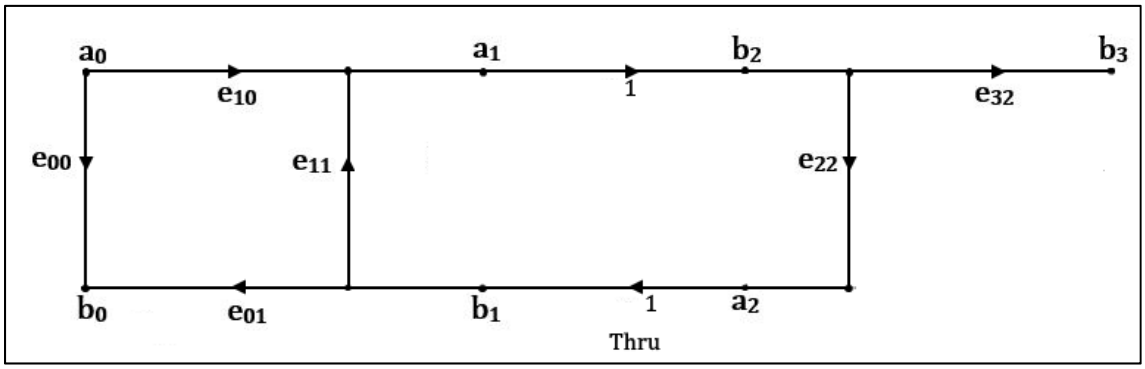

Figure 5.8 Signal flow calibration model for the Thru connection

The measured return loss S_{11M} corresponds to the value obtained during the measurement of the Thru calibration standard.

$$S_{11M}=\left.\frac{b_0}{a_0}\right|_{a_3=0}=e_{00}+\frac{e_{10}.e_{22}.e_{01}}{1-e_{11}.e_{22}} \tag{5.11}$$

This yields to:

$$S_{11M}=\frac{e_{00}-\Delta.e_{22}}{1-e_{11}.e_{22}} \tag{5.12}$$

Where $\Delta=e_{00}.e_{11}-e_{10}.e_{01}$.

The value of the error term e_{22} can be deduced from equation (5.12) in terms of S_{11M} and the known error terms from one-port calibration.

$$e_{22} = \frac{e_{00} - S_{11M}}{\Delta - e_{11}.S_{11M}} \tag{5.13}$$

The measured insertion loss S_{21M} corresponds to the value of the insertion loss obtained during the measurement of the Thru calibration standard.

$$S_{21M} = \left.\frac{b_3}{a_0}\right|_{a_3=0} = e_{30} + \frac{e_{10}.e_{32}}{1 - e_{11}.e_{22}} \tag{5.14}$$

This gives the error term $e_{10}.e_{32}$ in terms of S_{21M} and other known error terms.

$$e_{10}.e_{32} = (S_{21M} - e_{30}).(1 - e_{11}.e_{22}) \tag{5.15}$$

Once all the error terms are known for the two-port measurement system, the measurement S-parameter values of any device under test can then be corrected using equations (5.7) and (5.8). To validate the calibration method on the proposed six-port network analyzer, it is applied to measured reflection and transmission coefficients based on real experimental measurements in order to extract the corrected complex coefficients (S_{11C} and S_{21C}).

5.6 Applying calibration to experimental results

The six-port network analyzer of Figure 5.5 is used to measure the transmission and reflection coefficients of different loads connected as device under tests. As in the case of the six-port reflectometer, the diode detectors used are calibrated to have accurate results prior to make any measurements. Since the same diode detectors are used, this step has already been completed in chapter 4. Then, the first step is to calibrate Port 1 with well-known standards (Open, Short and Match) to obtain the error terms for port1 e_{00}, e_{11} and $e_{01}e_{10}$. This step is also accomplished in the six-port reflectometer calibration and the three error terms are found in Table 4.2. The next step is to find the crosstalk error e_{30} from port 1 to port 2 by connecting matched terminations to port 1 and port 2. In most cases, the isolation ports calibration error e_{30} is neglected (Henze et al., 2014) and is not carried out in the calibration process. Thus, this step is skipped since it has minor effect in the correction process. The final step is to connect the

Thru standard as DUT between port 1 and port 2 in order to find the error terms e_{22} and $e_{10}e_{32}$. By connecting the Thru standard between port 1 and port 2, two additional measured standard values Γ_{mstd4} and Γ_{mstd5} can be computed which correspond to the reflection (S_{11M}) and transmission (S_{21M}) coefficients of the Thru as DUT. At each frequency, the measured results of the reflection and transmission coefficients (Γ_{mstd4} and Γ_{mstd5}) are found from power readings P_3, P_4, P_5, P_6 and P_3', P_4', P_5', P_6' when the Thru is connected as DUT using equation 4.9. The power reading P_{ref} is taken from the experimental measurement of one-port calibration. The calculated complex values of the five measured standard values used for two-port calibration including the two complex values Γ_{mstd4} and Γ_{mstd5} in the frequency range 2.4 GHz to 4.0 GHz are shown in Table 5.1.

Table 5.1 Results of five measured standard values for two-port calibration

Freq.	***Γ*mstd1 (open)**	***Γ*mstd2 (short)**	***Γ*mstd3 (match)**	***Γ*mstd4 (Thru)**	***Γ*mstd5 (Thru)**
2.40E+09	0.7698-0.0397j	0.2572-1.1783j	0.363-0.4498j	*0.3157-0.2062j*	*0.3982-0.5366j*
2.50E+09	1.1047+0.0304j	-0.8044-1.8414j	0.3355-0.4617j	*0.2406-0.2258j*	*0.4599-0.9154j*
2.60E+09	1.2545+0.0164j	-1.014-0.8017j	0.2385-0.3379j	*0.2179-0.2779j*	*0.3027-1.2088j*
2.70E+09	1.135-0.1138j	-0.9377-0.2621j	0.1199-0.2349j	*0.1343-0.2933j*	*0.091-1.327j*
2.80E+09	0.9578-0.27j	-0.9389+0.0659j	0.0343-0.142j	*0.029-0.201j*	*0.0655-1.3515j*
2.90E+09	0.8707-0.4189j	-0.9209+0.3861j	0.0028-0.0499j	*-0.0056-0.0651j*	*0.12-1.3678j*
3.00E+09	0.8303-0.5811j	-0.7694+0.6691j	0.0158+0.0152j	*0.0273+0.0158j*	*0.1585-1.3805j*
3.10E+09	0.7304-0.7223j	-0.5477+0.8505j	0.0394+0.0363j	*0.0595+0.0227j*	*0.1724-1.2168j*
3.20E+09	0.5496-0.8375j	-0.3466+0.9326j	0.0489+0.021j	*0.0695-0.0011j*	*0.2004-1.3343j*
3.30E+09	0.3168-0.9584j	-0.1589+0.9696j	0.0473-0.0092j	*0.0555-0.023j*	*0.1856-1.3927j*
3.40E+09	0.0615-1.0745j	0.0754+0.9615j	0.0484-0.0529j	*0.0551-0.0417j*	*0.1424-1.3012j*
3.50E+09	-0.1722-1.1218j	0.3485+0.8843j	0.0488-0.1305j	*0.0845-0.1091j*	*0.1906-1.3705j*
3.60E+09	-0.3878-1.0505j	0.5703+0.6875j	0.015-0.2219j	*0.0745-0.2102j*	*0.2778-1.2377j*
3.70E+09	-0.7469-0.8832j	0.6455+0.3866j	-0.0443-0.257j	*0.0436-0.2373j*	*0.2154-1.0379j*
3.80E+09	-1.3957-0.7093j	0.6083+0.1251j	-0.06-0.2509j	*0.1011-0.2902j*	*0.0214-1.1747j*
3.90E+09	-1.1097-0.3043j	0.6188-0.0047j	-0.0002-0.2676j	*0.1271-0.3511j*	*-0.1495-1.2549j*
4.00E+09	-0.5132-0.285j	0.8251-0.1486j	0.0794-0.4319j	*0.0355-0.3207j*	*-0.2818-1.0195j*

It is to be noted that the calibration approach described here is a continuous process which begins with obtaining the first three standards used in the reflectometer for one-port calibration prior to obtaining the additional two complex values Γ_{mstd4} and Γ_{mstd5} corresponding to the Thru standard and needed to complete the two-port calibration.

By using the above analysis, these results allow to calculate the five error terms of the two error boxes at each frequency. Since the first three error terms have already been found for one-port calibration, all that remains is to find the additional two error terms e_{22} and $e_{10}.e_{32}$ for two port-calibration by using equations 5.13 and 5.15. The five error terms including the additional two error terms which will fully describe the error boxes for two-port calibration are shown in Table 5.2.

Table 5.2 Computed five error terms for two-port calibration

Freq.	e_{00}	e_{11}	$e_{01}.e_{10}$	e_{22}	$e_{10}.e_{32}$
2.40E+09	0.363-0.4498j	-0.1336-0.3244j	0.328+0.5968j	*0.24+0.2528j*	*0.4382-0.4653j*
2.50E+09	0.3355-0.4617j	-0.3314-0.14j	0.9552+0.7629j	*0.0445+0.201j*	*0.5204-0.8697j*
2.60E+09	0.2385-0.3379j	-0.1077-0.0094j	1.122+0.402j	*0.0004+0.0532j*	*0.3095-1.2065j*
2.70E+09	0.1199-0.2349j	-0.0172+0.0465j	1.0382+0.0759j	*0.0096-0.0569j*	*0.0889-1.3239j*
2.80E+09	0.0343-0.142j	-0.0326+0.0364j	0.949-0.1657j	*0.005-0.0611j*	*0.0624-1.3488j*
2.90E+09	0.0028-0.0499j	-0.0399+0.0195j	0.8953-0.4006j	*-0.0015-0.0175j*	*0.119-1.3673j*
3.00E+09	0.0158+0.0152j	-0.0061+0.0313j	0.8008-0.6254j	*0.0086+0.0075j*	*0.1582-1.3809j*
3.10E+09	0.0394+0.0363j	0.0111+0.057j	0.6401-0.7897j	*0.0229+0.0069j*	*0.1707-1.2172j*
3.20E+09	0.0489+0.021j	0.0001+0.0594j	0.4497-0.8882j	*-0.0292-0.0084j*	*0.1982-1.3353j*
3.30E+09	0.0473-0.0092j	-0.0069+0.0345j	0.2386-0.965j	*0.0153+0.0046j*	*0.185-1.3932j*
3.40E+09	0.0484-0.0529j	0.0033+0.0197j	-0.0071-1.0184j	*-0.0118+0.006j*	*0.1427-1.3013j*
3.50E+09	0.0488-0.1305j	-0.0205+0.0338j	-0.2591-1.0041j	*-0.0286+0.0281j*	*0.1928-1.3707j*
3.60E+09	0.015-0.2219j	-0.0727+0.0477j	-0.4716-0.8697j	*-0.0393+0.0471j*	*0.2842-1.2355j*
3.70E+09	-0.0443-0.257j	-0.0013-0.0114j	-0.6963-0.635j	*-0.083+0.0475j*	*0.2144-1.0375j*
3.80E+09	-0.06-0.2509j	0.2985-0.0832j	-0.8989-0.4327j	*-0.1273+0.1142j*	*-0.0304-1.2091j*
3.90E+09	-0.0002-0.2676j	0.2535-0.1748j	-0.8218-0.2213j	*-0.112+0.1407j*	*-0.2194-1.2514j*
4.00E+09	0.0794-0.4319j	-0.1456-0.3066j	-0.7239-0.0134j	*0.0604-0.1642j*	*-0.3039-1.0783j*

5.6.1 Corrected reflection and transmission coefficients

Once the error terms are known, we can easily find the corrected reflection and transmission coefficients of any device under test by using equation 4.18. For experimental validation, two attenuators (3 dB and 6 dB) have been used as DUTs to test the proposed six-port network analyzer. The measured complex reflection and transmission coefficients of the two DUTs are found by incrementing the frequency by steps of 0.1 GHz in the frequency range 2.4–4 GHz while maintaining the amplitude source signal level to 13 dBm. Therefore, for each frequency, the measured results of the complex reflection and transmission coefficients (S_{11M} and S_{21M}), which are found directly from power readings of the first and second junctions of the six-port network analyzer by applying equation 4.9 are shown in Table 5.3 below.

Table 5.3 Measured results of the reflection and transmission coefficients for 2 DUTs

Freq.	S_{11M} (DUT=3 dB attenuator)	S_{21M} (DUT=3 dB attenuator)	S_{11M} (DUT=6 dB attenuator)	S_{21M} (DUT=6 dB attenuator)
2.4E+09	0.3179∠-41.99	0.5073∠-52.21	0.2918∠-47.53	0.3904∠-51.31
2.5E+09	0.2871∠-48.74	0.7422∠-64.40	0.2686∠-52.20	0.5441∠-64.43
2.6E+09	0.313∠-51.81	0.8989∠-76.35	0.2932∠-51.77	0.6528∠-75.97
2.7E+09	0.2901∠-63.20	0.9581∠-84.99	0.0062∠-65.10	0.7211∠-1.13
2.8E+09	0.1838∠-80.51	0.9723∠-85.95	0.1908∠-79.70	0.7679∠-84.82
2.9E+09	0.0573∠-98.33	0.9816∠-84.29	0.0536∠-100.09	0.7017∠-83.70
3.0E+09	0.0302∠47.82	0.9824∠-83.14	0.0302∠56.63	0.6936∠-83.34
3.1E+09	0.0591∠30.73	0.8685∠-82.44	0.0581∠34.76	0.6139∠-83.24
3.2E+09	0.0634∠7.16	0.953∠-81.72	0.061∠11.64	0.6742∠-81.88
3.3E+09	0.0557∠-17.56	0.9955∠-81.97	0.0536∠-14.81	0.7061∠-81.61
3.4E+09	0.0697∠-38.94	0.9361∠-82.81	0.0696∠-39.52	0.6683∠-82.03
3.5E+09	0.1439∠-58.59	0.9829∠-80.93	0.1472∠-61.61	0.7292∠-80.27
3.6E+09	0.2302∠-79.61	0.9482∠-76.54	0.2355∠-83.76	0.7048∠-75.64
3.7E+09	0.2419∠-95.17	0.8159∠-76.44	0.2478∠-102.54	0.6236∠-74.70
3.8E+09	0.2677∠-90.24	0.9018∠-86.22	0.2597∠-102.27	0.6913∠-82.96
3.9E+09	0.3245∠-74.92	0.9945∠-92.67	0.2948∠-77.86	0.7731∠-87.70
4.0E+09	0.3055∠-74.92	0.8296∠-95.36	0.2951∠-69.86	0.651∠-87.05

Next, the experimental measured results and the error terms are used in equations 5.7 and 5.8 to obtain the corrected values of the complex reflection and transmission coefficients (S_{11C} and S_{21C}) at the frequency range 2.4 - 4 GHz. The corrected results obtained through the two-port calibration process are shown in Table 5.4.

Table 5.4 Corrected results of the reflection and transmission coefficients for 2 DUTs

Freq.	S_{11C} (DUT=3 dB attenuator)	S_{21C} (DUT=3 dB attenuator)	S_{11C} (DUT=6 dB attenuator)	S_{21C} (DUT=6 dB attenuator)
2.4E+09	0.1894∠-81.71	0.7626∠2.31	0.2841∠-79.64	0.5871∠3.15
2.5E+09	0.1242∠-96.05	0.7325∠0.91	0.1843∠-94.98	0.5398∠0.92
2.6E+09	0.0584∠-100.56	0.7225∠0.18	0.0875∠-100.33	0.5251∠-0.29
2.7E+09	0.0062∠-65.10	0.7211∠-1.13	0.0096∠-60.77	0.5217∠-2.30
2.8E+09	0.0094∠96.75	0.7195∠-1.31	0.0258∠82.87	0.519∠-2.54
2.9E+09	0.0073∠164.81	0.7149∠-0.71	0.0105∠162.78	0.511∠-1.30
3.0E+09	0.0069∠-137.95	0.707∠-0.33	0.0099∠-139.90	0.4992∠-0.14
3.1E+09	0.0017∠-79.99	0.7067∠0.46	0.0034∠-55.84	0.4995∠1.25
3.2E+09	0.0043∠144.46	0.7062∠0.23	0.0066∠144.87	0.4995∠0.38
3.3E+09	0.0017∠-54.46	0.7084∠-0.44	0.0024∠-55.01	0.5025∠-0.82
3.4E+09	0.0043∠-147.43	0.7151∠-0.95	0.0068∠-151.19	0.5105∠-1.73
3.5E+09	0.009∠-80.43	0.7106∠-1.13	0.0124∠-78.87	0.5273∠-1.77
3.6E+09	0.0138∠0.42	0.7487∠-0.60	0.0187∠-4.30	0.5571∠-1.41
3.7E+09	0.0306∠44.87	0.7708∠-1.70	0.0415∠49.10	0.5892∠-3.41
3.8E+09	0.0374∠18.73	0.7556∠-3.98	0.0515∠22.38	0.574∠-7.93
3.9E+09	0.0091∠-58.93	0.7893∠-5.31	0.0119∠-113.77	0.6145∠-11.08
4.0E+09	0.136∠124.27	0.8034∠-8.32	0.2088∠119.06	0.6401∠-15.85

In order to evaluate the two-port calibration process, the magnitudes of the measured reflection and transmission coefficients compared to corrected ones are extracted from the above results and are shown in Table 5.5. These results reveal the good performance of the two-port calibration process when applied to measured results of the proposed SPNA. As can be noticed from Table 5.5, the corrected results show a great improvement compared to measured results.

The correction method is able to remove the hardware imperfection errors present in the six-port network analyzer.

Table 5.5 Magnitudes of the measured and corrected results for 2 DUTs

Freq.	$\|S_{11M}\|_{3\ dB}$	$\|S_{21M}\|_{3\ dB}$	$\|S_{11M}\|_{6\ dB}$	$\|S_{21M}\|_{6\ dB}$	$\|S_{11C}\|_{3\ dB}$	$\|S_{21C}\|_{3\ dB}$	$\|S_{11C}\|_{6\ dB}$	$\|S_{21C}\|_{6\ dB}$
2.40E+09	0.3179	0.5073	0.2918	0.3904	0.1894	0.7626	0.2841	0.5871
2.50E+09	0.2871	0.7422	0.2686	0.5441	0.1242	0.7325	0.1843	0.5398
2.60E+09	0.313	0.8989	0.2932	0.6528	0.0584	0.7225	0.0875	0.5251
2.70E+09	0.2901	0.9581	0.0062	0.7211	0.0062	0.7211	0.0096	0.5217
2.80E+09	0.1838	0.9723	0.1908	0.7679	0.0094	0.7195	0.0258	0.519
2.90E+09	0.0573	0.9816	0.0536	0.7017	0.0073	0.7149	0.0105	0.511
3.00E+09	0.0302	0.9824	0.0302	0.6936	0.0069	0.707	0.0099	0.4992
3.10E+09	0.0591	0.8685	0.0581	0.6139	0.0017	0.7067	0.0034	0.4995
3.20E+09	0.0634	0.953	0.061	0.6742	0.0043	0.7062	0.0066	0.4995
3.30E+09	0.0557	0.9955	0.0536	0.7061	0.0017	0.7084	0.0024	0.5025
3.40E+09	0.0697	0.9361	0.0696	0.6683	0.0043	0.7151	0.0068	0.5105
3.50E+09	0.1439	0.9829	0.1472	0.7292	0.009	0.7106	0.0124	0.5273
3.60E+09	0.2302	0.9482	0.2355	0.7048	0.0138	0.7487	0.0187	0.5571
3.70E+09	0.2419	0.8159	0.2478	0.6236	0.0306	0.7708	0.0415	0.5892
3.80E+09	0.2677	0.9018	0.2597	0.6913	0.0374	0.7556	0.0515	0.574
3.90E+09	0.3245	0.9945	0.2948	0.7731	0.0091	0.7893	0.0119	0.6145
4.00E+09	0.3055	0.8296	0.2951	0.651	0.136	0.8034	0.2088	0.6401

In order to better see the good performance of the calibration method, the corrected transmission coefficients magnitude and phase results for the two chosen DUTs are shown in Figure 5.9 and Figure 5.10 respectively.

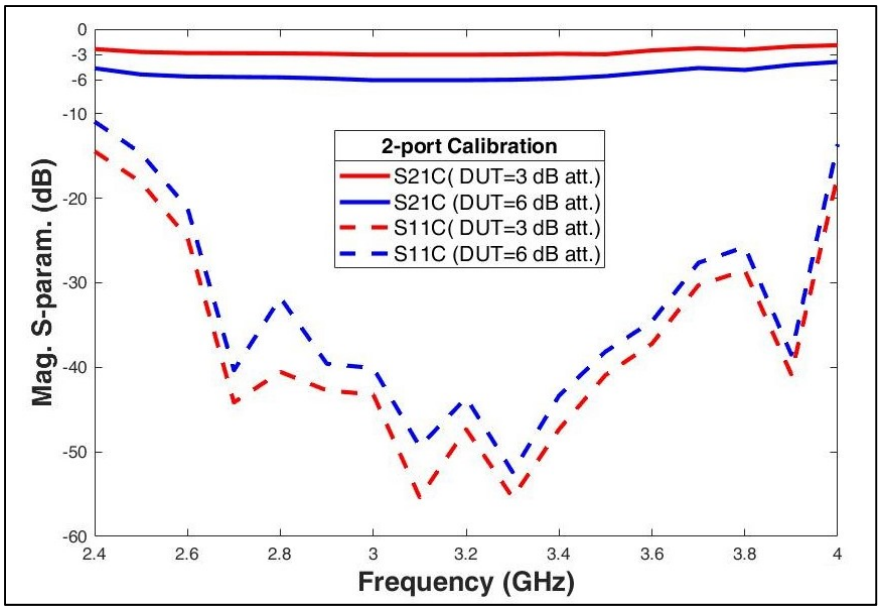

Figure 5.9 Corrected results for two different attenuators

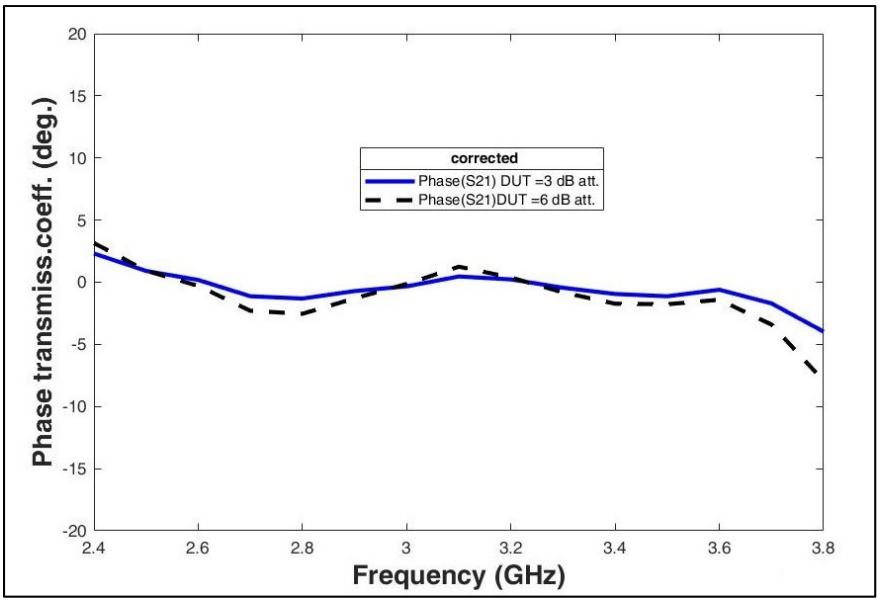

Figure 5.10 Phase transmission coefficients for two different attenuators

As can clearly be noticed from Figure 5.9 and Figure 5.10, the two-port calibration process works as expected to correct the hardware imperfection of the entire measurement system across the frequency operating bandwidth of interest. The corrected transmission coefficients

for the two attenuators have the values of – 3 ± 0.2 dB and – 6 ± 0.44 dB in the range 2.6 GHz–3.5 GHz. In addition, the transmission phase response of the two attenuators is 0 ± 2.5 degrees in the frequency range 2.5–3.7 GHz.

5.7 Conclusion

In this chapter, a low-cost six-port network analyzer (SPNA) has been presented and fabricated at microwave-wave S-band frequencies in order to find the reflection and transmission coefficients of a DUT. The circuit consists of two six-port junctions and an additional circuit to feed the two circuits. The proposed six-port network analyzer is then tested to find the corrected reflection and transmission coefficients using a two-port calibration process. The calibration method uses four standards to get the five error terms needed to get the corrected reflection and transmission coefficients of two attenuators used as DUTs. As in the case of the six-port reflectometer, the calibration method's advantage is its simplicity and ease of use compared to the conventional six-port calibration techniques used in the literature. After calibration, the obtained measurement results with the proposed SPNA were accurate over a large frequency band from 2.6 GHz to 3.5 GHz.

CONCLUSION AND FUTURE WORK

The literature on the six-port technology can be mainly divided into two major applications. On one hand, it is used as a measurement device to measure the reflection and transmission coefficients of a device under test (DUT). On the other hand, it is used as a multiport direct digital receiver for high-speed wireless communication systems. “Both approaches take advantage of the capability of easily and precisely retrieving the magnitude and phase of a complex-valued signal. For the reflectometer, the complex reflection coefficient of a device under test (DUT) can be identified; for the communication receiver, the modulated in-phase and quadrature (I/Q) signal can be calculated” (Koelpin et al., 2010). However, “the targeted performances of the six-port circuits in terms of S-parameters are the same. The main difference versus its initial application as reflectometer is the addition of a fourth q_i point, which allows a straightforward correspondence with the complex plane” (Tatu & Wu, 2013) and an additional circuit connected to a power detector is used for reference.

The calibration methods used in the literature for six-port reflectometers are mostly based on the intersection of three circles (centered in qi points) as originally described by Engen, which means three q_i points are used. As described by Engen (1978), before reducing the six-port to a four-port, the SPR requires eleven constants for the calibration process. In addition, the calibration process is often complicated due to the mathematical complexity of the equations or matrices used to find the reflection coefficient. Therefore, there was a critical need to develop a simplified calibration process that will replace the traditional calibration method in which the reflection coefficient was very difficult to obtain, with a new analytical method. For that reason, a new calibration process adapted to six-port is applied to correct the measured results from any hardware imperfections. This error correction method is based on the use of four q_i points and a straightforward analytical solution for the complex reflection coefficient as in the case of the six-port receiver, which means a significant simplification in the mathematical analysis and computational efforts.

To our knowledge, although the error-correction method has traditionally been employed to calibrate industrial network analyzers, it was never solely used with success in the six-port calibration process especially when applied to two-port measurements. The reason we chose it is that it is both accurate and easy to use, and most users can be familiar with it especially that it is widely used with commercial network analyzers. This would allow adapting a universal technique known in the industry to the six-port measurement technique. The calibration process, which uses the three-term error model (with three known calibration standards) for one-port calibration and the five-term error model (with only four standards) for two-port calibration, is simple, reliable, and relatively fast compared with the complicated methods used in the literature and at the same time, it reduces the complexity of the calibration process.

In this thesis, a compact, low-cost wideband microwave six-port measurement system that can be used to measure the transmission and reflection coefficients of a DUT has been presented. The thesis begins by viewing the existing research on the six-port technology through a literature review. The basic theoretical concepts and operation principles of the six-port measurement system are then described. After choosing the best six-port architecture to implement, the main challenge was to optimize the performance of its main components in the desired operating bandwidth. Next, the design and optimization of the main components constituting the proposed measurement system are accomplished in chapter 3.

One of the major contributions in this thesis is the design and fabrication of a new ring power divider, which has been modified by adding an SIR to the old structure to improve its operational bandwidth. To validate the theoretical analysis and simulations, a prototype is fabricated on a single layer substrate. This power divider shows a bandwidth enhancement up to 27.2 % compared to the conventional ring structure and will be used in our six-port measurement system in order to increase its bandwidth. The experimental results show that the proposed circuit is broadband with a high factor amplitude balance over the considered bandwidth covering the frequency bandwidth of 1.7 GHz to 4.6 GHz. This contribution resulted in the following journal article publication:

- **Barakat, Rabih**, Nerguizian, V., Hammou, D., & Tatu, S. O. (2020). Modified ring power divider using stepped-impedance resonator. Journal of Microwaves, Optoelectronics and Electromagnetic Applications, 19, 26-38.

In addition, a new rounded 90-degree coupler composed of two sections has been proposed. The measured results show the good performance of the proposed coupler having less than ±1 dB between 2.6 GHz and 3.7 GHz.

The second major contribution is the design and fabrication of a new six-port reflectometer operate at the center frequency of 3 GHz whose main characteristics are low design complexity and low cost. The presented reflectometer is constructed by using a six-port junction and an additional circuit. The proposed six-port junction having 47 % fractional bandwidth is built in microstrip single-layer low-cost technology and overweighs all other similar works present in the literature in terms of better S-parameter performance and wider fractional bandwidth as was clearly shown in Table 4.1. The proposed six-port reflectometer uses a simplified calibration technique based on one-port error correction. This contribution resulted in the following journal article submission:

- **Barakat, Rabih** & Tatu, S. O. (2022). Wideband six-port reflectometer for microwave applications. International Journal of Electrical and Computer Engineering (IJECE).

Finally, the six-port network analyzer is built by fabricating two six-port junctions and an additional circuit to feed the two circuits. The system is analyzed and tested to find both the complex reflection and transmission coefficients of a DUT. The two-port calibration process is applied to the obtained measured results in order to reduce any imperfections present in the system and to achieve accurate results. It is to be noted that another major contribution in this thesis is the achievement of a simplified calibration approach where only three standards are used in the six-port reflectometer and four standards in the six-port network analyzer compared to other similar previous methods using at least four and more standards for six-port reflectometers as seen the literature review. The proposed calibration approach uses a

simplified analytical method compared to complicated and time-consuming calibration six-port methods previously reported in the literature.

For future work, some potential research activities can be proposed. For example, the two-section branch-line coupler design can be enhanced by adding some open circuited stubs to it in order to improve its bandwidth. Also, the additional circuit and the six-port junction can be integrated in the same circuit so that the final circuit has two inputs (one for the source and the other for the DUT) and five outputs for power detectors. This would decrease transmission line effects and reduce the hardware imperfections present in the six-port reflectometer. In addition, for two-port measurements, the two six-port junctions and the additional circuit can be integrated in the same circuit. The final circuit will have one input for the source signal, eight outputs connected to power detectors and two additional ports to connect the DUT. Moreover, the power detectors can be integrated in the same substrate of the six-port circuit over the same PCB as explained in (Petrocchi et al., 2019) where a Skyworks SMS7630-079 zero-bias Schottky diode can be used. This allows to improve the measurement responses of the overall six-port measurement device and reduces hardware deficiencies from the system, which releases some burden from the calibration process. This in turn will give rise to more accurate results for the calibrated reflection and transmission coefficients. Besides, the six-port network analyzer can be used in the future in measuring any type of load. In particular, it can be used to measure reflection and transmission coefficients of biological tissues and cells where the derived complex permittivity determination is used for cancer detection (Nerguizian et al., 2017).

BIBLIOGRAPHY

Ahmed, U. T., & Abbosh, A. M. (2015). Design of wideband single-layer in-phase power divider using microstrip to slotline coupled structure. *Microwave and Optical Technology Letters*, *57*(4), 789–791.

Arriola, W. A., Lee, J. Y., & Kim, I. S. (2011). Wideband 3 dB Branch Line Coupler Based on /4 Open Circuited Coupled Lines. *IEEE Microwave and Wireless Components Letters*, *21*(9), 486–488.

Barakat, R., Nerguizian, V., Hammou, D., & Tatu, S. O. (2020). Modified ring power divider using stepped-impedance resonator. Journal of Microwaves, Optoelectronics and Electromagnetic Applications, 19, 26-38.

Barbara, S., & Yevhen, Y. (2020). Design of millimeter-wave six-port device for LTCC technology. *International Journal of Electronics and Telecommunications*, *66*(1), 37–43.

Basu, D., & Purkait, K. (2019). A Hypothetical Analysis to Study the Variations of Complex Dielectric Permittivity for Detection of Various Stages of Cancer of a Biological Target using Microwave Tomography. In 2019 Devices for Integrated Circuit (DevIC) (pp. 433-440). IEEE.

Bialkowski, M. E., Seman, N., & Khor, W. C. (2006). Design of a six-port reflectometer for a microwave breast cancer detection system. In AusWireless 06 Conference.

Bianco, B., Corana, A., Ridella, S., & Simcich, C. (1978). Evaluation of errors in calibration procedures for measurements of reflection coefficient. *IEEE Transactions on Instrumentation and Measurement*, *IM–27*(4), 354–358.

Bilik, V., Raffaj, V., & Bezek, J. (1990). A new extremely wideband lumped six-port reflectometer. In 1990 20th European Microwave Conference (Vol. 2, pp. 1473-1478). IEEE.

Boutejdar, A., Challal, M., Das, S., & El Hani, S. (2019). Design and Manufacturing of a Novel Compact 2.4 GHz LPF Using a DGS-DMS Combination and Quasi Octagonal Resonators for Radar and GPS Applications. *Progress In Electromagnetics Research C*, *90*, 15–28.

Chagtmi, N., Boulejfen, N., & Ghannouchi, F. M. (2017). Conception of a Dual-band Six-port Based Reflectometer. In 2017 Mediterranean Microwave Symposium (MMS) (pp. 1-4). IEEE.

Chang, T. J., Huang, T. J., & Hsu, H. T. (2017). A new design of wilkinson power divider using radial stubs featuring size reduction and bandwidth enhancement with physical isolation. In 2017 IEEE 18th Wireless and Microwave Technology Conference (WAMICON) (pp.

1-4). IEEE.

Chen, Y., Zhou, J., Yu, Z., Yin, Y., & Peng, G. (2017). Design of an ultra-wideband compact 90-degree 3dB coupler for image-rejection up-converter. In 2017 Sixth Asia-Pacific Conference on Antennas and Propagation (APCAP) (pp. 1-3). IEEE.

Chew, P. S., Yeo, K. S., Ma, K., & Kong, Z. H. (2015). A 57 to 66 GHz novel six-port correlator. In 2015 IEEE 11th International Conference on ASIC (ASICON) (pp. 1-4). IEEE.

Chun, Y. H., & Hong, J. S. (2006). Compact wide-band branch-line hybrids. IEEE Transactions on Microwave Theory and Techniques, 54(2), 704-709.

De Sousa, F. R., & Huyart, B. (2003). A new method for automatic calibration of 5-port reflectometers. In Proceedings of the 2003 SBMO/IEEE MTT-S International Microwave and Optoelectronics Conference-IMOC 2003.(Cat. No. 03TH8678) (Vol. 2, pp. 1063-1068). IEEE.

Engen, G. F. (1997). A (historical) review of the six-port measurement technique. IEEE Transactions on Microwave Theory and Techniques, 45(12), 2414-2417.

Engen, G. F. (1978). Calibrating the six-port reflectometer by means of sliding terminations. IEEE Transactions on Microwave Theory and Techniques, 26(12), 951-957.

Engen, G. F. (1977). The six-port reflectometer: An alternative network analyzer. IEEE Transactions on microwave theory and techniques, 25(12), 1075-1080.

Engen, G. F., & Hoer, C. A. (1972). Application of an arbitrary 6-port junction to power measurement problems. IEEE transactions on Instrumentation and Measurement, 21(4), 470-474.

Fang, X. T., Zhang, X. C., & Tong, C. M. (2011). A novel miniaturized microstrip six-port junction. Progress In Electromagnetics Research Letters, 23, 129-135.

Ferrero, A., & Pisani, U. (1991). QSOLT: A new fast calibration algorithm for two port S parameter measurements. In 38th ARFTG Conference Digest (Vol. 20, pp. 15-24). IEEE.

Gao, L., Wen, J. M., & Zheng, S. Y. (2019). Coupling Enhanced Single-layer Couplers Based on Multi-section Coupled-line Sections. In 2019 IEEE MTT-S International Wireless Symposium (IWS) (pp. 1-3). IEEE.

Gao, S. S., Sun, S., & Xiao, S. (2013). A novel wideband bandpass power divider with harmonic-suppressed ring resonator. IEEE Microwave and Wireless Components Letters, 23(3), 119-121.

Ghannouchi, F M, & Bosisio, R. G. (1988). An alternative explicit six-port matrix calibration formalism using five standards. *IEEE Transactions on Microwave Theory and Techniques*, *36*(3), 494–498.

Ghannouchi, F. M., Bosisio, R. G., & Demers, Y. (1989). Load-pull characterization method using six-port techniques. In 6th IEEE Conference Record., Instrumentation and Measurement Technology Conference (pp. 536-539). IEEE.

Ghannouchi, Fadhel M, Larose, R., Bosisio, R. G., & Demers, Y. (1990). Six-port network analyzer load-pull system for active load tuning. *IEEE Transactions on Instrumentation and Measurement*, *39*(4), 628–631.

Ghannouchi, F. M., & Mohammadi, A. (2009). The six-port technique with microwave and wireless applications. Artech House.

Gutierrez Miguelez, C., Huyart, B., Bergeault, E., & Jallet, L. P. (2000). A new automobile radar based on the six-port phase/frequency discriminator. *IEEE Transactions on Vehicular Technology*, *49*(4), 1416–1423.

Haddadi, K. (2007). Systèmes à base de six-port en gammes micro-onde et millimétrique et techniques de calibrage associées: application à l'analyse de réseaux, aux télécommunications et contrôle non destructif (Doctoral dissertation, Lille 1).

Haddadi, K., & Lasri, T. (2012). Formulation for complete and accurate calibration of six-port reflectometer. IEEE transactions on microwave theory and techniques, 60(3), 574-581.

Hammou, D., Moldovan, E., & Tatu, S. O. (2011). Novel MHMIC millimeter wave power divider/combiner. In 2011 24th Canadian Conference on Electrical and Computer Engineering (CCECE) (pp. 280-283). IEEE.

Hammou, D., Nedil, M., & Tatu, S. O. (2016). New Implementation of Mm-Wave Heterodyne Receiver Based on Six-Port Technology: Circuit Characterization and High Data-Rate Demodulation Results. *Progress In Electromagnetics Research C*, *65*, 139–151.

Hammou, D., Nedil, M., & Tatu, S. O. (2017). Design of improved ring Wilkinson power divider for millimetre wave applications. *Electronics Letters*, *53*(8), 542–544.

Hannachi, C., Hammou, D., Djerafi, T., Ouardirhi, Z., & Tatu, S. O. (2013). Complete characterization of novel MHMICs for V-band communication systems. Journal of Electrical and Computer Engineering, 2013.

Hassan, A., & Abbas, O. (2018). Design of a wide band six port reflectometer using broadside coupled lines. *Microwave and Optical Technology Letters*, *60*(9), 2101–2103.

Henze, A., Tempone, N., Monasterios, G., & Silva, H. (2014). Incomplete 2-port vector

network analyzer calibration methods. In 2014 IEEE Biennial Congress of Argentina (ARGENCON) (pp. 810-815). IEEE.

Hoer, C. A. (1977). A network analyzer incorporating two six-port reflectometers. IEEE Transactions on microwave theory and techniques, 25(12), 1070-1074.

Hofmann, M., Linz, S., Weigel, R., Fischer, G., & Kissinger, D. (2013). A multiband 2-port VNA for biomedical applications based on two six-port-junctions. In 2013 IEEE MTT-S International Microwave Symposium Digest (MTT) (pp. 1-4). IEEE.

Hung, C.-Y., Weng, M.-H., Su, Y.-K., Yang, R.-Y., & Wu, H.-W. (2007). Design of compact and sharp-rejection ultra wideband bandpass filters using interdigital stepped-impedance resonators. *IEICE Transactions on Electronics*, *90*(8), 1652–1654.

Hunter, J. D., & Somlo, P. I. (1985). An Explicit Six-Port Calibration Method Using Five Standards (Short Papers). IEEE transactions on microwave theory and techniques, 33(1), 69-72.

Ibrahim, S. Z., Razalli, M. S., Hoon, W. F., & Karim, M. N. A. (2016). Six-Port interferometer for direction-of-arrival detection system. In 2016 IEEE International Symposium on Systems Engineering (ISSE) (pp. 1-4). IEEE.

Iqbal, M., Camarchia, V., Pirola, M., & Quaglia, R. (2016). A miniaturized wilkinson power divider for ultra wide-band operation. In 2016 21st International Conference on Microwave, Radar and Wireless Communications (MIKON) (pp. 1-4). IEEE.

Johnosono, S., Fujii, T., & Ohta, I. (2006). Design of broadband CPW branch-Line 3-dB couplers. In 2006 European Microwave Conference (pp. 36-39). IEEE.

Julrat, S., & Trabelsi, S. (2017). Portable six-port reflectometer for determining moisture content of biomass material. IEEE Sensors Journal, 17(15), 4814-4819.

Juroshek, J. R., & Hoer, C. A. (1984). A dual six-port network analyzer using diode detectors. IEEE transactions on microwave theory and techniques, 32(1), 78-82.

Kim, H. J., Wang, S. J., Jung, W. J., & Kim, J. H. (2015). Wideband 3 dB quadrature microstrip line coupler with unequally reduced wave impedances and asymmetrical configuration in parallel lines. In 2015 IEEE 16th Annual Wireless and Microwave Technology Conference (WAMICON) (pp. 1-4). IEEE.

Kissinger, D., Laemmle, B., Nasr, I., & Weigel, R. (2013). Millimeter-wave integrated reflectometer architectures for biomedical applications. In 2013 IEEE Topical Conference on Biomedical Wireless Technologies, Networks, and Sensing Systems (pp. 61-63). IEEE.

Koelpin, A., Vinci, G., Laemmle, B., Kissinger, D., & Weigel, R. (2010). The six-port in modern society. IEEE Microwave Magazine, 11(7), 35-43.

Kothari, A., Ghasr, M. T., & Zoughi, R. (2013). Sensitivity analysis of a single-port vector reflectometer with a wideband phase-shifter. In 2013 IEEE International Instrumentation and Measurement Technology Conference (I2MTC) (pp. 381-386). IEEE.

Kumar, M., Islam, S. N., Sen, G., Parui, S. K., & Das, S. (2018). Design of Wideband Wilkinson Power Divider with Improved Performances. In 2018 IEEE Indian Conference on Antennas and Propogation (InCAP) (pp. 1-4). IEEE.

Kumar, S., Tannous, C., & Danshin, T. (1995). A multisection broadband impedance transforming branch-line hybrid. *IEEE Transactions on Microwave Theory and Techniques*, *43*(11), 2517–2523.

Kuo, J.-T., & Shih, E. (2003). Microstrip stepped impedance resonator bandpass filter with an extended optimal rejection bandwidth. *IEEE Transactions on Microwave Theory and Techniques*, *51*(5), 1554–1559.

Kuwahara, Y., Nakada, Y., Nozaki, A., & Fujii, K. (2019). Measurement and Analysis of Complex Permittivity of Breast Cancer in Microwave Band. In 2019 41st Annual International Conference of the IEEE Engineering in Medicine and Biology Society (EMBC) (pp. 2929-2932). IEEE.

Lee, C. Y., You, K. Y., Tan, T. S., Then, Y. L., Lee, Y. S., Zahid, L., Lim, W. L., & Lee, C. H. (2016). Enhanced five-port ring circuit reflectometer for synthetic breast tissue dielectric determination. *Progress In Electromagnetics Research C*, *69*, 83–95.

Li, J., Bosisio, R. G., & Wu, K. (1994). A collision avoidance radar using six-port phase/frequency discriminator (SPFD). In 1994 IEEE MTT-S International Microwave Symposium Digest (Cat. No. 94CH3389-4) (pp. 1553-1556). IEEE.

Li, J., Bosisio, R. G., & Wu, K. (1995). Modeling of the six-port discriminator used in a microwave direct digital receiver. In Proceedings 1995 Canadian Conference on Electrical and Computer Engineering (Vol. 2, pp. 1164-1165). IEEE.

Li, S., & Bosisio, R. G. (1982). Calibration of multiport reflectometers by means of four open/short circuits. IEEE Transactions on Microwave Theory and Techniques, 30(7), 1085-1090.

Nadera, A. A., Kok Yeow, Y. O. U., Chia Yew, L. E. E., Khamis, N. H., & Dimon, M. N. (2018). Wideband and compact Wilkinson power divider utilizing series delta-stub and folded stepped-impedance transmission line. Radioengineering, 27(1), 200–206.

Zeier, M., Allal, D., & Judaschke, R. (2018). Guidelines on the evaluation of vector network analyzers (VNA). EURAMET Calibration Guide, 3(12).

Mishra, B., Rahman, A., Shaw, S., Mohd, M., Mondal, S., & Sarkar, P. P. (2014). Design of an ultra-wideband Wilkinson power divider. In 2014 First International Conference on Automation, Control, Energy and Systems (ACES) (pp. 1-4). IEEE.

Moubarek, T., Almanee, M., & Gharsallah, A. (2019). Calibrating Six-Port Compact Circuit using a New Technique Program. *International Journal of Advanced Computer Science and Applications*, *10*(5), 491–497.

Murmu, L., Bage, A., & Das, S. (2017). Wideband bandpass filter using stepped impedance resonator with susceptibility test. *Revue Roumaine Des Sciences Techniques, Serie Electrotechnique et Energetique*, *62*(3), 294–298.

Nerguizian, V., Alazzam, A., Stiharu, I., & Burnier Jr, M. (2017). Characterization of several cancer cell lines at microwave frequencies. Measurement, 109, 354-358.

Nor, M. Z. B. M., Rahim, S. K. A., Sabran, M. I. B., & Rani, M. S. B. A. (2013). Wideband planar wilkinson power divider using double-sided parallel-strip line technique. *Progress In Electromagnetics Research C*, *36*, 181–193.

Ou, X. P., & Chu, Q. X. (2008). A modified two-section UWB Wilkinson power divider. In 2008 International Conference on Microwave and Millimeter Wave Technology (Vol. 3, pp. 1258-1260). IEEE.

Pazoki, R., Fard, M. G., & Fard, H. G. (2007). A modification in the single-stage wilkinson power divider to obtain wider bandwidth. In 2007 Asia-Pacific Microwave Conference (pp. 1-4). IEEE.

Petrocchi, A., Raffo, A., Bosi, G., Avolio, G., Resca, D., Vannini, G., & Schreurs, D. (2019). An Ultra-Wideband Sensing Board for Radio Frequency Front-End in IoT Transmitters. Electronics, 8(10), 1191.

Pozar, D. M. (2012). Microwave Engineering. Fourth Editions, University of Massachusetts at Amherst, John Wiley & Sons, Inc, 26-30.

Qayyum, S., & Negra, R. (2017). Compact six-port junction using broadside-coupled CPW couplers for a broadband six-port receiver. In 2017 47th European Microwave Conference (EuMC) (pp. 347-350). IEEE.

Qian, C. Z. (1985). An improved method for six-port reflectometer calibration. IEEE transactions on instrumentation and measurement, (4), 611-615.

Rumiantsev, A., & Ridler, N. (2008). VNA calibration. *IEEE Microwave Magazine*, *9*(3), 86–99.

Staszek, K. (2018). Six-Port Calibration Utilizing Matched Load and Unknown Calibration Loads. *IEEE Transactions on Microwave Theory and Techniques*, *66*(10), 4617–4626.

Staszek, K., Kaminski, P., Rydosz, A., Gruszczynski, S., & Wincza, K. (2013). A least-squares approach to the calibration of multiport reflectometers. In IEEE MTT-S International Microwave and RF Conference (pp. 1-4). IEEE.

Staszek, K, Rydosz, A., Maciak, E., Wincza, K., & Gruszczynski, S. (2017). Six-port microwave system for volatile organic compounds detection. *Sensors and Actuators B: Chemical*, *245*, 882–894.

Staszek, Kamil, Gruszczynski, S., & Wincza, K. (2016). Six-Port Reflectometer Providing Enhanced Power Distribution. *IEEE Transactions on Microwave Theory and Techniques*, *64*(3), 939–951.

Sun, S., Wu, Y., Li, M., Zhang, W., Liu, Y., & Huang, S. (2017). A novel wideband six-port correlator with filter-integration and DC-block functions. In 2017 IEEE 5th International Symposium on Electromagnetic Compatibility (EMC-Beijing) (pp. 1-4). IEEE.

Sun, Y., & Freundorfer, A. P. (2004). Broadband folded Wilkinson power combiner/splitter. *IEEE Microwave and Wireless Components Letters*, *14*(6), 295–297.

Sunil, P. A., Dey, S., & Dey, S. (2020). Compact Six-Port Network Using Lange Coupler For Sub-6 GHz Fifth Generation Communication. In 2020 IEEE International IOT, Electronics and Mechatronics Conference (IEMTRONICS) (pp. 1-6). IEEE.

Tang, C.-W., Chen, M.-G., Lin, Y.-S., & Wu, J.-W. (2006). Broadband microstrip branch-line coupler with defected ground structure. *Electronics Letters*, *42*(25), 1458–1460.

Tatu, S. O., & Moldovan, E. (2006). V-band multiport heterodyne receiver for high-speed communication systems. EURASIP Journal on Wireless Communications and networking, 2007, 1-7.

Tatu, S. O., & Wu, K. (2013). Six-port technology and applications. In 2013 11th International Conference on Telecommunications in Modern Satellite, Cable and Broadcasting Services (TELSIKS) (Vol. 1, pp. 239-248). IEEE.

Tatu, S. O., Moldovan, E., Wu, K., & Bosisio, R. G. (2001). A new direct millimeter-wave six-port receiver. IEEE Transactions on microwave theory and techniques, 49(12), 2517-2522.

Vinci, G., Lindner, S., Barbon, F., Hofmann, M., Fischer, G., Kissinger, D., & Kölpin, A. (2012). 24 GHz six-port medical radar for contactless respiration detection and heartbeat monitoring. In 2012 9th European Radar Conference (pp. 75-78). IEEE.

Wiedmann, F, Huyart, B., Bergeault, E., & Jallet, L. (1999). A new robust method for six-port reflectometer calibration. *IEEE Transactions on Instrumentation and Measurement*, *48*(5), 927–931.

Wiedmann, F., Huyart, B., Bergeault, E., & Jallet, L. (1997). New structure for a six-port reflectometer in monolithic microwave integrated-circuit technology. IEEE transactions on Instrumentation and Measurement, 46(2), 527-530.

Wilkinson, E. J. (1960). An N-Way Hybrid Power Divider. *IEEE Transactions on Microwave Theory and Techniques*, *8*(1), 116–118.

Woods, D. (1980). Analysis of a dual-six-port network analyser and derivation of calibration equations. *IEE Proceedings A (Physical Science, Measurement and Instrumentation, Management and Education, Reviews)*, *127*(8), 541–548.

Xu, H.-X., Wang, G.-M., & Lu, K. (2011). Microstrip rat-race couplers. *IEEE Microwave Magazine*, *12*(4), 117–129.

Xu, X., Wu, K., & Bosisio, R. G. (2005). Six-Port Networks. Encyclopedia of RF and microwave engineering.

Yakabe, T., Kinoshita, M., & Yabe, H. (1994). Complete calibration of a six-port reflectometer with one sliding load and one short. *IEEE Transactions on Microwave Theory and Techniques*, *42*(11), 2035–2039.

Yoon, H.-J., & Min, B.-W. (2017). Two Section Wideband 90 Hybrid Coupler Using Parallel-Coupled Three-Line. *IEEE Microwave and Wireless Components Letters*, *27*(6), 548–550.

Yu, J. D., Ban, K. S., Shin, C. Y., & Kim, Y. W. (2008, December). Various Six-Port Correlators Using Coupler and Power Divider. In Proceedings of the 2008 Second International Conference on Future Generation Communication and Networking-Volume 01 (pp. 445-448).

Zeier, M., Hoffmann, J., Ruefenacht, J., & Wollensack, M. (2017). Contemporary evaluation of measurement uncertainties in vector network analysis. Tm-Technisches Messen, 84(5), 348-358.

Zhang, W., Hasan, A., Ghannouchi, F. M., Helaoui, M., Wu, Y., & Liu, Y. (2017). Concurrent dual-band receiver based on novel six-port correlator for wireless applications. IEEE Access, 5, 25826-25834.